2017-12-19

Environmental Durability and Degradation of Fiber-Reinforced Bismaleimide/Quartz Composite for Aircraft Radome Applications

Luis Alberto Rodriguez
University of Miami, l.rodriguez47@umiami.edu

UNIVERSITY OF MIAMI

ENVIRONMENTAL DURABILITY AND DEGRADATION OF FIBER-REINFORCED BISMALEIMIDE/QUARTZ COMPOSITE FOR AIRCRAFT RADOME APPLICATIONS

By

Luis A. Rodriguez

A DISSERTATION

Submitted to the Faculty
of the University of Miami
in partial fulfillment of the requirements for
the degree of Doctor of Philosophy

Coral Gables, Florida

December 2017

UNIVERSITY OF MIAMI

A dissertation submitted in partial fulfillment of
the requirements for the degree of
Doctor of Philosophy

ENVIRONMENTAL DURABILITY AND DEGRADATION OF FIBER-REINFORCED BISMALEIMIDE/QUARTZ COMPOSITE FOR AIRCRAFT RADOME APPLICATIONS

Luis A. Rodriguez

Approved:

_____	_____
Landon R. Grace, Ph.D. Assistant Professor of Mechanical and Aerospace Engineering North Carolina State University	Michael R. Swain, Ph.D. Associate Professor of Mechanical and Aerospace Engineering
_____	_____
Emrah Celik, Ph.D. Assistant Professor of Mechanical and Aerospace Engineering	Guillermo Prado, Ph.D. Dean of the Graduate School
_____	
Francisco J. De Caso y Basalo, Ph.D. Associate Scientist of Civil, Architectural and Environmental Engineering	

RODRIGUEZ, LUIS A. (Ph.D., Mechanical and Aerospace Engineering)
Environmental Durability and Degradation of Fiber-Reinforced Bismaleimide/Quartz Composite for Aircraft Radome Applications (December 2017)

Abstract of a dissertation at the University of Miami.

Dissertation supervised by Professor Landon R. Grace.
No. of pages in text. (136)

Bismaleimide (BMI) is a polymeric thermoset material that is suitable for high temperature structural and electrical applications, particularly when used as a matrix in fiber-reinforced composites for radar-protecting structures (radomes) on commercial and military aircraft. In this role, BMI's high service temperature and high strength-to-weight ratio are of significant importance in supersonic aircraft. A main disadvantage of this material is the propensity to absorb environmental and aircraft related fluids in many applications, even in hot, dry environments. Moisture absorption has been known to be a deleterious factor in the service life of aircraft structures, especially in the case of dielectric property degradation. In this thesis, the effects of hygrothermal aging conditions and elevated temperatures on quartz-fiber-reinforced bismaleimide specimens were investigated via a split-post dielectric resonant technique at X-band (10 GHz), dynamic mechanical analysis (DMA), and flexural strength assessments. Furthermore, BMI/quartz moisture absorption kinetics were modeled by the three-dimensional hindered diffusion model (3D HDM) and its one-dimensional version of the Langmuir-type absorption model. These methods utilize least square regression to recover composite diffusivities, equilibrium moisture content, and molecular binding and unbinding probabilities with an error of less than 1%.

In split-post dielectric experiments, a 1% increase in contaminant content by weight resulted in a 7.8%, 4.5%, and 2.5% increase in relative permittivity of the material due to water, deicing fluid, and propylene glycol, respectively. A more significant impact was seen in the material's loss tangent, where a 1% increase in contaminant content by weight is responsible for a 378.5%, 592.99%, and 441.49% increase in loss tangent due to the aforementioned fluids, respectively. Since water is the most ubiquitous, a simple desorption method was performed and it was found that relative permittivity and loss tangent increase were reversed, relative to the initial moisture content. Exposure to temperatures at approximately 60% of T_g (316°C) coupled with relatively low moisture content (1.21%) and cyclical (1 Hz) flexural strain on the order of 10^{-5} were sufficient to induce fiber-matrix debond. This debond was confirmed by scanning electron microscopy (SEM) and was associated with a discrete decrease in flexural strength of up to 26%. The sensitivity of the DMA to the fiber-matrix interface integrity provides a beneficial tool for assessing the effects of thermal and moisture conditions on the onset of fiber-matrix debond, which can be detrimental to radomes in operation.

Acknowledgements

First and foremost I would like to thank my number one supporter, my mom. Without your unwavering support and love, I would not have accomplished all that I have. Love you mom. Furthermore, I would like to thank each one of my siblings and the rest of my family for being there through all my joys and hardships, love you all. To my incredible, creative, wonderful, crazy, and awesome friends thank you all for your friendship, for all the good times we had, and for all the good times we will have. To my beautiful, strong willed, caring, always loving, smart, and hardworking girlfriend, thank you for your understanding, encouragement, and love.

Many thanks to Dr. Michael Swain, Dr. Emrah Celik, and Dr. Francisco De Caso y Basalo for being part of my advisory committee. Thank you all for your brilliant comments and suggestions. A very special gratitude goes out to my advisor Dr. Landon Grace. Since day one, he has been supportive and has always believed that I would persevere through my doctoral studies. Your advice on research, as well as on my career, has been invaluable.

"And, when you want something, all the universe conspires in helping you achieve it"

-Paulo Coelho

Table of Contents

List of Figures

List of Tables

CHAPTER 1: Introduction

1.1 Background

Fiber-reinforced polymer composites have been garnering substantial popularity in the aerospace, marine, automotive, and electronics industries as a result of their desirable electrical, mechanical and thermal characteristics. Combinations of fiber and matrix systems, different fiber orientations, and heat treatments have led to desirable properties in advanced applications. Correspondingly, an increase in the use of fiber composites has been noticed in the past several decades. Bismaleimide composites are a subset of these materials that are rapidly developing and finding use in many diverse applications due to their durability and suitability in high-performance or extreme-environment applications. In comparison to other advanced resins such as epoxies and polyimides, BMI provides an increase in thermal stability with analogous processability [1] and no generation of volatiles as side product [2]. During cure volatiles can produce a higher void content [3] in composites, which can result in deleterious effects. These effects include degradation of mechanical properties [4-6], an increase in equilibrium moisture content, and an increase in rate of moisture absorption [7, 8]. The thermosetting nature of BMI, which involves a three-dimensional crosslinking network, is what allows thermal and environmental resistance [9]. As a result the polymer provides excellent property retention due to its unique properties, such as its high glass transition temperature (T_g) of 316 °C [10], chemical/corrosion resistance, relatively high tensile stress [11], and constant electrical properties over an extensive spread of temperatures [12]. Its exceptional corrosion resistance allows the material to withstand a combination of high temperature and high humidity. The resin has outstanding flame retardant characteristics that are incorporated in

advanced fiber-reinforced matrices [13, 14]. In bonding applications, BMI is used in electrical circuits, rubber to glass bonding, and anti-fouling of ship hulls (crustaceans and algae growth prevention) [15]. In aerospace applications, BMI is used in the wings, empennage and fuselage of the F-22 Raptor, tail boom of the Bell Model 412 helicopter, the aft flap hinge fairing in a C-17, and aircraft nacelle structures (inner core cowl of the Pratt and Whitney 4168 engine) [16, 17]. In addition, BMI-based composites have excellent dielectric properties and are often used in conjunction with quartz or glass fiber reinforcement in radar protecting structures [18, 19]. While numerous studies have verified the ability of BMI-based composites to withstand singular aspects of extreme environments, research has shown that environmentally induced damage on polymer composites has a significant effect on their thermal, electrical, and mechanical properties. Substantial evidence has been garnered on potential degradation conditions such as ultra violet radiation [20, 21], lightning strikes [22, 23], thermo-oxidative aging at elevated temperatures [24, 25], galvanic corrosion in presence of other metals [26, 27], and exposure to moisture. Since moisture is the most pervasive, it is of primary concern in the long-term service life of fiber-reinforced polymer composites.

In contrast to the advantages over conventional materials, polymeric composites are susceptible to degradation due to heat and moisture in severe operating environments. Sensitivity to moisture absorption [28-32] and exposure to high temperatures [33-35] has been addressed in polymer-reinforced composites over the past twenty years. Similarly, the interwoven effects of both moisture contamination and elevated temperature have been analyzed [36-39]. The moisture diffusion process begins by a fluid migrating into a polymeric resin through available microchannels and volumetric changes in the polymer

chain configuration. Not only can moisture ingress into the matrix via free space, but it can also diffuse through the fiber-matrix interphase region. In BMI/quartz laminates, diffusivity in the fiber direction is approximately 11 times greater than diffusivity transverse to the fibers [40]. Microchannels at this interphase region become an essential route for water penetration, and as water ingress advances, the interphase pathways widen in response to a dilatational expansion [41]. Consequently, the product of swelling leads to an increment in chain spacing and motion, resulting in plasticization that can be reflected in viscoelastic properties [42]. Research performed on epoxy resins has concluded that interchain debonding is the culprit. This type of debonding is constituted of Van der Waals and hydrogen bonds that are disturbed when moisture diffuses into the resin [43]. The disturbance evokes breaking of chains, causing chain mobility and swelling in the epoxy. With a combination of increasing temperature, a local molecular moisture vapor pressure is induced inside the resin and increases with increasing temperature [39]. Increasing thermal energy causes moisture to diffuse rapidly as a result of hydrogen sites becoming readily available and matrix swelling. At a critical temperature, when the moisture vapor pressure exceeds the local polymer-matrix yield stress during hygrothermal diffusion, matrix cavitation may take place [38]. Likewise, as a result of high temperatures, compressive stresses in the fibers are induced due to the polymer matrix having a greater thermal expansion coefficient than the fibers. In addition to the mismatch of thermal expansion coefficients, a significant mismatch between moisture expansion coefficient emerges if the fiber is almost non-absorbent, thus causing the interphase to swell and resulting in water penetration, causing localized stresses and strain fields that lead to debonding [44, 45].

In hygrothermal studies of BMI, it has been demonstrated how the interlaminar shear strength of carbon-fiber-reinforced BMI decreases by about 67% after 14 days of moisture ingress [46]. Bao and Yee noticed interfacial debonding and cracking in uni-weave carbon-fiber-reinforced BMI panels during SEM imaging due to exposure to moisture at 90°C for about 17 months [47]. The SEM micrographs show that most of the cracks are located near resin rich regions where the highest stresses occur due to matrix swelling. Bao and Yee performed a similar study on woven carbon fiber BMI composite immersed in water for 25 months at 70°C and observed cracks near the resin rich and interply regions [48]. In both of the aforementioned studies, cracks were not noticed in dry composites raised to similar or higher temperatures. Furthermore, it has been hypothesized that strong interface adhesion between fiber and matrix induces an increase in the Tg of the composite due to polymer chains having decreased mobility [49]. Thus, when hygrothermal conditioning is introduced, interface adhesion and Tg decrease as a result of increased chain movement [43]. DMA testing reveals that Tg in carbon-fiber-reinforced BMI samples decreases with increasing moisture content [49].

1.2 BMI/quartz Composite

The composite under investigations is bismaleimide/quartz. BMI is a type of polyimide resin trade name HexPly® F650 [10], reinforced with an eight-harness satin weave quartz fabric, style 581 [50]. Formation of the resin can occur by thermal or chemical polymerization [15]. Figure 1 displays the resin chemical structure constructed of two maleimide groups at each end with different possible main chain variations of R, illustrated in Figure 2 [15].

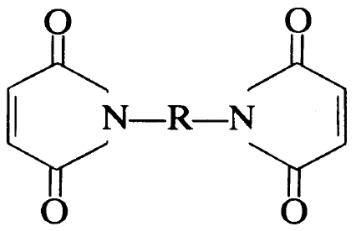

Figure 1. Bismaleimide monomer [15].

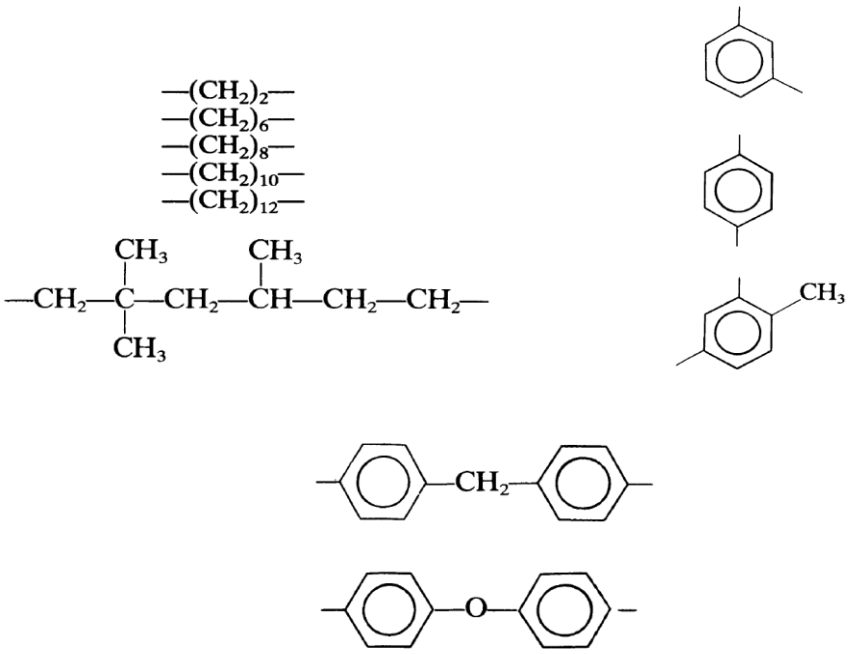

Figure 2. Possible R variations of main chain [15].

The F650 resin is structurally stable up to 316 °C (600 °F) dry, and 232 °C (450 °F) wet. The quartz eight-harness weave is a hot-melt, addition-type, polyimide resin impregnated cloth, which is typically used for laminates that have a heat resistance of 230 °C (446 °F), for long-term service time, and of 260 °C (500 °F) for short-term service time [50]. Composites panels were fabricated from a continuous 500-yard roll of prepreg material. The laminate lay process for the test panels and actual layup for the processed panel are shown in Figure 3 and Figure 4 respectively [10].

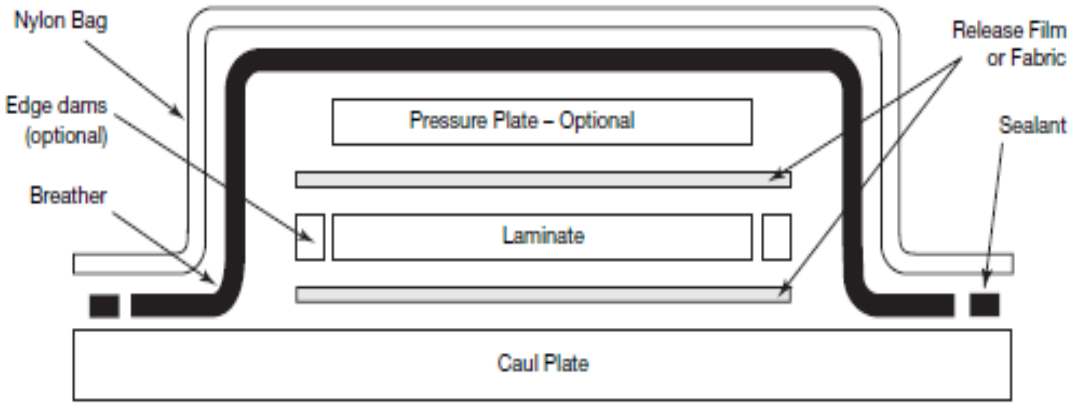

Figure 3. Typical BMI/quartz layup used for processing panels [10].

Figure 4. Actual processed BMI/quartz panel [51].

Test panels were then cured in an autoclave, according to manufacturer recommendations, which are as follows [10]:

A. Apply vacuum, 22 in. Hg (74 kPa), and 85 psi (586 kPa) autoclave pressure at ambient temperature.

B. Hold at 80-100°F (27-38°C) for 30 minutes, then vent vacuum.

C. Raise temperature to "option."

a. 375°F at 1-5°F (191°C at 0.6-3°C) per minute, hold for four hours.

b. 350°F at 1-5°F (191°C at 0.6-3°C) per minute, hold for six hours.

D. Cool and remove from autoclave.

E. Postcure four hours at 475°F (232°C). Raise temperature from ambient to 375°F (191°C) at a rate of 5-10°F (3-6°C) per minute and a rate not to exceed 3.3°F (2°C) per minute above 375°F (191°C).

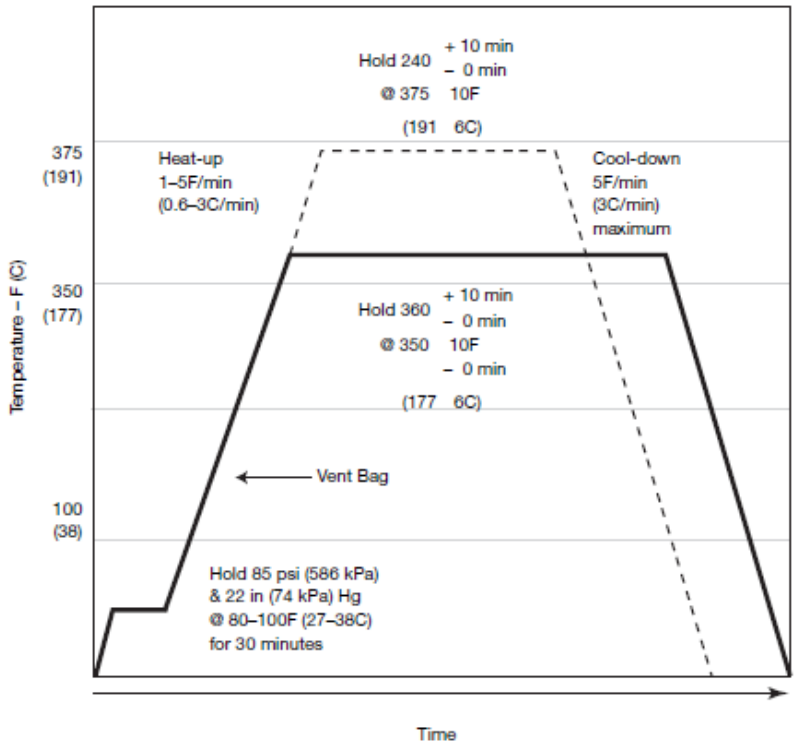

Figure 5. Cure process suggested by Hexcel [10].

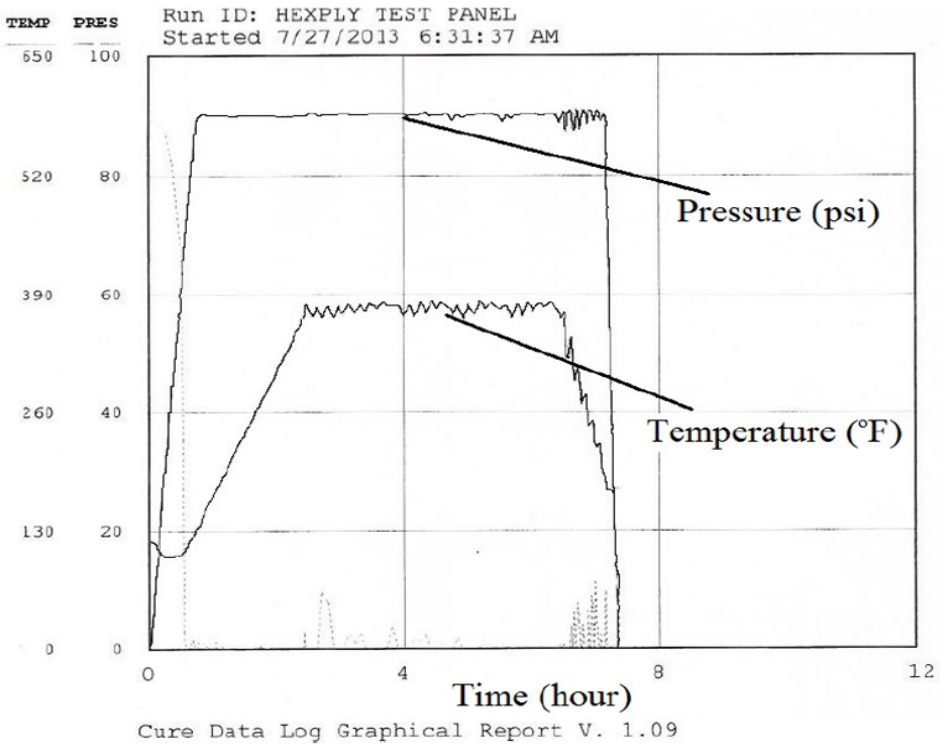

Figure 6. Actual cure process of fabricated panels [51].

A graphical representation of the pressure/temperature vs. time is illustrated by the manufacturer in Figure 5. The actual pressure/temperature vs. time data gathered during the autoclave curing procedure is presented in Figure 6 [51]. Commercially-reported equilibrium moisture content for the neat resin without reinforcement is 4.3% by weight, which is consistent with a 1.38% moisture content by weight for the BMI/quartz composite, assuming the fibers of satin weave are impermeable [10]. The mechanical properties of BMI/quartz are reported by manufacturer in Table 1. In Table 2, the dielectric properties of the dry specimen are given within the X-band frequency range (9.375 GHz).

Table 1. BMI/quartz mechanical properties reported by Hexcel [10].

	Room Temperature	350°F (177°C)	450°F (232°C).
Tension Strength ksi (MPa) Modulus msi (GPa)	 77.10 (531.6) 3.90 (26.9)	 66.60 (459.2) 3.60 (24.8)	 62.80 (433.0) -
Compression Strength ksi (MPa) Modulus msi (GPa)	73.20 (504.7) 4.06 (28.0)	54.50 (375.8) 3.85 (26.5)	42.40 (292.3) -
Short Beam Shear Strength ksi (MPa)	8.80 (60.7)	7.20 (49.6)	6.10 (42.1)

Table 2. Dielectric properties of BMI/quartz as reported by Hexcel [10].

Temperature	Dielectric Constant	Loss Tangent
75°F (24°C)	3.31	.003
300°F (149°C)	3.33	.004
450°F (232°C) at 9.375 GHz	3.34	.005

1.3 Motivation and Application of Bismaleimide/quartz in Radomes

In the aerospace industry, BMI is sometimes reinforced with quartz fibers for use in radomes due to the resultant low dielectric properties, heat retardant characteristics, relatively low vulnerability to moisture ingress [51], and long-term structural rigidity when subjected to moisture rich environments [52]. Furthermore, the matrix is often a viable option when utilized in high temperature and humidity environments as a result of its corrosion resistance, high glass-transition temperature, and mechanical durability in these extreme surroundings [40].

Radomes are protective housing structures that are typically used for object and weather detection in ground-based, maritime, or aircraft-based radar installations. These structures form a critical component of the radar detection system by shielding its constituent antenna from hazardous conditions such as lightning, debris, moisture, hail or bird strike, and aircraft-related fluids such as fuels, lubricants, and solvents. The ability to provide structural integrity and impact protection while maintaining transparency to electromagnetic energy is crucial to the service life of a radome [53]. Therefore, these

protective structures on aircraft are typically fabricated from polymers or fiber-reinforced polymer composites due to their aforementioned excellent high strength to weight ratio, mechanical, thermal, and electrical properties. However, one of the pivotal drawbacks of these polymeric composite structures is their sensitivity to moisture absorption in nearly all operational environments [54], which may lead to irreparable damage to radome composites.

Structural property degradation of polymeric composites is often coupled with absorption of environmental and aerospace service-related fluids. Contaminants include precipitation, humidity, salt water and condensation, as well as aircraft-related contaminants such as fuels, lubricant, solvents, and deicing fluids [54, 55]. Significant research has been performed in the area of fluid ingress and its effects on the electrical, mechanical and thermal properties of polymeric materials. Several studies have focused on the effects of fluids typically present in the aircraft environment. Sugita et al. [56] investigated the degradation of mechanical properties due to bio-based and synthetic deicing fluids on carbon/epoxy composites and noticed a decrease in ultimate tensile load in specimens immersed in bio-based deicing fluid after eight days at a 1% weight gain. The degradation of carbon/epoxy lap joints due to water, jet fuel, hydraulic fluid, and an anti-icing fuel additive was reported by Sugita et al. [57]. It was observed that the anti-icing additive had the most significant effect on specimens by lowering the relative hardness by 12.5%. Moreover, the effect of two commonly used aerospace detergents, an aircraft surface cleaner (Penair C5572) and a nonionic detergent (MEK), on the rheological properties of neat epoxy is reported by Moffet and La Saponara [58]. They noticed fracture of laminates due to absorption of MEK after a three month period of exposure and storage

modulus variations of -18% at 99°C due to Penair C5572 after a six month exposure. As of now, extensive research has been performed on the moisture absorption behavior and its damage to epoxy and epoxy fiber-reinforced composites [28, 59]. In comparison, BMI/quartz has not been investigated at the same level as epoxy, but it has been examined in varying detail. Investigations include aerospace grade hydraulic fluid absorption and its effects on flexure properties as a result of the coupled effects of humidity exposure (prior to laminate fabrication) and cure fabrication pressure [60]. In addition, Grace and Altan [40] have characterized the anisotropic moisture absorption of the polymeric composite using a three-dimensional hindered diffusion model. The occasional studies of quartz-reinforced BMI are most likely a result of its use for specialized advanced application.

In radomes, the ubiquitous nature of water and its high dielectric constant of about 80 are of crucial importance to radar performance. When moisture is absorbed in aircraft, radome properties can degrade due to various conditions. These events include thickness swelling (cracks or delamination), conducting high temperature (steam pressure delamination), thermal spiking (cracking and higher absorption of moisture), and freeze/thaw cycles (delamination and micro-cracking) [61]. Water's high dielectric constant can have a significant effect on over all radar performance by inducing shadows on radar images [62]. Thickness swelling can also attenuate transmitted waves and return echoes due to a change in electrical thickness. This is a result of electrical radome thickness being related to physical thickness, operating frequency, type of material, and type of design [63]. Moisture contaminated radome structures located on the tail of an aircraft can also be affected by the high temperature exhaust gases emitted (~500°C) from turbofan [64] and turbojet engines [65]. Moreover, at X-band frequency, the accumulation of rain

and ice on a radome surface will also have a pernicious effect on the received and transmitted signals beyond the attenuation of its dry counterpart [66] . As moisture being absorbed begins to freeze, accumulation of ice increases on the surface of the radome structure. Morgan et al. have reported that as ice increases, the flashover voltage due to lightning strikes increased by a factor of about 2 to 3 [67]. Lightning plasma pathways can generate a current of up to 200 kA. This type of discharge on a non-conducting polymer composite can generate joule heating and high temperatures. Resistive heating can induce delamination and fiber breakdown/sublimation (sublimation for a carbon fiber is at a temperature of about 3300 °C) [68]. The Federal Aviation Administration (FAA) reports that radomes usually have conductive lightning protection strips bonded to their surface to dissipate the electrical energy of lightning, but strip failure may occur causing high temperature resistance and shorts [62]. The highest probability of lightning strike events takes place during the climb and descent phase in the presence of moisture, and occur on radome, nacelles, wingtips, and horizontal stabilizers tips [69] (all possible locations for BMI composites).

The regulations set by the FAA, RTCA/DO-213 proposed by governmental experts, industry, and military give basic requirements of low dielectric properties and structural stability that can be found to be short and non-specific regarding issues of allowable moisture ingress and dielectric performance [63, 70, 71] in regards to radome structures. For example, the FAA states that a radome should allow radar signals to be transmitted with minimal distortion and that holes, regardless of size, can be detrimental due to moisture absorption. NATO's Advisory Group for Aerospace Research and Development (AGARD) published an advisory report regarding suitable radome material for avionic

systems that provides guidance to better asses environmental degradation on aircraft composites [53]. In this report, test methods to evaluate dielectric, moisture absorption, and flexural properties include a resonant cavity method, ASTM D570, and ASTM D790 respectively. The aforementioned guidance and past research in the environmental degradation of BMI/quartz and its composites is of crucial importance to the estimation of service life, maintenance, cost, and the prevention of catastrophic events.

The research performed on the BMI/quartz radome composite in this thesis focuses on circumstances in which the polymeric material could fail that would otherwise have not been identified or tested in the certification process, as a direct result of moisture ingress. For this reason, the characterization of BMI/quartz systems is concerned with the moisture diffusion kinetics and its effects on the dielectric, viscoelastic and flexural properties. ASTM standards D790 [72] (flexure), D5229 [73] (moisture absorption), D7028 [74] (viscoelastic properties), and a resonant cavity method [75] were used to evaluate material performance. The synergistic effects of elevated temperature and moisture content were also investigated to address their cumulative effect on the long-term service life of the radome composite. Furthermore, in regards to the combined moisture/elevated temperature coupling, it was found that the sensitivity of the DMA to the fiber-matrix interface can be used as an advantageous tool to evaluate debonding.

1.4 Modeling Moisture Diffusion in BMI/quartz Specimen

Mathematical modeling of diffusion in polymer composite systems is of critical importance in order to predict the extent of degradation as a result of moisture ingress and to identify diffusion mechanisms. Therefore, accurate prediction of moisture content at a specified time within polymeric composites must be known in order to assess structure

failure over time. Fick in 1855 [76] laid down one of the first significant investigation of moisture diffusion in a solid. The Fickian absorption model still is being widely used in polymer composites [28, 30, 77, 78]. The most frequently used is the one-dimensional case, which is based on Fick's second law and its commonality emerges from the ASTM D30 committee recommendations for characterization of moisture uptake. This is outlined in the ASTM D5229 [73]. Moisture ingress in this model occurs through a semi-infinite plate and diffusion through the edges is neglected. The concentration profile is governed by the equation

$$\frac{\partial c}{\partial t} = D_z \frac{\partial^2 c}{\partial z^2} \tag{1}$$

A dry plane sheet with a thickness of h exposed to moisture on both sides is assumed, with initial and boundary conditions (for all t) given respectively by,

$$c(z,0) = 0 \ \text{ for } \ |z| < \frac{h}{2}$$
$$c\left(\frac{h}{2}, t\right) = c\left(-\frac{h}{2}, t\right) = c_\infty \tag{2}$$

In these equations, c is the moisture concentration, c_∞ is the moisture equilibrium concentration, D_z is the diffusion coefficient, t describes time, and z is a spatial coordinate. Solving Fick's Second Law with the given boundary and initial conditions gives the following solution

$$c(z,t) = c_\infty - 4\frac{c_\infty}{\pi}\sum_{p=0}^{\infty}\frac{(-1)^p}{(2p+1)}\cos\left(\frac{\pi(2p+1)}{h}z\right) \times e\left[-\left(\frac{\pi(2p+1)}{h}\right)^2 D_z t\right] \quad (3)$$

Integration of Equation (3) over the surface and time yields the mass gain function for the one-dimensional Fickian absorption

$$M(t)_F = M_\infty - \frac{8M_\infty}{\pi^2}\sum_{p=0}^{\infty}\frac{1}{(2p+1)^2}e^{-\pi^2 t\left(\frac{D_z(2p+1)^2}{h^2}\right)} \quad (4)$$

Here $M(t)_F$ is the percent mass gain of the specimen and describes the total mass entering as a function of time. M_∞ is the equilibrium percent mass content. The diffusion directions, geometry, and coordinate system described in the predictive model used are demonstrated in Figure 7.

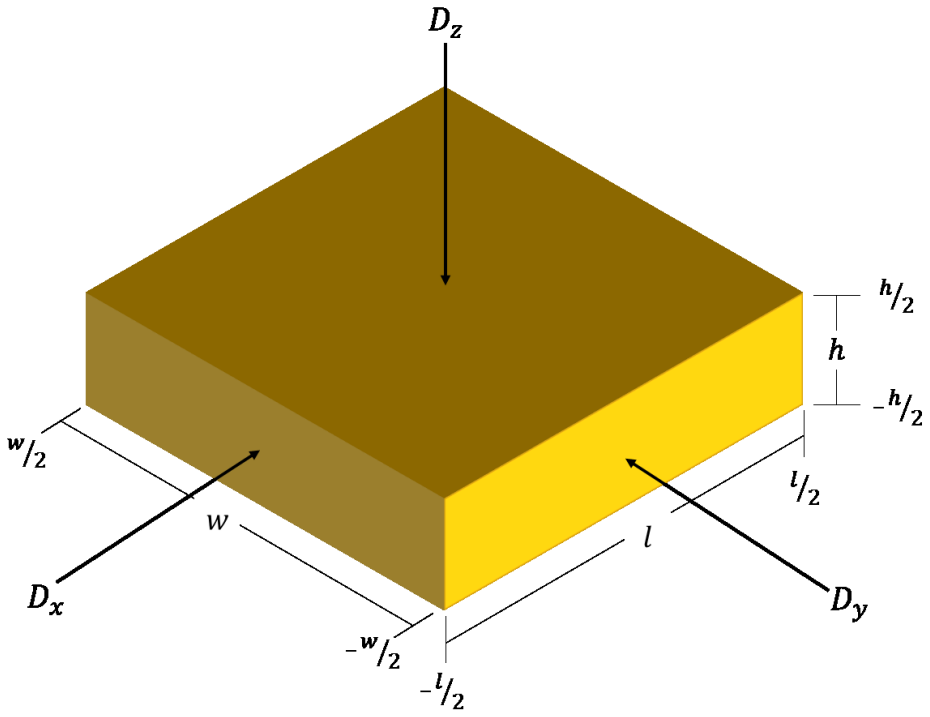

Figure 7. Dimensions and diffusion coordinates of predictive models

In 1976, Shen and Springer [79] proposed an edge correction to account for diffusion through the edges of a thin plate. The correction is described by

$$D_{EC} = D_z\left(1 + \frac{h}{l} + \frac{h}{w}\right)^{-2} \tag{5}$$

where h and l are the height and width of the plate, respectively. Furthermore, since D_z, initially varies linearly with the square root of time, the coefficient can be written as,

$$D_z = \pi\left[\left(\frac{M_2 - M_1}{\sqrt{t_2} - \sqrt{t_1}}\right)\frac{h}{4M_\infty}\right]^2 \tag{6}$$

In Equation (6), the slope is used with corresponding coordinates of $\left(\sqrt{t}_1, M_1\right)$ and $\left(\sqrt{t}_2, M_2\right)$. These points are located on the initial linear portion of the uptake curve and the subscripts 1 and 2 describe initial and secondary points.

Fick's Second Law is beneficial when characterizing moisture ingress through the thickness of a single-phase, semi-infinite, thin solid plate. However, there have been many cases where non-Fickian behavior has been noticed in polymeric systems [31, 47, 48, 80-84]. The varying degree of absorption behavior often necessitates the utilization of non-linear models. Among these are the time-varying diffusivity model [85] (variation in diffusion coefficient with temperature represented as a time dependent function), a dual-diffusivity model [86] (takes into account the two-phases of the composite), a coupled diffusion relaxation model [87, 88] (net moisture is separated by diffusion controlled and polymer relaxation controlled), and the dual-mode sorption model or the "Langmuir-type" [89] (accounts for the modes of penetrant interaction within the medium). Although the one-dimensional Fickian and non-Fickian based models may be valid in some cases, significant error can be introduced from a high degree of material anisotropy, finite dimension of composite specimen, and hindrance of moisture in the composite network. Anisotropy in polymeric laminated composites is of much importance in moisture diffusion when comparing diffusivity in the direction along the fibers and the bulk diffusivity in all other directions [77]. Diffusivity due to capillary action along the fiber direction is expected to be significantly higher, which may result in higher absorption rates across the side surfaces of the laminates, even with a thin laminate. Furthermore, the effect of micropores [90], mechanical loading [91], and chemical interactions between the diffusant and polymer [92] have been reported to hinder diffusion. Therefore, in an effort to reduce

error, Grace and Altan [93, 94] have developed a three-dimensional hindered diffusion model (3D HDM) that considers anisotropic diffusion and polymer penetrant (physical and chemical) interactions. The 3D HDM stems from the non-Fickian absorption behavior of the one-dimensional "Langmuir-type" model proposed by Carter and Kibler [89]. This model assumes polymer-penetrant interaction between both polar water molecules and polar molecular groups of the polymer resin. It does this by adding an additional term of sources and sinks to the one-dimensional Fickian model. The nature of this addition can be described by the probabilities of bound molecules becoming mobile and mobile molecules becoming bound. The one-dimensional Langmuir coupled expressions that are satisfied by a concentration at a position z and a time t are given by

$$D_z \frac{\partial^2 n}{\partial z^2} = \frac{\partial n}{\partial t} + \frac{\partial N}{\partial t}$$
$$\frac{\partial N}{\partial t} = \gamma n - \beta N \tag{7}$$

The number of mobile molecules per unit volume are represented by n and the number of bound molecules per unit volume are represented by N. The probability per unit time that a bound molecule will become mobile is β and the probability per unit time that a mobile molecule will become bound is γ. Equilibrium is expressed by ∞, and is reached when the following relation is attained

$$\gamma n_\infty = \beta N_\infty \tag{8}$$

The relations describe a dry slab of thickness h exposed to constant moisture on both sides with the initial and boundary conditions (for all t) being

$$n(z,0) = 0,\ N(z,0) = 0 \quad \text{for } |z| < \frac{h}{2}$$
$$n\left(\frac{h}{2},t\right) = n\left(-\frac{h}{2},t\right) = n_\infty \tag{9}$$

Exact solutions for the spatial distribution of bound and mobile molecules are obtained via Laplace transforms and contour integration [89]. The solution for bound molecules is described by

$$N(z,t) = n_\infty \frac{\gamma}{\beta}\left\{1 - \frac{4}{\pi}\sum_{p=1}^{\infty(odd)} \frac{(-1)^{\frac{p-1}{2}}}{p\left(r_p^+ - r_p^-\right)} \times \left[r_p^+ e^{\left(-r_p^- t\right)} - r_p^- e^{\left(-r_p^+ t\right)}\right]\cos\frac{p\pi z}{h}\right\} \tag{10}$$

where,

$$r_p^\pm = \frac{1}{2}\left[(kp^2 + \gamma + \beta) \pm \sqrt{(kp^2 + \gamma + \beta)^2 - 4k\beta p^2}\right] \tag{11}$$

and

$$k = \frac{\pi^2 D_z}{h^2} \tag{12}$$

Here the parameter k determines the rate of saturation. The solution for the mobile molecules is given by

$$n(z,t) = n_\infty \left\{ 1 - \frac{4}{\pi} \sum_{p=1}^{\infty(odd)} \frac{(-1)^{\frac{p-1}{2}}}{p\left(r_p^+ - r_p^-\right)} \times \left[r_p^+ e^{\left(-r_p^- t\right)} - r_p^- e^{\left(-r_p^+ t\right)} \right] \cos\frac{p\pi z}{h} \right\} + n_\infty \frac{4}{\pi\beta} \sum_{p=1}^{\infty(odd)} \frac{(-1)^{\frac{p-1}{2}}}{p\left(r_p^+ - r_p^-\right)} r_p^+ r_p^- \left[e^{\left(-r_p^- t\right)} - e^{\left(-r_p^+ t\right)} \right] \cos\frac{p\pi z}{h} \tag{13}$$

Integration of the exact solution over a laminate thickness h results in the total moisture content of the Langmuir model, $M(t)_L$, at time t.

$$M(t)_L = M_\infty \left\{ 1 - \frac{8}{\pi^2} \sum_{p=1}^{\infty(odd)} \frac{r_p^+ e^{\left(-r_p^- t\right)} - r_p^- e^{\left(-r_p^+ t\right)}}{p^2\left(r_p^+ - r_p^-\right)} + \frac{8}{\pi^2}\left(\frac{k\beta}{\gamma+\beta}\right) \sum_{p=1}^{\infty(odd)} \frac{e^{\left(-r_p^- t\right)} - e^{\left(-r_p^+ t\right)}}{\left(r_p^+ - r_p^-\right)} \right\} \tag{14}$$

In Equation (14), M_∞ is the moisture equilibrium content. It should be noted that in polymer composites, $k \ll \gamma$ and β. Therefore, when k is large, a judicious approximation is given by

$$M(t)_L = \frac{\beta}{\gamma+\beta} M_\infty \left(1 - \frac{8}{\pi^2}\sum_{p=0}^{\infty} \frac{1}{(2p+1)^2} e^{-\pi^2 t\left(D_z \frac{(2p+1)^2}{h^2}\right)}\right) + M_\infty \left(1 - \frac{\gamma}{\gamma+\beta} e^{-\beta t} - \frac{\beta}{\gamma+\beta}\right) \tag{15}$$

Further simplification of $M(t)_L$ leads to

$$M(t)_L = \mu M_\infty (M(t)_F) + (1-\mu)\left(1 - e^{-\beta t}\right) \tag{16}$$

where

$$\mu = \frac{\beta}{\gamma+\beta} \tag{17}$$

The parameter μ is the hindrance coefficient and it governs diffusion hindrance as a result of chemical and physical interaction [94]. This dimensionless coefficient varies from 0 to 1 and it shows the important relationship between γ and β. Therefore, as mobile molecules enter a polymer composite, the rate of change will be varied over time. Also, it can be observed that Equation (16) is a linear superposition of the one-dimensional Fickian and "Langmuir-type" models.

A similar approach was taken to arrive at an analytical solution for the 3D HDM. The coupled pair of partial differential equations that are satisfied by a moisture content at a time t and spatial positions x, y, and z are given by

$$D_x \frac{\partial^2 n}{\partial x^2} + D_y \frac{\partial^2 n}{\partial y^2} + D_z \frac{\partial^2 n}{\partial z^2} = \frac{\partial n}{\partial t} + \frac{\partial N}{\partial t}$$

$$\frac{\partial N}{\partial t} = \gamma n - \beta N \tag{18}$$

where D_x, D_y, and D_z are the diffusion coefficients in the x, y, and z directions. The auxiliary initial and boundary conditions (for all t) for a dry laminate of thickness h, width w, and length l are

$$n(x,y,z,0) = 0,\ N(x,y,z,0) = 0 \ \text{ for } \ |x| < \tfrac{l}{2},\ |y| < \tfrac{w}{2},\ |z| < \tfrac{h}{2} \tag{19}$$

$$\begin{aligned} n\left(x,y,\frac{h}{2},t\right) &= n\left(x,y,-\frac{h}{2},t\right) = n_\infty \\ n\left(x,\frac{w}{2},z,t\right) &= n\left(x,-\frac{w}{2},z,t\right) = n_\infty \\ n\left(\frac{l}{2},y,z,t\right) &= n\left(-\frac{l}{2},y,z,t\right) = n_\infty \end{aligned} \tag{20}$$

The solution for the 3D HDM is not invertible by means of Laplace transforms as its one-dimensional version is. Therefore, Grace [51] outlined the moisture concentration profile in the three-dimensional anisotropic model by the use of the forward-time, centered-space finite difference (FTCS) scheme. The numerical inversion method has been previously used to successfully model moisture diffusion, for over 5 years, in BMI/quartz specimens [52]. It should be noted that one can arrive at an approximation of the 3D HDM via the

three-dimensional Fickian mass gain function. The anisotropic three-dimensional Fickian model outlined by Aktas [77] is described by

$$D_x \frac{\partial^2 n}{\partial x^2} + D_y \frac{\partial^2 n}{\partial y^2} + D_z \frac{\partial^2 n}{\partial z^2} = \frac{\partial n}{\partial t} \tag{21}$$

where the initial and boundary conditions (for all t) for a dry laminate of thickness h, width w, and length l are

$$n(x, y, z, 0) = 0 \text{ for } |x| < \frac{l}{2},\ |y| < \frac{w}{2},\ |z| < \frac{h}{2} \tag{22}$$

$$\begin{aligned} n\left(x, y, \frac{h}{2}, t\right) &= n\left(x, y, -\frac{h}{2}, t\right) = n_\infty \\ n\left(x, \frac{w}{2}, z, t\right) &= n\left(x, -\frac{w}{2}, z, t\right) = n_\infty \\ n\left(\frac{l}{2}, y, z, t\right) &= n\left(-\frac{l}{2}, y, z, t\right) = n_\infty \end{aligned} \tag{23}$$

The solution for spatial concentration in a laminate is given by

$$
\begin{aligned}
&n(x,y,z,t) \\
&\quad = n_\infty \left(1 - \frac{64}{\pi^3} \sum_{p=0}^{\infty} \sum_{q=0}^{\infty} \sum_{r=0}^{\infty} \frac{(-1)^{p+q+r}}{(2p+1)(2q+1)(2r+1)} \right. \\
&\quad \times \cos\frac{(2p+1)\pi z}{h} \cos\frac{(2q+1)\pi y}{w} \cos\frac{(2r+1)\pi x}{l} \\
&\quad \left. \times e^{-\alpha_{p,q,r} t} \right)
\end{aligned}
\tag{24}
$$

where

$$
\alpha_{p,q,r} = \pi^2 \left(\frac{D_z (2p+1)^2}{h^2} + \frac{D_y (2q+1)^2}{w^2} + \frac{D_x (2r+1)^2}{l^2} \right) \tag{25}
$$

Integration was performed to find, $M(t)_{3DF}$, the percent mass gain equation for the three-dimensional Fickian model,

$$
\begin{aligned}
M(t)_{3DF} = M_\infty \left(1 - \frac{512}{\pi^6} \sum_{p=0}^{\infty} \sum_{q=0}^{\infty} \sum_{r=0}^{\infty} \frac{1}{(2p+1)^2 (2q+1)^2 (2r+1)^2} \times \right. \\
\left. \times e^{-t\pi^2 \left(\frac{D_z (2p+1)^2}{h^2} + \frac{D_y (2q+1)^2}{w^2} + \frac{D_x (2r+1)^2}{l^2} \right)} \right)
\end{aligned}
\tag{26}
$$

As in Equation (16) Grace [94] concludes that the 3D HDM can be approximated by a linear superposition of the three-dimensional Fickian mass gain function and the

"Langmuir-type" model when $k \ll \gamma$ and β. Hence, the 3D HDM analytical mass gain function can be given by

$$M(t)_{3DHDM} = \mu M_{\infty}(M(t)_{3DF}) + (1-\mu)\left(1 - e^{-\beta t}\right) \tag{27}$$

CHAPTER 2: Dielectric Property Degradation and Reversibility of BMI/quartz Specimens

2.1 Dielectric Property Degradation

The purpose of an aircraft radome is to protect its constituent radar system while sustaining structural integrity and maintaining minimum transmission loss. Toward that end, polymers and their composites have gained favorability in radome construction as a result of their high strength to weight ratio [95], thermo-resistivity [13] and low dielectric properties [78]. Most significantly is the sustainability of the material's dielectric properties, which include relative permittivity and loss tangent. The relative permittivity of a material is the ability of the material to store electrostatic energy in an applied electric field and the loss tangent is a measure of dissipated energy through induction or conversion into thermal energy [96]. Low relative permittivity and loss tangent allows transparency to electromagnetic waves at the operating frequency of the radar antenna. Therefore, changes to a material as a result of operational environment can induce degradation in antenna performance and accuracy. In the service life of an aircraft, damage to a radome can result in the form of object impact and environmental effects. The most widespread and damaging source of degradation to polymer composite radomes is moisture contamination. Moisture's ubiquitous nature and the propensity of a composite to absorb it is of paramount importance to the protective radar structure. Assessment of the deleterious effects of moisture ingress on the mechanical properties of fiber-reinforced composites has garnered much focus throughout several decades of research [45, 56, 97, 98]. In contrast, quantifying and assessing dielectric property degradation as a result of

absorbed moisture has not received equivalent attention, though some studies have been performed [99-101]. During rainfall on stationary radomes, transmission loss and degradation of dielectric constant has been observed in the presence of water on the structure's surface [102, 103]. During aircraft operation, rainfall is not of great concern to signal transmission as a result of airflow during flight and the beading of water around the radome structure [19]. On the contrary, moisture absorption and its impact within the polymer composite network is not extensively understood in regards to radar wave transmission. Although there is a lack in literature, it has been observed that even a small amount of absorbed water can have a significant effect on the transmitted signal [104]. It is well known that changes to signal transmittance and absorption are directly correlated to moisture content inside the composite structure. Accuracy in prediction is of crucial importance when classifying the degree of signal attenuation. In the BMI/quartz composite, deviation from Fickian diffusion has been reported based on the (free and bound) water polymer interaction [40] with excellent accuracy. Furthermore, the non-linear onset of dielectric constant degradation with respect to moisture content has been observed to correspond to the onset of pseudo-equilibrium of the BMI composite [19]. The latter relation theorizes on the bound and free water molecule states during the absorption process.

The focus of this chapter is twofold. Primarily the goal is to report on the dielectric effects of aircraft contaminants contained within the polymer network. Although precipitation is known to produce a thin film of water on the surface of the radome, contributing to transmission loss [105], the effects of contaminants within the polymer are much more permanent than losses associated with precipitation-induced surface films.

Secondly, this study provides a more thorough understanding of the magnitude and reversibility of dielectric property changes as a result of water absorption within the fiber-reinforced polymer network. A comparison of water uptake and reversibility of dielectric properties is made to two readily used aircraft radome composites to further comprehend the degradation occurring in the BMI composite. To the best of our knowledge, this work represents the first investigation into the dielectric properties of BMI/quartz exposed to typical aerospace fluids.

2.2 Materials, Machining and Moisture Measurements

2.2.1 Aerospace Fluids Absorption in BMI/quartz

The material under investigation is a three-ply bismaleimide resin reinforced with an eight-harness satin weave quartz fabric. Fifteen samples, shown in Figure 8, were cut by the wet diamond saw in Figure 9. The cutting method is the typical machining method for this type of composite material. Specimen dimensions were cut to 63.5 x 63.5 mm and thicknesses of 0.755 mm.

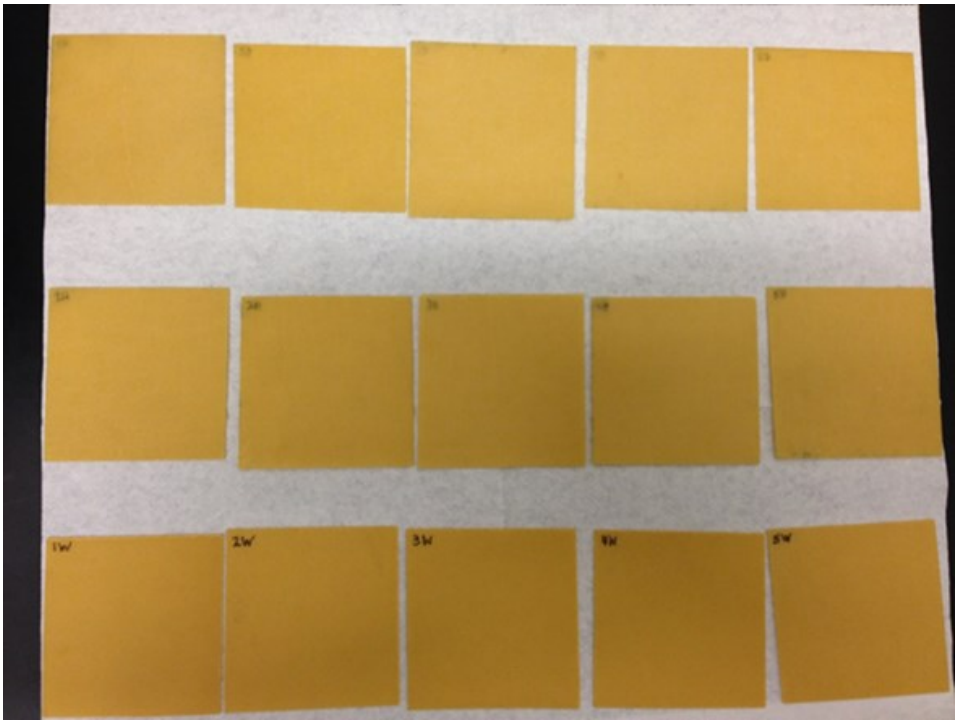

Figure 8. BMI/quartz specimen for dielectric analysis

Figure 9. Diamond saw

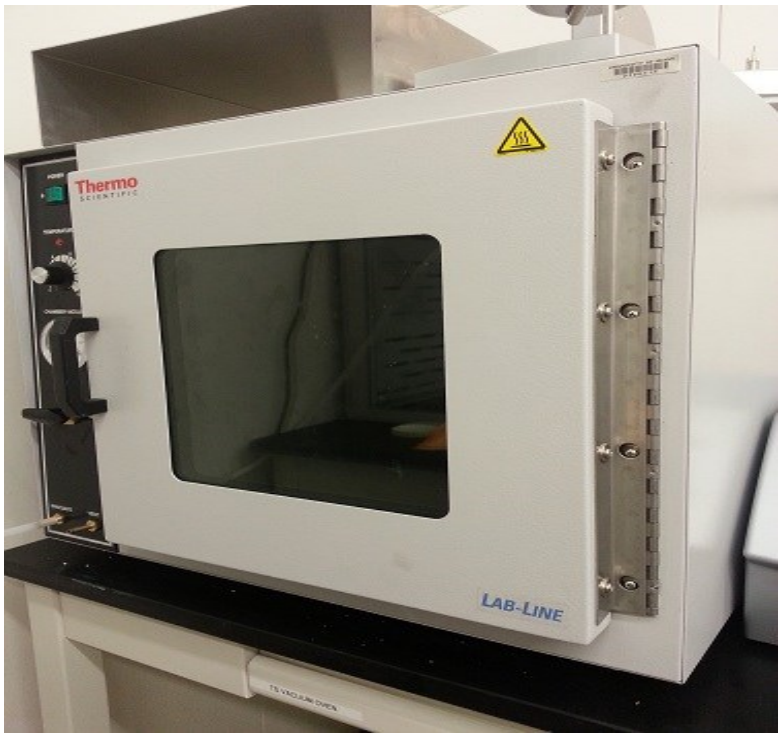

Figure 10. Vacuum oven

Figure 11. Aerospace contaminants

Samples were dried at 80°C by vacuum oven in Figure 10 and stored in a desiccator in order to remove all residual moisture. After removal from oven and desiccator, dry samples were weighed and measurements were recorded. Figure 11 shows propylene glycol, deicing fluid, and distilled water as the aerospace contaminants used in this study. Five samples were then fully immersed in each fluid type. Propylene glycol in this study represents the pure form of a common component in some types of deicing fluid. The deicing contaminant used is commercially available under the trade name TKS Anti-Icing De-Icing Fluid, and is composed of 85-95 wt. % ethylene glycol, 0-5 wt. % isopropanol, and 0-10 wt. % water [106]. After samples were fully immersed in each respective fluid (Figure 12), they were maintained at 25°C in a constant temperature water bath (Figure 12).

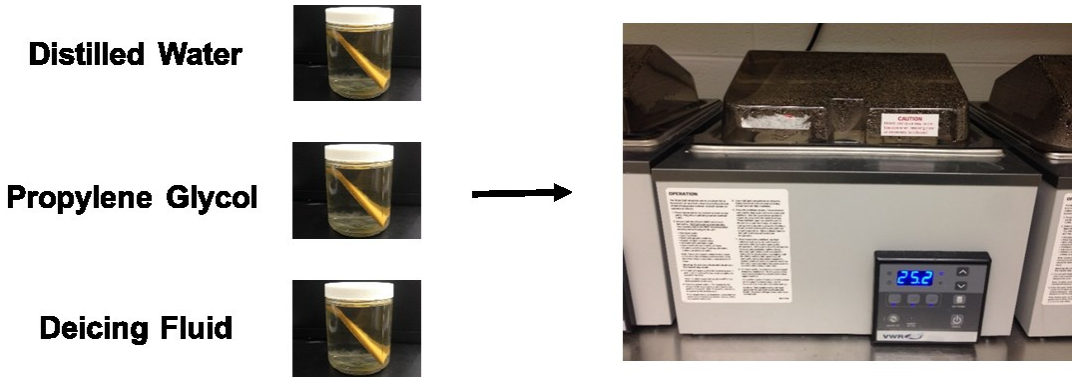

Figure 12. Full immersion in constant-temperature water bath

Gravimetric weight gain data was periodically recorded using a high precision analytical balance according to ASTM D5229 [73], as the average percent moisture content, $M\%$, given by

$$M\% = \frac{W_i - W_o}{W_o} \tag{28}$$

Here, W_i is the current sample mass and W_o is the oven-dried sample mass. Upon removal for periodic weighing, samples were dried with a lint-free cloth in order to remove all surface fluid. Immediately, the gravimetric and dielectric data was recorded at 10 GHz. The documented data is an average of all five samples for each respective fluid, with an uncertainty level calculated using a 95% confidence interval.

2.2.2 BMI/quartz, Epoxy/7781, Epoxy/4180 and Distilled Water Absorption/Desorption Measurements

The polymeric composites used in the desorption study are a three-ply BMI resin reinforced with an eight-harness satin weave quartz fabric, a four-ply epoxy resin reinforced with a four-harness glass satin weave (Style 4180), and a similar four-ply epoxy resin reinforced with an eight-harness glass satin weave (Style 7781). The trade names for the BMI/quartz and the two epoxy systems are HexPly® F650 and Cycom 919®, respectively. The BMI composite is the same used in the previous section. Epoxy composites were autoclave-cured at 121 °C and 23 inHg vacuum for two hours. Five specimens each for BMI/quartz, 7781 style epoxy, and 4180 style epoxy with dimensions of 63.5 x 63.5 mm and thicknesses of 0.755, 0.866, 0.373 mm, respectively, were cut with a wet diamond saw, and are shown in Figure 13.

Figure 13. BMI/quartz (top), epoxy/7781 (middle), and epoxy/4180 (bottom) machined composites

The same procedure is repeated from section *2.2.1*, but it is presented here for a better insight of techniques used. Specimens were dried at 80 °C and stored in a desiccator. Samples were then weighed and the dry weight was recorded. Composite specimens were under full immersion in water and maintained in a constant temperature water bath at 25 °C for nearly four months. Upon removal for periodic weighing, samples were dried with a lint-free cloth to remove all surface water. Gravimetric weight gain data during moisture uptake was periodically recorded using a high precision analytical balance according to ASTM D5229 [73]. Immediately following weighing, sample dielectrics were analyzed at 10 GHz. Following the monitoring of dielectric property loss during the absorption phase, desorption was performed in an oven at 50 °C and gravimetric data was recorded periodically until the initial sample weight stabilized, indicating the absence of absorbed

water. Dielectric measurements during desorption were performed in the same manner as the absorption process. The dielectric data recorded is an average of all five samples for each material type, with an uncertainty level calculated using a 95% confidence interval.

2.3 Dielectric Property Theory and Equipment

Relative permittivity and loss tangent are important factors that determine the performance of a radome structure. These parameters are part of or can be derived from the complex permittivity, ε^*, which is shown by

$$\varepsilon^* = \varepsilon_o(\varepsilon' - j\varepsilon'') \tag{29}$$

Here, ε_o, ε', and ε'' are the permittivity of free space, the relative permittivity (dielectric constant), and the loss factor respectively. The ratio of energy lost per energy stored per cycle of an alternating electromagnetic wave is the loss tangent, which is given by

$$\tan\delta = \frac{\varepsilon''}{\varepsilon'} \tag{30}$$

The analysis of measuring dielectric properties was performed with the aid of a split-post dielectric resonator (SPDR) manufactured by QWED© of Warsaw, Poland. The device is linked to an Agilent Programmable Network Vector Analyzer (PNA). The SPDR is shown schematically in Figure 14 and the PNA coupled to the resonator is shown in Figure 15. SPDR devices are capable of measuring the relative permittivity (dielectric constant) and loss tangent of a material at a range of 1 to 20 GHz [107]. To be applicable to aircraft

radome materials, the frequency used was 10 GHz. This frequency is the middle of X-band frequency (8-12 GHz), which is common to aircraft radar systems. Composites utilized in the suitable frequency range should have a thickness that is uniform and less than the 1 mm air gap in the SPDR in order for dielectric properties to be accurately measured [75]. When a material sample is placed between two dielectric resonators inside a metallic enclosure, an azimuthal evanescent electric field is generated between the gap of the resonator [108]. The electric field in the resonator is parallel to the surface of the sample, thus creating a continuous electric field on the dielectric surface [75]. The resultant variations in power loss of the system (Q factor) and resonant frequency of the cavity in response to the presence of the sample were used to calculate the dielectric constant and loss tangent of the material at 10 GHz.

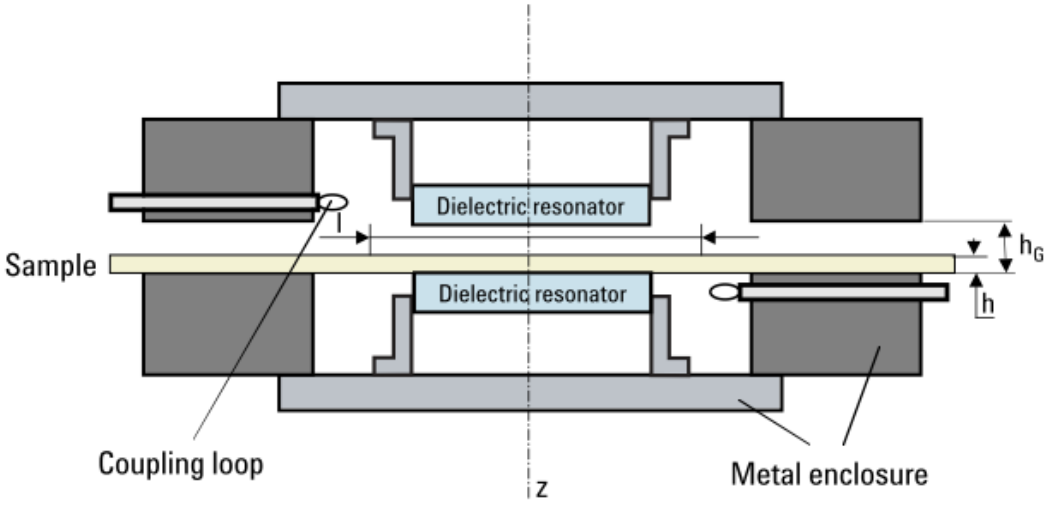

Figure 14. Split-Post dielectric resonator cross-section [75]

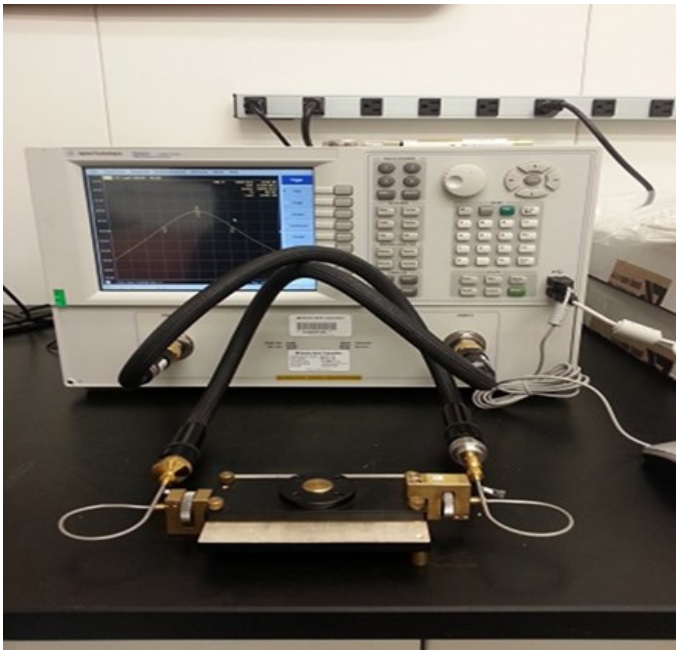

Figure 15. Network vector analyzer coupled with SPDR

The Rayleigh-Ritz iterative based solution [107] is used to determine dielectric properties of absorbed laminates with and without contaminant. This solution is based on the resonant frequency of the empty resonator shift produced by the sample. The real part of permittivity, ε', in this device is calculated by the iterative function [108],

$$\varepsilon' = 1 + \frac{f_o - f_s}{h f_o K_{\varepsilon'}(\varepsilon', h)} \tag{31}$$

where f_0 is the resonant frequency of the empty resonator, f_s is the resonant frequency with the sample inside the resonator, h the is thickness of the sample, and $K_{\varepsilon'}$ is a function of ε' and h that is calculated for every distinct resonator. Loss tangent can be determined from

$$\tan\delta = \frac{Q_U^{-1} - Q_{DR}^{-1} - Q_C^{-1}}{P_{es}} \quad (32)$$

where Q_U is the unloaded Q factor of the inner section of the resonator that contains the sample, Q_{DR} is the Q factor due to the dielectric losses of the resonator, Q_C is the Q factor that depends on the metal losses of the inner section of the resonator containing the specimen, and P_{es} is the electric energy filling factor. The latter parameter is a ratio of the electric energy stored in the specimen to the electric energy stored in the resonator [108]. The split-post resonator method is an already well established technique for measuring the complex permittivity of dielectric laminar materials, including fused silica, ferrite, low-loss isotropic dielectrics, and low loss anisotropic dielectrics [109-114]. Providing that the thickness of the sample under analysis is measured with an accuracy of $\pm$ 0.7% or better, the uncertainty of the real part of the complex permittivity will be better than $\pm$ 1%. Typical loss tangent uncertainty is $\pm$ 0.5% with a resolution of 2 x 10^{-5}.

2.4 Dielectric Property Degradation Results and Discussion of Aerospace Fluid Absorption in BMI/quartz

The moisture uptake of three aerospace contaminants in three-ply BMI/quartz composites is illustrated in Figure 16. This figure represents the average moisture mass percent change of the BMI/quartz as a function of the square root of time. The 95% confidence interval is also plotted for all five samples with respect to distilled water, deicing fluid, and propylene glycol. Respectively, from the aforementioned fluids, it can be observed that water, propylene glycol, and deicing fluid achieved an average weight percent content of 1.31%, 4.28%, and 3.41% at approximately 1300 hours, accordingly. The expected equilibrium water content of the neat resin is 4.3% [10] and according to the

laminate properties given by the manufacturer, the equilibrium content of HexPly® F650 is approximately 1.38% [40]. However, as observed by Grace [52], equilibrium content for water has not been reached as moisture ingress continues at a slow rate. Propylene glycol has the greatest fluid uptake rate and has reached the highest fluid content by weight for the experimental time frame. The latter fluid was followed relatively close by deicing fluid, with distilled water having a significant lower pseudo-equilibrium than the other contaminants. Results in regards to the final moisture content for each fluid type have a similarity with their appropriate viscosity and molecular weight. Distilled water, propylene glycol, and deicing fluid have viscosities of 0.89 cP, 40.4 cP, and 16.1 cP [115], respectively. Molecular weights of the respective aforementioned fluids are 18 g/mol, 62 g/mol, and 76 g/mol. A pattern between viscosities, molecular weights, and moisture content (1300 hours) in the BMI composite is noticed, with water having the lowest of the three parameters and propylene glycol having the highest. It should be noted that the properties for deicing fluid used for viscosity, molecular weight, and dielectric properties are that of ethylene glycol, since it makes up about 85-95 wt.% of the total concentration. Contaminant physical properties are shown in Table 3.

Table 3. Physical properties of aerospace fluids

	Molecular Weight *(g/mol)*	**Viscosity** *(Cp)*	**Fluid Content at 1300 hr.** *(wt. %)*
Water	18	0.89	1.31
Propylene Glycol	76	40.4	4.28
Deicing Fluid	62	16.1	3.41

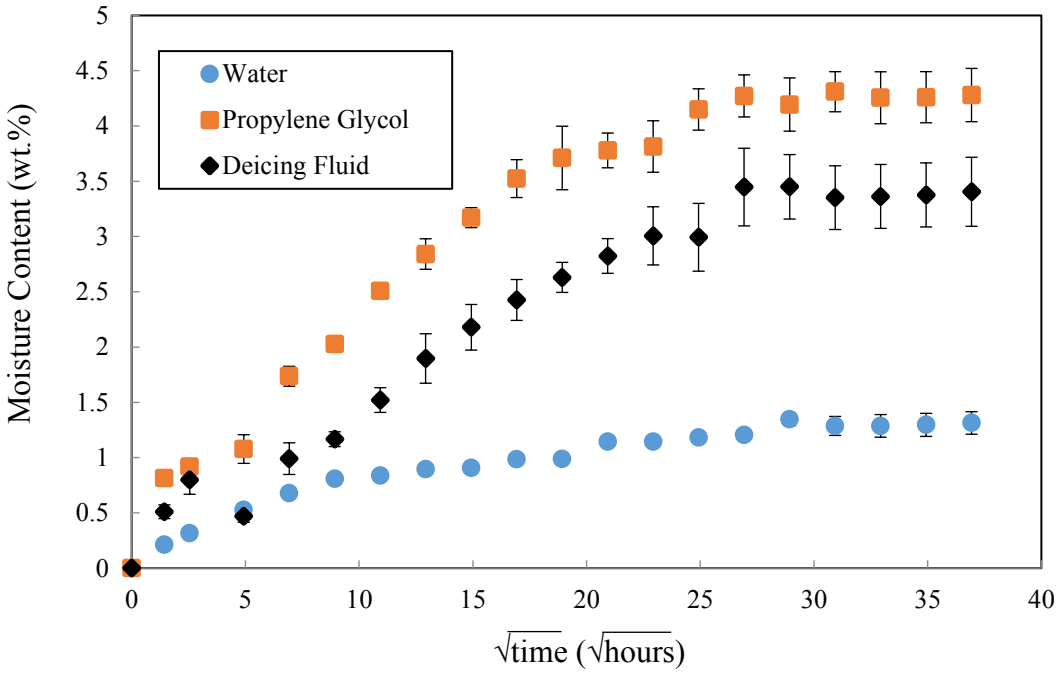

Figure 16. BMI/quartz aerospace contaminant absorption

In terms of relating dielectric properties of the composite to the fluids used, it is evident that the dielectric properties of the immersed specimens are related to the properties of each fluid. Therefore, the respective relative permittivity at 25°C and 10 GHz for water, propylene glycol, and deicing are 55, ~4.9, and ~5.5 respectively. Loss tangents for the same fluids at equivalent temperature and frequency are 0.54, ~0.71, and 0.78 [116, 117]. Figure 17 illustrate the changes in relative permittivity and Figure 18 shows changes in the loss tangent. The initial relative permittivity and loss tangent of the material was measured at 2.99 and 0.0041. A roughly linear relationship between dielectric properties and percent weight fluid content is observed for each fluid type until final immersion time. The presence of 1% fluid content for water, propylene glycol, and deicing fluid resulted in an

increase of 7.9%, 2.4%, and 4.4% in relative permittivity of the material, respectively. The final relative permittivity for the previously mentioned fluids is 3.31, 3.27, and 3.37 with respect to the moisture content at 1300 hours. Composite loss tangent is observed to be significantly affected by the aforementioned fluids. The existence of 1% contaminant content for water, propylene glycol, and deicing fluid contributed to a considerable increase of 379.8%, 326.2%, and 567.3% in loss tangent, correspondingly. Final loss tangents for the aforesaid contaminants are 0.0239, 0.0466, and 0.0710, respectively, at the maximum fluid content. Deicing fluid has the greatest overall effect on the relative permittivity and loss tangent of the material during the experimental time frame as a result of its relatively high fluid content by weight and corresponding dielectric properties.

To make more of a profound relationship between moisture ingress and dielectric degradation, the number of molecules were calculated with respect to molecular weight, moisture mass, and Avogadro's number (6.022×10^{23}) at moisture content of 1% and at 1300 hours of immersion. The latter is shown in Table 4 and Table 5, accordingly, with experimental results of dielectric properties of specimen with diffused contaminant and dielectric properties of contaminants at 25°C and 10 GHz. At 1% moisture content, it can be inferred that water's high relative permittivity and number of water molecules inside the composite produced the greatest permittivity increase in comparison to the other fluids. On the contrary, the ability of deicing fluid to predominantly degrade the material's dielectric properties can be explained via the fluid's physical and electrical properties. Although the deicing solution has an intermittent molecular weight, viscosity, and number of molecules (less than water but greater than propylene glycol), the cause of dissipative loss in Figure 18 is dependent on the electric dipole moment and molecule rotation in the BMI composite

[118]. Electric dipole rotation is provoked when an electric field induces a torque on the dipolar molecules. Consequently, the molecule will rotate to align itself with the electric field and if the field changes, so will the torque. Reorientation of the dipoles makes a contribution to the loss tangent in the form of friction. The electric dipole moments for distilled water, propylene glycol, and deicing fluid in the liquid phase are 3.00 D, 3.52 D, and 3.66 D [119, 120], respectively. Therefore, although propylene glycol had the greatest pseudo-equilibrium moisture content and water has a high relative permittivity, ethylene glycol's dominant dipole moment and number of molecules play a paramount role in the dielectric properties of the contaminated BMI/quartz composite.

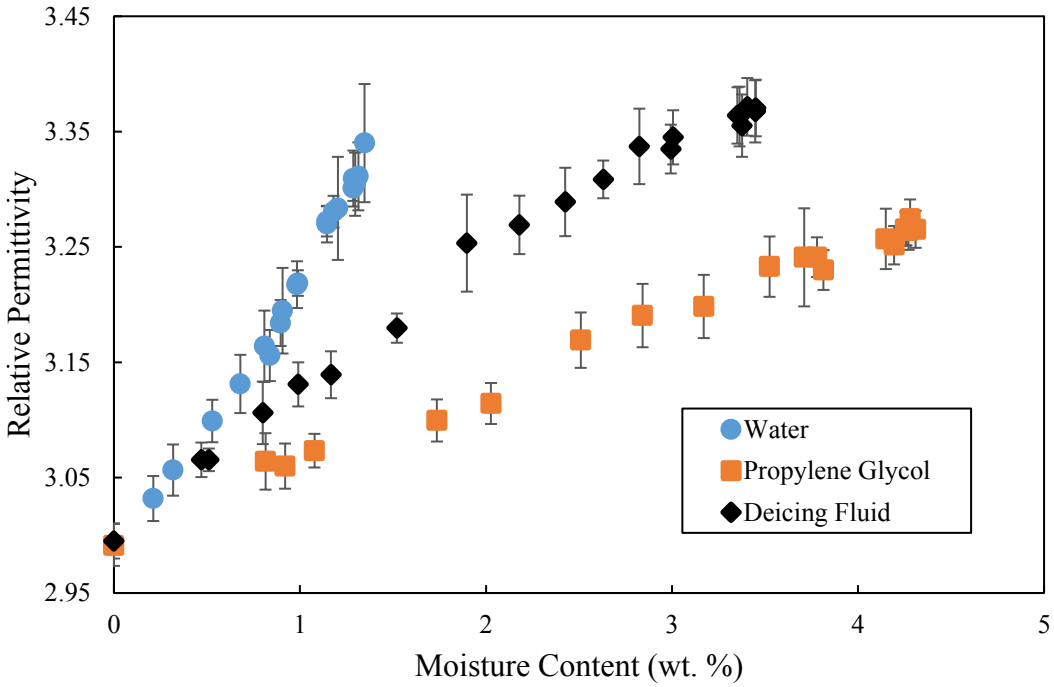

Figure 17. BMI/quartz relative permittivity with respect to absorbed aerospace contaminant volume

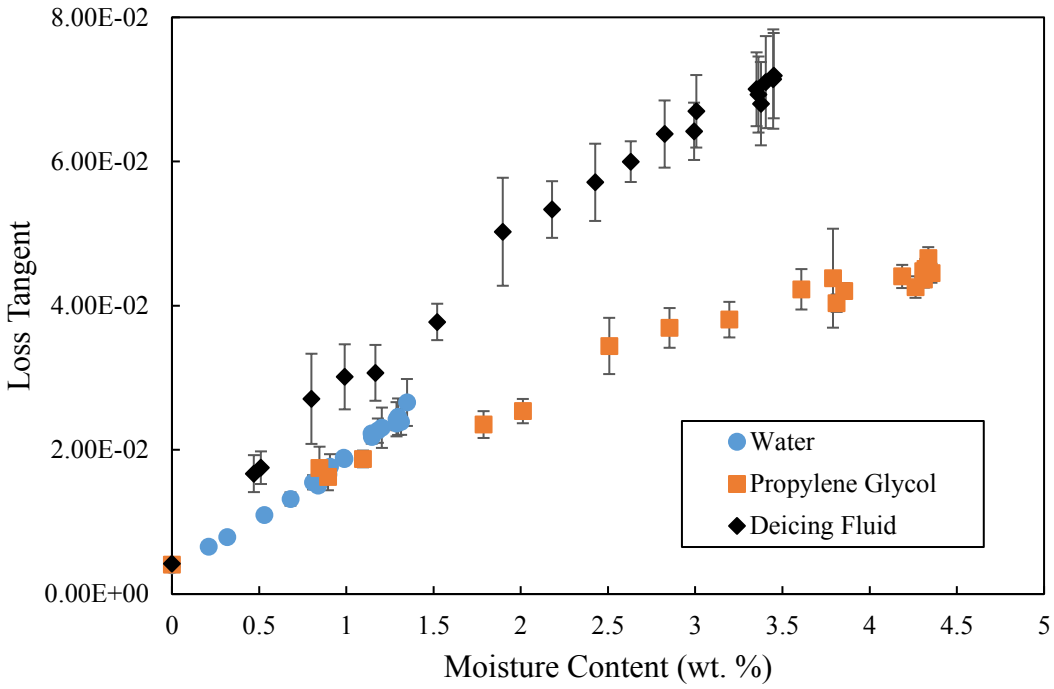

Figure 18. BMI/quartz loss tangent with respect to absorbed aerospace contaminant volume

Table 4. Number of molecules and dielectric properties at 1% fluid content with respect to dielectric properties of each contaminant at 25°C and 10 GHz

	ε' *25°C 10 GHz*	$tan\,\delta$ *25°C 10 GHz*	**Dipole Moment** *(Debye)*	ε' *(1 wt.%)*	$tan\,\delta$ *(1 wt.%)*	**Number of Molecules**
Water	55	0.54	3.00	3.23	0.0193	1.51E+23
Propylene Glycol	4.5	0.71	3.52	3.06	0.0174	3.61E+22
Deicing Fluid	7	0.78	3.66	3.13	0.0282	4.42E+22

Table 5. Number of molecules and dielectric properties at final fluid content with respect to dielectric properties of each contaminant at 25°C and 10 GHz

	ε' *25°C 10 GHz*	$tan\,\delta$ *25°C 10 GHz*	**Dipole Moment** *(Debye)*	ε' *(final)*	$tan\,\delta$ *(final)*	**Number of Molecules**
Water	55	0.54	3.00	3.31	0.0239	1.52E+23
Propylene Glycol	4.5	0.71	3.52	3.27	0.0466	3.72E+22
Deicing Fluid	7	0.78	3.66	3.37	0.071	4.53E+22

2.5 Moisture Uptake and Reversibility of BMI/quartz's Dielectric Degradation Compared to Epoxy/Glass Radome Composites: Results and Discussion

To develop a deeper understanding of the deleterious effects of moisture ingress in the BMI polymeric composite, specimen moisture uptake of distilled water is plotted up to 1300 hours, in Figure 19, against that of the epoxy/7781 style and epoxy/4180 style radome composites. Moisture uptake curves relatively demonstrate the significant level of free volume inside a three-ply bismaleimide specimen, which is attributed to the higher than typical void content of about 8% by volume [19]. Moisture contents, relative permittivity and loss tangents for each composite are shown in Table 6. As suspected in the BMI samples, such increase in moisture content had a substantial impact on the percent increase of dielectric properties, particularly in loss tangent. Figure 20 displays the linearity of relative permittivity and Figure 21 the loss tangent for all three material types. Despite BMI's increase in moisture content, its relative permittivity is remarkably the lowest out of the composites. The material loss tangent had a significant increase for all samples, but had the most deleterious effects on the BMI composite. The much larger relative increase of 495% in loss tangent for the BMI specimen is likely a result of the higher void content

in these samples, leading to a higher water content in the liquid, bulk phase. In an aircraft radar system the dipolar rotation as a result of electromagnetic wave transmission can induce shadow effects on radar screen leading to a decrease in performance.

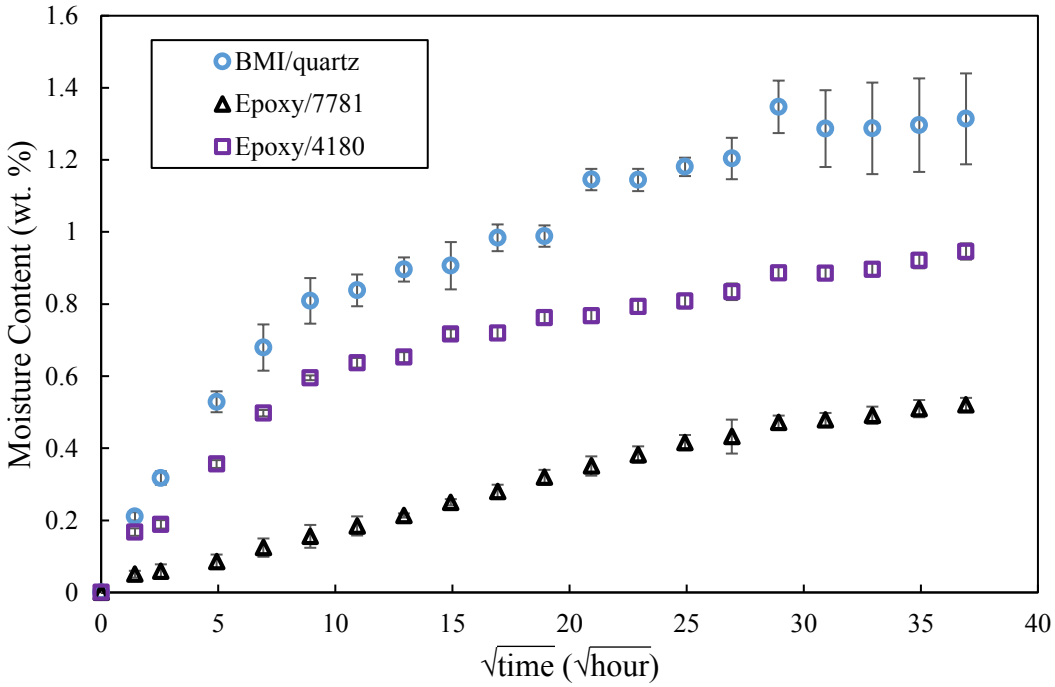

Figure 19. Moisture absorption of BMI and epoxy reinforced composites at 1300 hours of immersion

Table 6. BMI and epoxy composites final moisture content with corresponding dielectric properties

	Moisture Content *(wt. %)*	$\boldsymbol{\varepsilon'}$ *(% increase)*	$\boldsymbol{\tan\delta}$ *(% increase)*
BMI/quartz	1.31	10.7	495
Epoxy/7781	0.52	2.64	51.9
Epoxy/4180	0.95	5.64	84.6

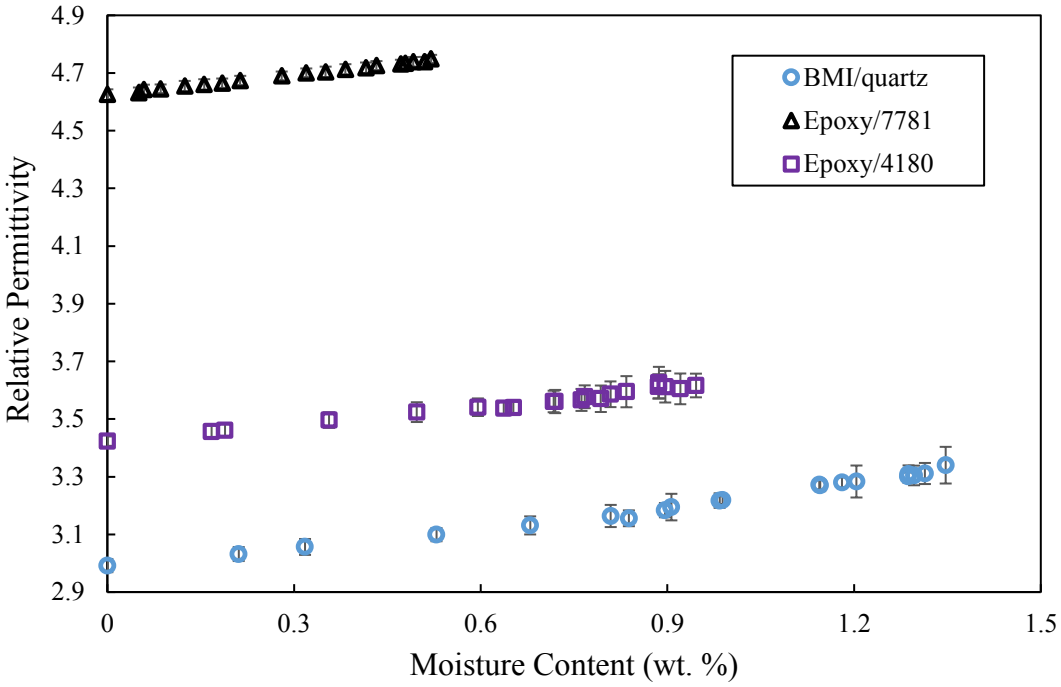

Figure 20. Relative permittivity of BMI and epoxy reinforced composites at 1300 hours of immersion

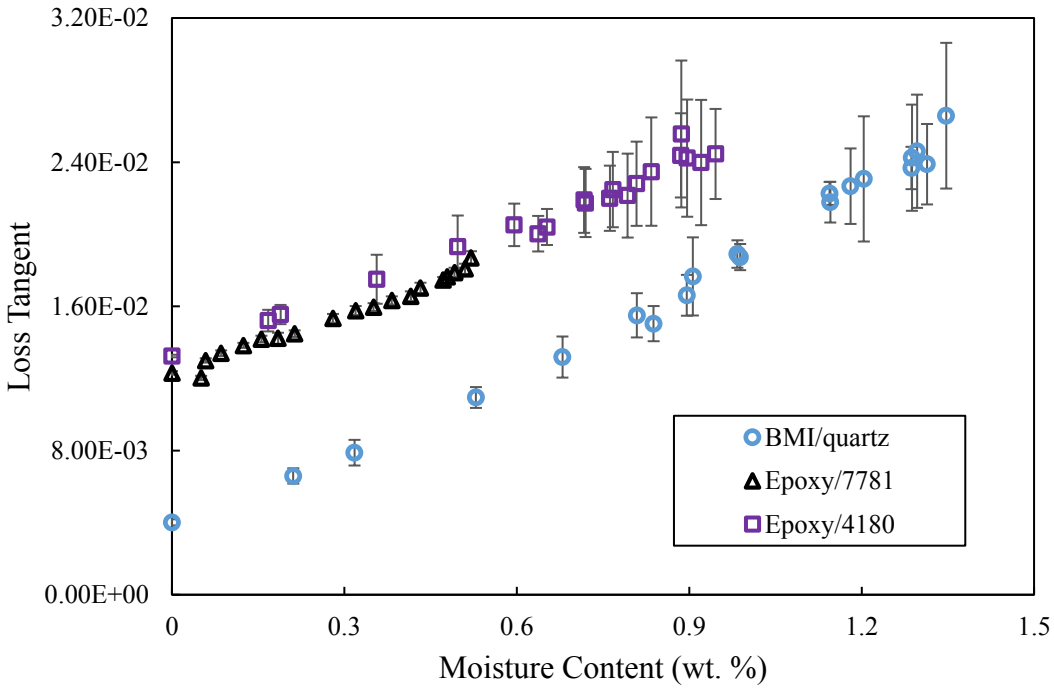

Figure 21. Loss tangent of BMI and epoxy reinforced composites at 1300 hours of immersion

The same composites were utilized to verify reversibility of dielectric properties by a simple method of drying. Although this method removed a considerable amount of moisture initially, the importance of this study is the recovery of the original dielectric characteristics. In order to simulate practical conditions, in which the time allowed for moisture desorption via moderate heating or vacuum conditions would be limited, desorption was terminated when the rate of weight loss for the samples decreased dramatically. As a result, the moisture content before absorption and after desorption are slightly different. This is indicative of a small amount of firmly bound water molecules still existing within the polymer network. Given enough time, it is expected that this moisture could also be removed. As such, dielectric constant and loss tangent is reported at the projection of the best fit line of the desorption data points. By this method, the difference in dielectric constant after desorption with respect to the initial absorption dielectric constant measurements was 0.144 % in the BMI/quartz samples, 0.084% in the style 7781 epoxy, and 0.003% in the style 4180 epoxy. Dielectric constant as a function of moisture content is shown in Figure 22, Figure 23, and Figure 24 for BMI/quartz, 7781 epoxy, and 4180 epoxy, accordingly. Moisture uptake in the aforementioned specimens resulted in a 4.66%, 3.35%, and 4.01% increase in dielectric constant for a 0.68%, 0.61%, and 0.72% increase in water content by weight, respectively. Loss tangent as a function of moisture content is shown in Figure 25, Figure 26, and Figure 27. The same water content responsible for the increase in dielectric constant is responsible for a 228%, 71.4%, and 64.1% increase in loss tangent for BMI/quartz, epoxy 7781 style, and epoxy 4180 style materials, respectively. In the preceding composites, the changes in loss tangent after desorption were 2.63%, 1.71%, and 4.51%, respectively. The dielectric constant and loss

tangent as a function of water content for all three material types during the desorption phase were approximately equivalent to those measured during the absorption phase. An analogous linear relationship of dielectric properties as a function of moisture content is observed for each composite system during both periods of moisture absorption and desorption. Though not relevant at radar frequencies, Cotinaud et al. performed a similar investigation on glass fiber-reinforced epoxy at a much lower frequency of 50 Hz and concluded that although mechanical properties after 0.6 to 0.7 % of water concentration are irreversible, dielectric properties are reversible and are a function of moisture content [121]. This most importantly signifies that the dielectric property loss associated with low levels of moisture contamination within the polymeric composite samples is recoverable by a simple desorption method.

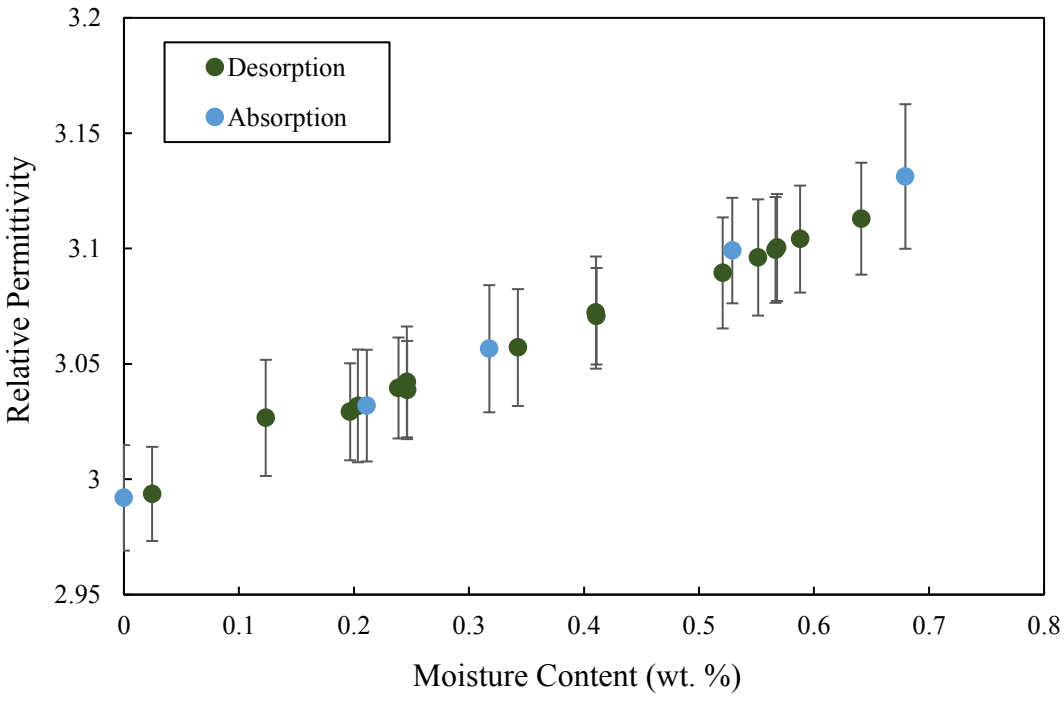

Figure 22. BMI/quartz relative permittivity as a function of moisture content

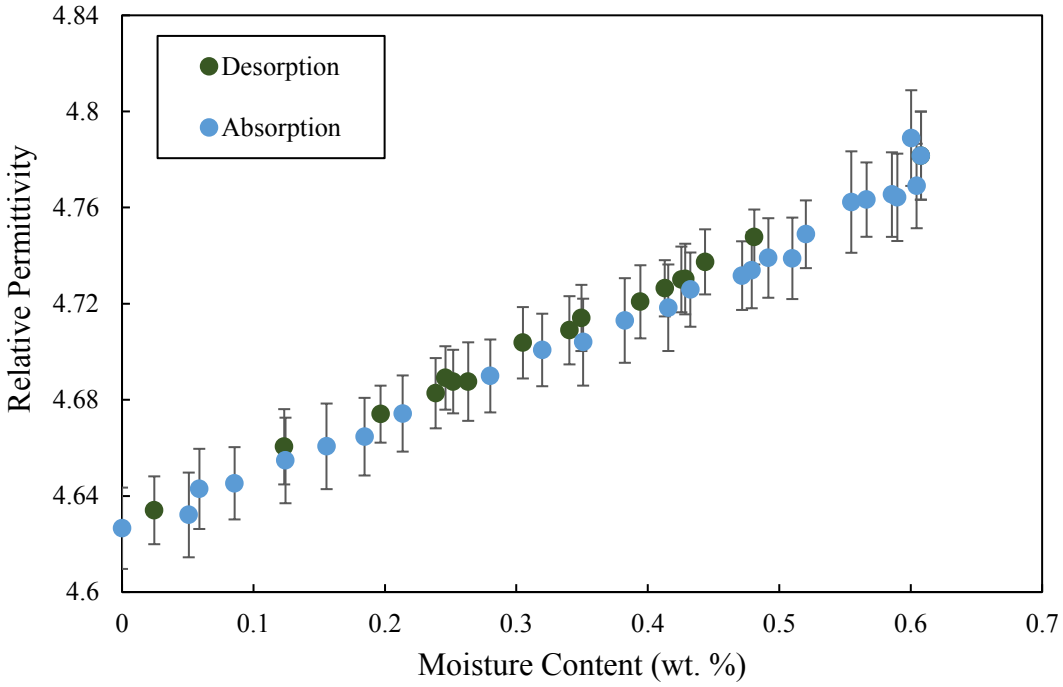

Figure 23. Epoxy/7781 relative permittivity as a function of moisture content

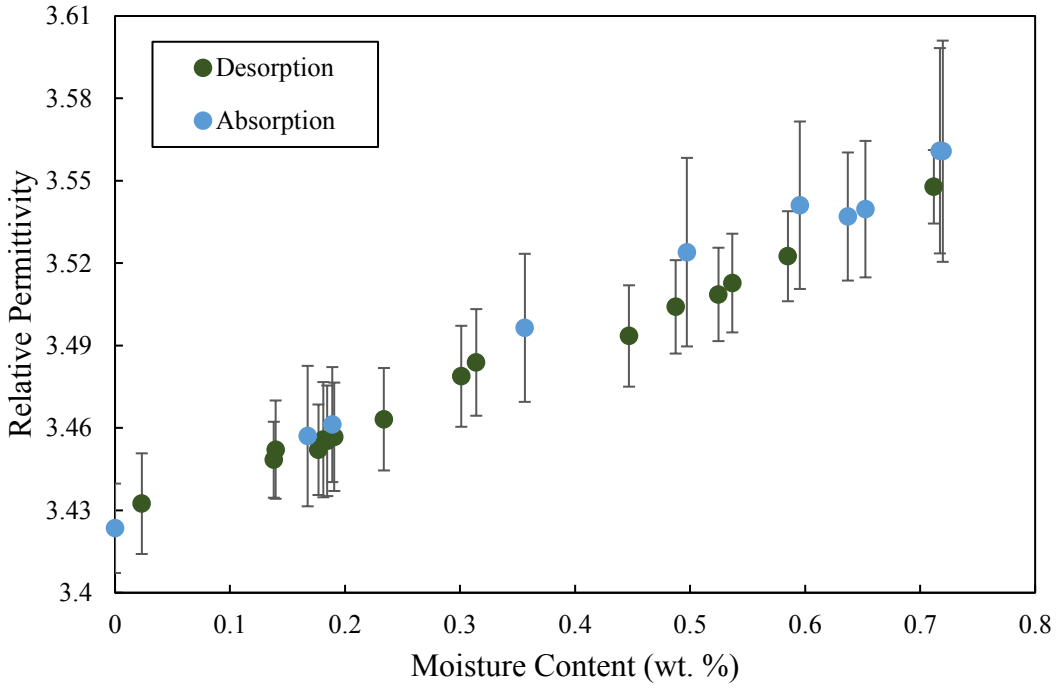

Figure 24. Epoxy/4180 relative permittivity as a function of moisture content

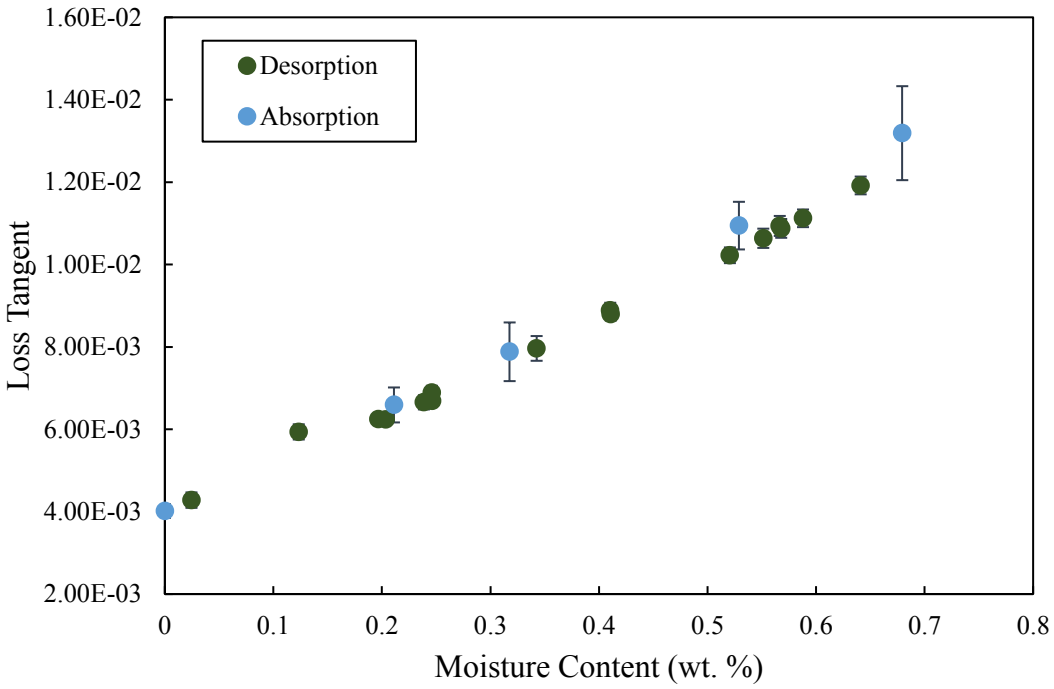

Figure 25. BMI/quartz loss tangent as a function of moisture content

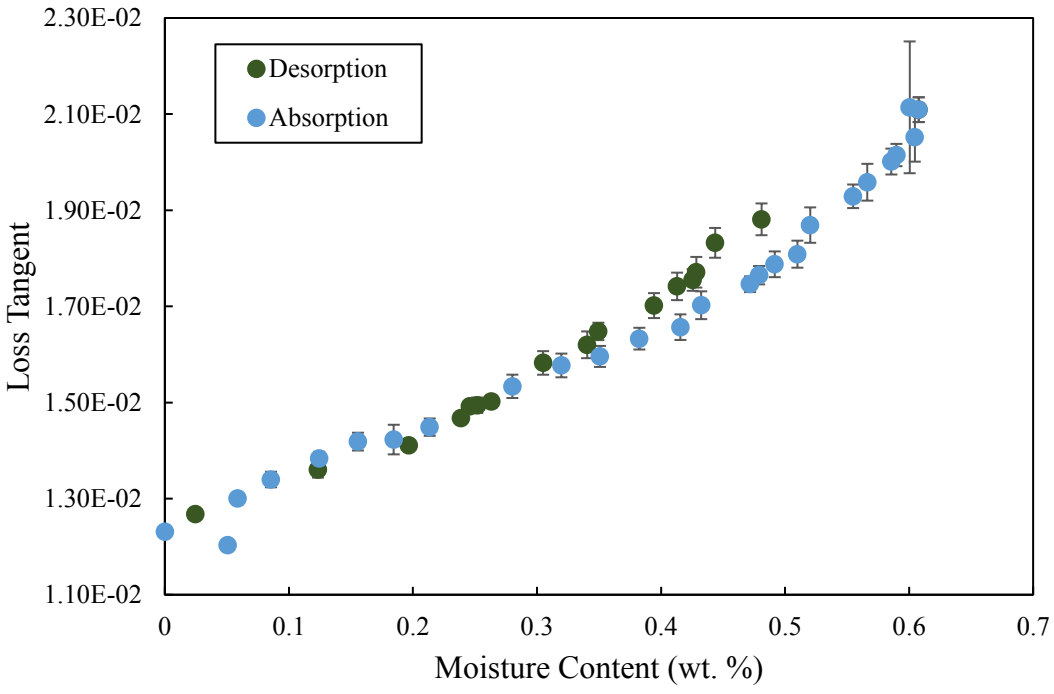

Figure 26. Epoxy/7781 loss tangent as a function of moisture content

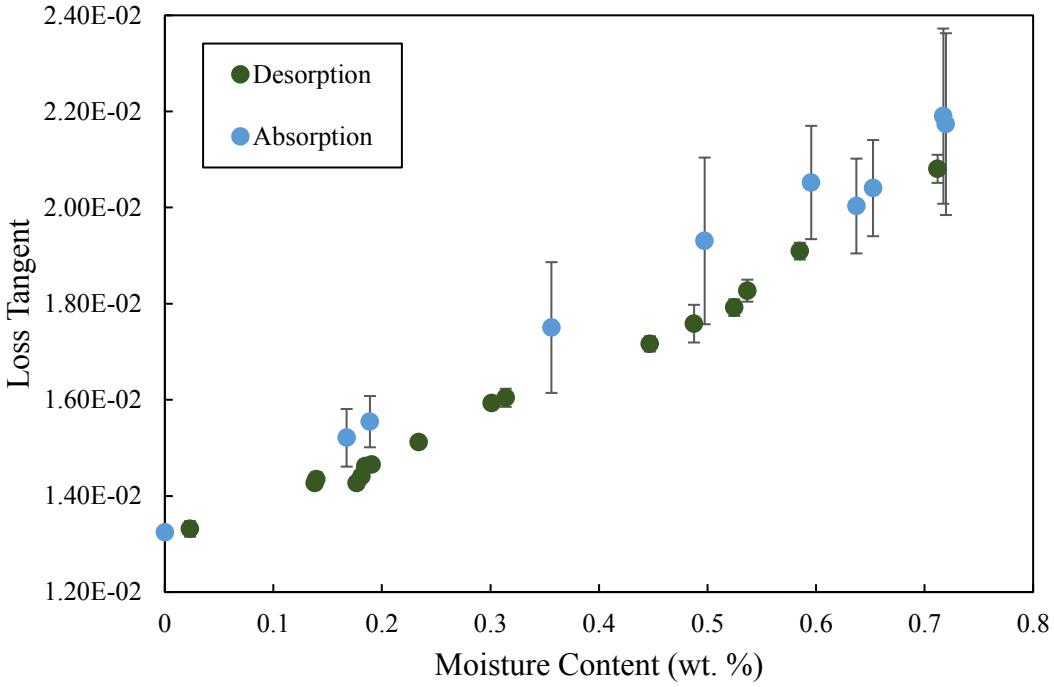

Figure 27. Epoxy/4180 loss tangent as a function of moisture content

2.6 Conclusion

Dielectric property degradation is likely related to the energy loss associated with the reorientation of a dipole molecule to align with an oscillating electric field. The trend of dielectric property loss due to water, propylene glycol, and deicing fluid contamination highlights the necessity for further investigation into polarity of each fluid and the polarity of the polymeric bismaleimide composite. During water desorption for BMI/quartz and epoxy/glass laminates, the similarity of dielectric constant and loss tangent in samples prior to absorption and after desorption suggests that any chemical or morphological changes induced by the presence of water have not caused irreversible changes in the dielectric properties of the specimen. Therefore, compromised dielectric properties and the associated loss of radar performance due to moisture contamination of a polymer

composite radome may be mitigated by a simple desorption method such as moderate heating or vacuum conditions. Furthermore, the significant loss of dielectric properties at relatively low fluid contents indicates a need for monitoring all types of contamination in radome structures

CHAPTER 3: Long-Term Durability of Water-Contaminated BMI/quartz Composite

3.1 Degradation of BMI Composites and Predictive Moisture Models

The disadvantage of polymer fiber-reinforced composites, including those based on the bismaleimide resin, is the susceptibility to absorb fluids in many applications [56, 57], even in typically hot, dry environments [122]. When considering the effects over the expected service-life of composite structures, which can span many years, degradation can become unstable. However, characterization of moisture ingress and subsequent degradation of BMI and BMI composites is far less common and extremely limited for long-term service conditions. Research performed on BMI composites indicates that short-term water contamination moderately degrades dielectric, viscoelastic, mechanical properties in general [19, 49], and precisely the fiber-matrix interface [47]. In particular, the variation of T_g and the mechanism behind it is one of the more consistently reported effects of water contamination in polymers and polymer composites. As moisture gradually increases, the dominant theory identifies resin plasticization as the resultant cause of deterioration in glass transition temperature [49]. Zhou and Lucas [123] have reported that this plasticization is related to the disturbance of interchain bonding by the presence of moisture within the polymer network of an epoxy resin, resulting in polymer chain scission, chain mobility, and swelling. A similar occurrence in carbon-fiber reinforced BMI is credited for decreasing T_g with increasing moisture content, resulting in a 30 °C reduction in service temperature for 2.4% moisture content by weight [49]. Delasi [124] proposes that the state of absorbed water has a significant effect on the associated variation in T_g. On the contrary, water contained in clusters or bound in hydroxyl-water groupings has little

to no effect on T_g. Water that disrupts interchain hydrogen bonds, however, depressed T_g significantly. This relation of absorbed moving water and bound cluster has been modeled in BMI, which has been observed to exhibit hindered diffusion behavior [40].

Constitutive models that allow prediction of fluid absorption behavior over time are necessary to relate property loss to service life and in-service conditions of a radome composite structure. Grace and Altan proposed the 3D HDM (Chapter 1), which includes interaction of diffusing molecules with the host medium [93, 94]. The model has been successfully applied to BMI/quartz laminates with varying ply-count and aspect ratio [40]. Critical to the prediction of structural life and performance is the water content at any given occasion, which is in turn crucial to preventing radome deterioration. Moreover, long-term moisture exposure and the resultant composite degradation are not well-defined in the existing open literature. Thus, the objective of this work is to further develop an understanding of the long-term behavior of BMI/quartz composites in a fully immersed water-contaminated state. Toward that end, BMI/quartz laminates are analyzed in the fully dry state, the saturated state achieved through four years of full immersion, and states between these conditions are examined in order to correlate water content with any characteristic changes.

3.1 Materials and Experimental Set Up

3.1.1 Material Machining and Environmental Conditioning

A six-ply, eight-harness satin weave quartz fiber embedded within a BMI matrix is the material under investigation. Specimens were prepared for environmental conditioning in five separate sets of seven specimens each, for a total of 35 specimens. Samples were cut from the same panel with a wet diamond saw. A set of five specimens served as the

control, and was not exposed to contamination. The remaining groups were allotted for two week, one month, six month, and four year immersion lengths. The effect of aging of the matrix, regardless of the environment to which the composite is exposed, is removed from consideration in this case due to the simultaneous fabrication and cure of all tested samples. As such, specimens exposed to four years of moisture immersion are equivalent in total age since cure, but not in exposure duration. Three specimens within each set were used for DMA testing, while the remaining four were designated for flexure tests. DMA specimen measurements were 25 mm by 12.5 mm with a thickness of 1.35 mm for dry, two week, and one month exposure duration conditions. DMA dimensions for six months and 51 months were 40 mm by 10 mm with a thickness of 1.35 mm. Though of different overall lengths (25 mm and 40 mm) as a result of sample (panel) size limitations, the DMA span of 20 mm was consistent for all specimens. Four composite samples were used for flexure analysis, with dimensions (for each immersion duration) of 40 mm by 10 mm, and thickness of 1.35 mm.

3.1.2 BMI/quartz Immersion

After machining the bismaleimide specimen, specimens were dried in a furnace at a constant temperature of 65 °C until an equilibrium weight was attained. Specimens were then fully immersed in separate containers of distilled water, which were then immersed in a constant temperature water bath at a temperature of 25 °C for their corresponding durations. Samples were periodically removed, weighed, and dried with a lint-free cloth to ensure removal of all residual surface water. This accumulation of gravimetric uptake data followed the standard procedure outlined in ASTM D5229 [73].

3.1.3 Dynamic Mechanical Analysis and Flexure Evaluation

The control dried and water-contaminated specimens were tested in a *TA Instruments* Q800 DMA (Figure 28) using a three-point bending clamp (Figure 29).

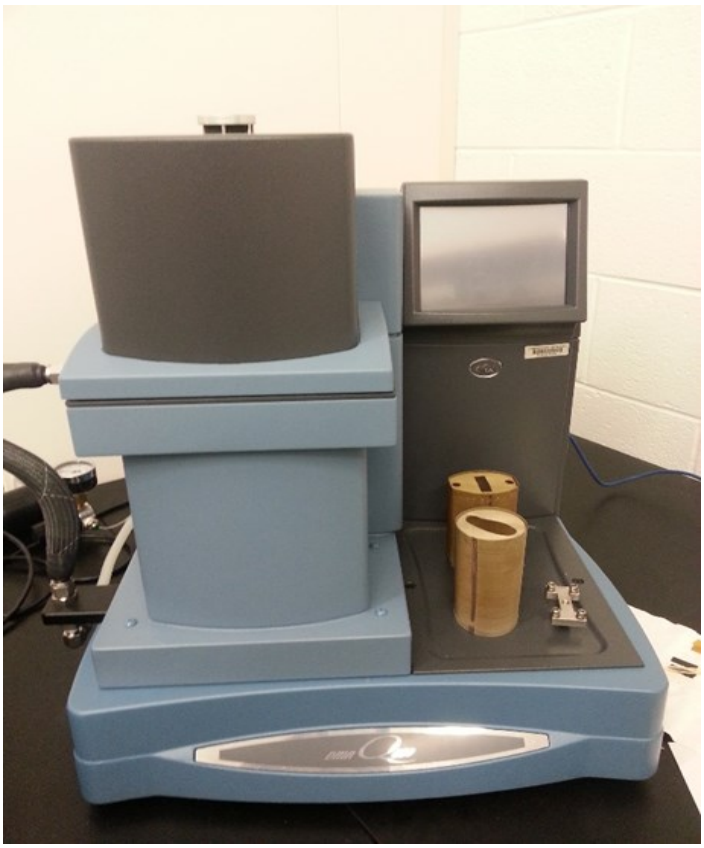

Figure 28. DMA Q800

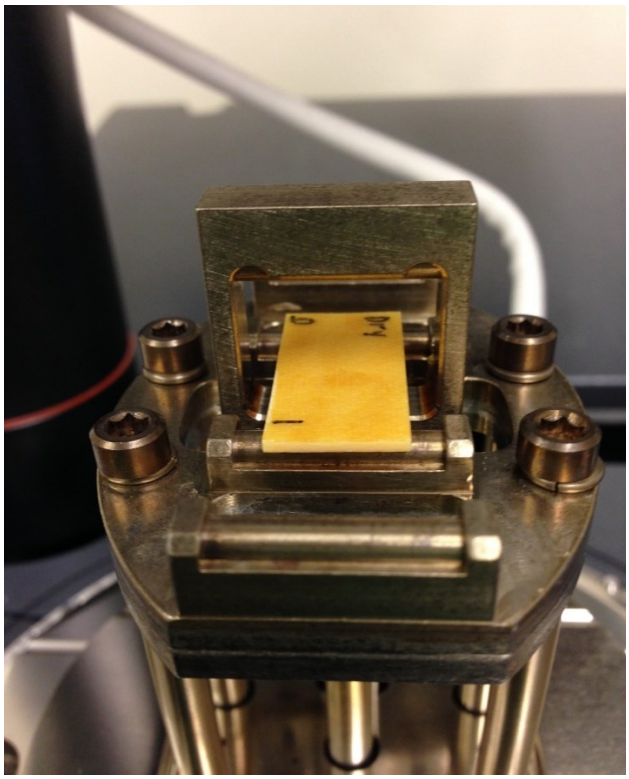

Figure 29. Three-point bending clamp

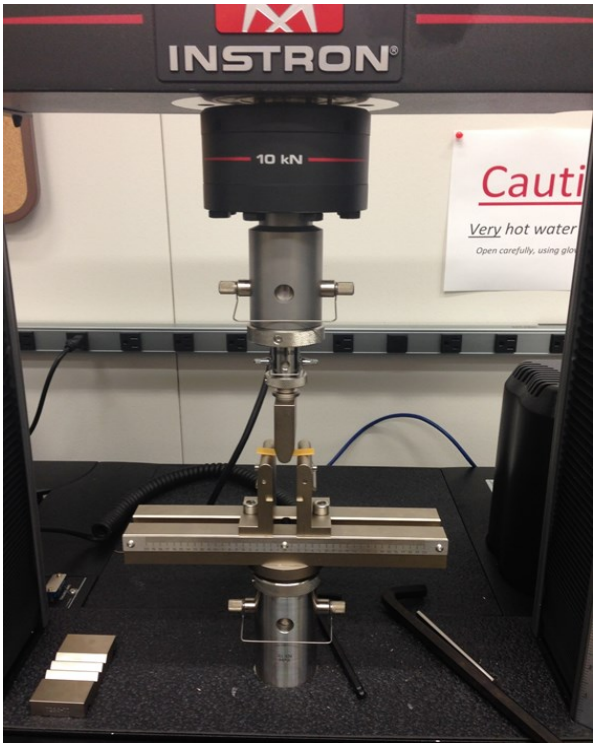

Figure 30. Instron dual column table frame and three-point bending fixture

DMA testing was executed at a constant heating rate of 5 °C/min, a frequency of 1 Hz, and an amplitude of 15 μm. T_g was found by slope change in the storage modulus (E′) as a function of temperature, in accordance with ASTM D7028 [74]. Figure 30 shows an Instron 5960-dual column table frame, with a three-point bending 5 kN flexure fixture that was used to perform flexure evaluations on the specimens. A constant crosshead rate of 0.9 mm/min, and span to thickness ratio of 20:1 were used for all samples. All flexure properties were determined according to ASTM D790 [72]. The data presented represents an average of all samples tested. A 95% confidence interval was computed for specimens used in flexure tests and an analysis of variance with the same confidence level was used to verify difference in means.

3.2 Long-Term Contamination Results and Discussion

3.2.1 Distilled Water Diffusion

The average moisture ingress of the BMI/quartz specimens immersed for about 51 months (> 4years) is shown in Figure 31, with the respective 3D HDM prediction. During initial stages of moisture ingress, the short-term moisture uptake is characterized by its proportionality to the square root of time. Deviation from the typical Fickian diffusion behavior is noticed and is succeeded by a pseudo-equilibrium at which moisture uptake does not diverge from 0.01% for a time period of 100 days [40]. Grace has observed that equilibrium moisture plateau has not been reached after five years of immersion [52] and this phenomenon has been tied to the effect of diffusion hindrance as a result of molecular binding of distilled water to polar sites within the host material. The presence of bound water molecules within polymer systems has been verified experimentally through nuclear magnetic resonance (NMR) [59], and hydrogen bonding has been identified as a

contributor to non-Fickian moisture absorption in BMI [125]. In like manner, gravimetric water absorption data [40] and X-band relative permittivity analysis [19] are allusive of the existence of firmly bound water in BMI/quartz. Conversely, during long-term submersion, the assumption that polymer chain relaxation is the prime culprit of Fickian divergence is valid to some degree.

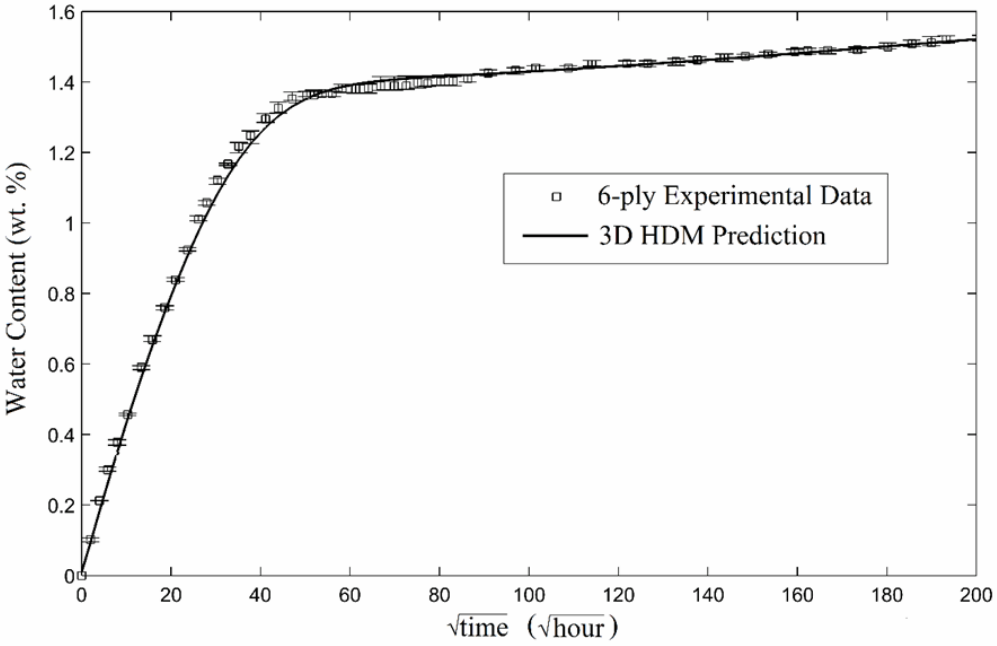

Figure 31. BMI/quartz four-year moisture uptake data and 3D-HDM prediction [126]

Equilibrium moisture content of this 6-ply composite has been projected at 1.723% by weight based on the approximate 51-month period. As noted in Ref. [52], the predicted moisture equilibrium occurs at 1.726 % by weight for a time frame of 5 years. Parameters extracted from a least-squares curve-fit to the three-dimensional hindered diffusion model were determined after 21 months of immersion and are given in Table 7. The error in this table is based on the assumption that the most recent parameters recovered are the most accurate. The associated diffusivity edge error, $D_{e,}$ is noticed to have a far lesser influence

on the adequacy of the fit. Hence, this parameter is more difficult to predict in thin laminates due to the relative smaller surface area. Errors with binding probabilities γ and β are moderately high, but have a far lesser impact than their combined ratio of the hindrance coefficient (μ). Moisture content for the experimental time frame of 51 months, in Figure 31, is 1.529% by weight and it is in excellent agreement with the model prediction. The error between the previously published projection based on 21 months of gravimetric data [40], the 4 year data, and 5 year experimentally recorded data show reasonable consistency.

Table 7. Comparison of parameters recovered with 3D HDM during ~4 years and 5 years of immersion [52]

	D_e *(mm^2/h)*	D_z *(mm^2/hr)*	M_∞ *(wt. %)*	γ (10^{-6}) *(hr^{-1})*	β(10^{-6}) *(hr^{-1})*	μ
6-ply (~ 4 years)	1.98×10^{-3}	1.73×10^{-4}	1.723	2.98	12.5	0.807
6-ply (5 years)	3.04×10^{-3}	1.67×10^{-4}	1.726	3.32	13.7	0.805
Error (%)	34.8	3.59	0.17	10.2	8.76	0.25

3.2.2 Flexural Analysis of Moisture-Contaminated BMI/quartz Laminates

Data gathered from the experimental stress vs. strain tests of BMI/quartz laminates are shown in Figure 32 and Figure 33. Maximum flexure stress, strain at maximum flexure stress, and flexure modulus are shown in Table 8. Specimens were tested in flexure in order to provide a measure of degradation as a result of moisture diffusion, particularly with respect to the fiber-matrix interface. BMI/quartz laminates were removed from immersion

after the time periods of two weeks, one month, six months, and four years. Following final weighing, specimens were immediately tested until failure in flexure was achieved.

Analysis of variance (ANOVA) was performed to determine whether flexure strength at different immersion times is considerably dissimilar. The significance level for the ANOVA analysis is 0.05 (using a 95% confidence interval), with a p-value of 0.274 gathered from the experimental data. According to ANOVA, if the p-value is equal or less than the significance level, means are different. If the p-value is larger than the significance level, means are not significantly different. The results of this analysis confirmed that, while an overall drop of 5% in flexural strength was measured in the worst case (four years of immersion), changes in flexural properties are not significant. The combination of BMI's highly crosslinked density, polar resin, polar contaminant, and quartz reinforcement creates a tortuous path for water molecules to diffuse into the composite matrix. Consequently, this restriction in water mobility leads to a very slow composite material degradation, which is reported by Grace [52] . Flexural strength preservation after four years of full immersion was not expected. The diffusivity through the edges along and parallel to fiber direction is approximately 11 times higher than diffusivity transverse to the fibers [40]. Therefore, the flexural load transferring ability was expected to be weakened due to the relative high concentration of water in the matrix-fiber interface regions. Although the conservation of flexural strength was unforeseen, early onset of structural failures at approximately 600 MPa and 0.025 mm/mm was detected for samples that were submerged for longer than six months. This occurrence is credited to the origin of fiber-matrix debond and delamination. It should be noted that a similar less significant event is seen for control samples.

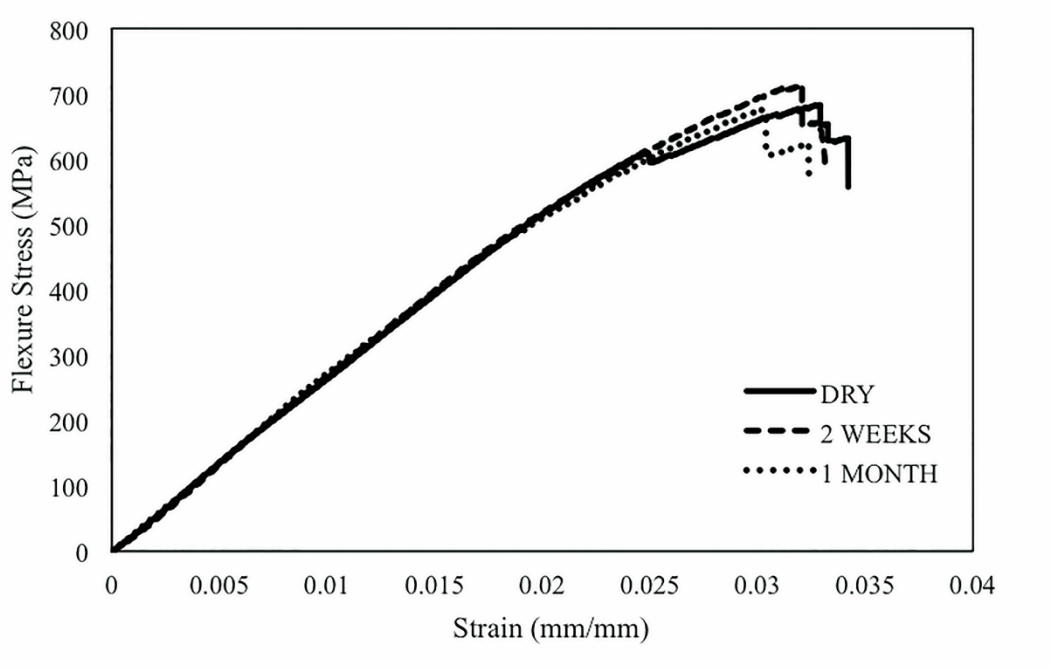

Figure 32. Flexure stress vs. strain of immersed (2 week and 1 month) and dry 6-ply BMI/quartz laminates [126]

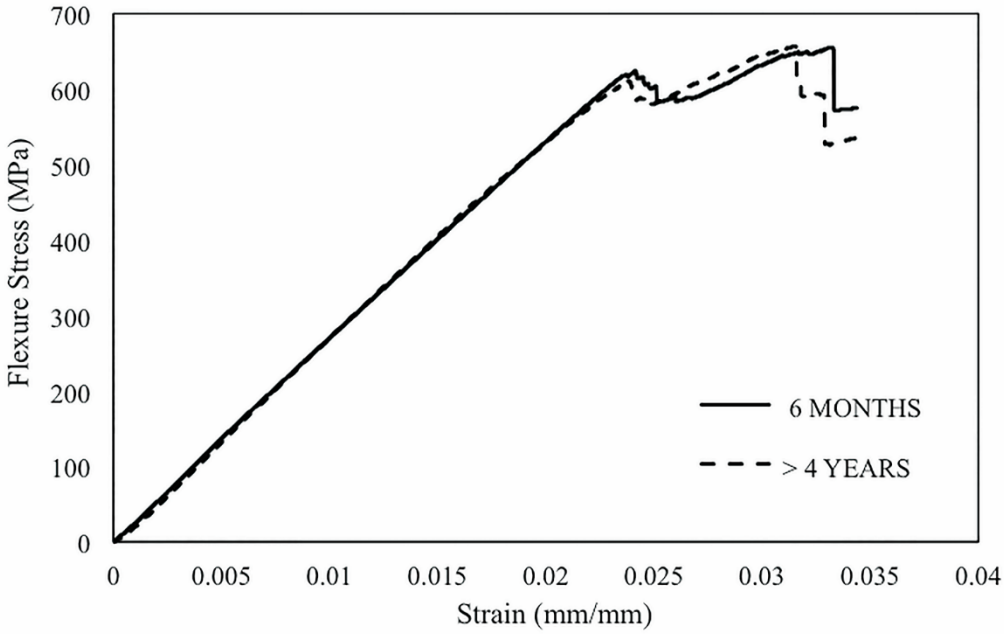

Figure 33. Flexure vs. strain of immersed (6 months and > 4 years) 6-ply BMI/quartz laminates [126]

Table 8. Water-contaminated BMI/quartz laminate flexure characteristics [126]

Immersion Time	Water Content *(wt. %)*	Max. Flexure Stress *(MPa)*	Strain at Max. Flexure Stress *(mm/mm)*	Flexure Modulus *(GPa)*
Dry	0	699	0.0314	27.9
2 Weeks	0.59	726	0.0329	28.0
1 Month	0.79	702	0.0326	27.4
6 Months	1.21	669	0.0325	27.9
> 4 Years	1.52	667	0.0309	28.6

Flexure strength at each immersion period and the dry state are shown in Figure 34 with corresponding error bars utilizing a 95% confidence interval. An increase in flexural strength is noticed at two weeks of moisture ingress, which is succeeded by a downward trend with increasing immersion time. As previously mentioned, no significant change in flexural strength is evident from the available data, but of note is the phenomenon at two weeks. This event has been reported in BMI and epoxy fiber-reinforced composites [45, 49, 127] and is associated to the rapid early stages of water molecule-polymer chain bonding, which act as a matrix reinforcement along with moisture-induced matrix plasticization [45, 49]. The theory behind the composite strengthening is that this type of behavior is estimated to last for the first month of submersion. Thereafter, diffusion of water molecules continues and at subsequent immersion times, hydrostatic pressure at the fiber-matrix interface will result in degradation.

The low variation in strength after four years of immersion at 25 °C is paramount to the durability and applicability of BMI/quartz in future aircraft radome structure designs, which are routinely exposed to moisture. Magid et. al [45] has, paradoxically, postulated

that the durability of the radome composite can be associated to saturation at the interface. Moisture in this region may increase the contact region between matrix and fiber, in which adhesive interactions allow load transferability and retention of material strength [45]. BMI's unanticipated long-term durability may similarly be attributed to its cure technique, where it is noticed that, for a BMI/carbon fiber composite, an addition of a post cure may have resulted in its strength retention [49].

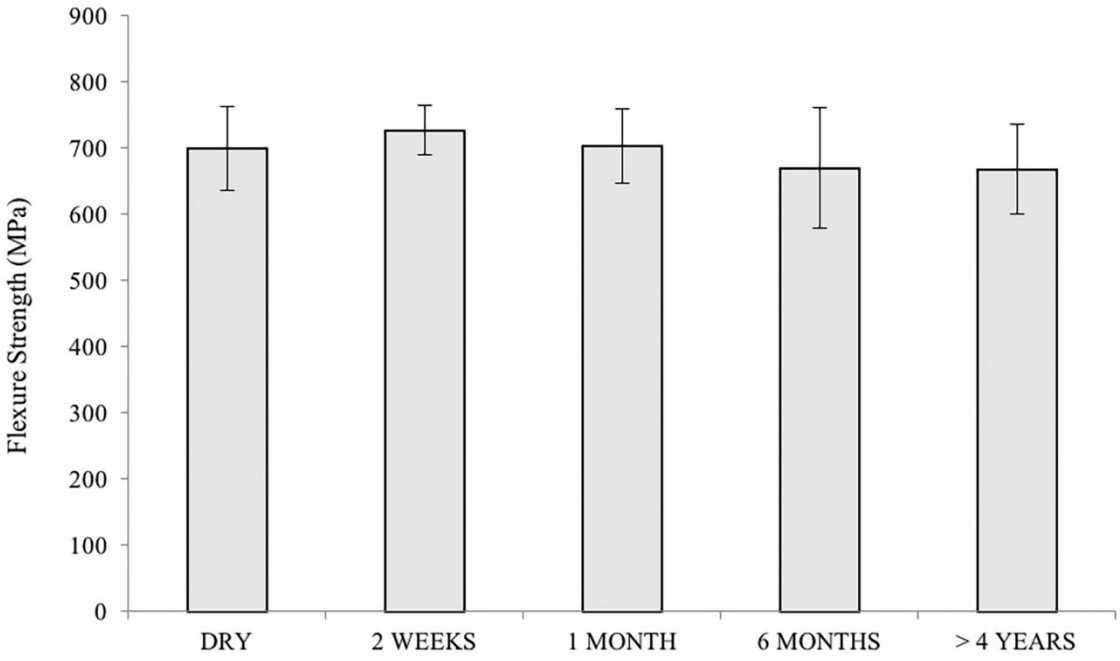

Figure 34. Flexure strength as a function of immersion time of BMI/quartz specimen [126]

3.2.3 Dynamic Mechanical Analysis of Dry and Moisture Contaminated BMI/quartz Laminates

Dynamic mechanical analysis was performed in order to provide an insight into the coupled moisture/temperature effects on the quality of the viscoelastic storage modulus. Figure 35, Figure 36, and Figure 37 show storage modulus as a function of temperature for

dry, six-month immersion, and four-year immersion BMI/quartz sets, respectively. ASTM D7028 is the standard method for determining glass transition temperature, which can be defined by the intersection of two tangent lines during the rapid slope change in storage modulus in the latter figures. By this method the T_g was approximately observed to be 380 °C. This value is misleading and artificially inflated as a consequence of choosing where the tangent lines lie. The reported manufacturer values for BMI/quartz is 316 °C. For many thermosetting polymers, the sudden drop in storage modulus is rather unusual, as they experience a slower descent.

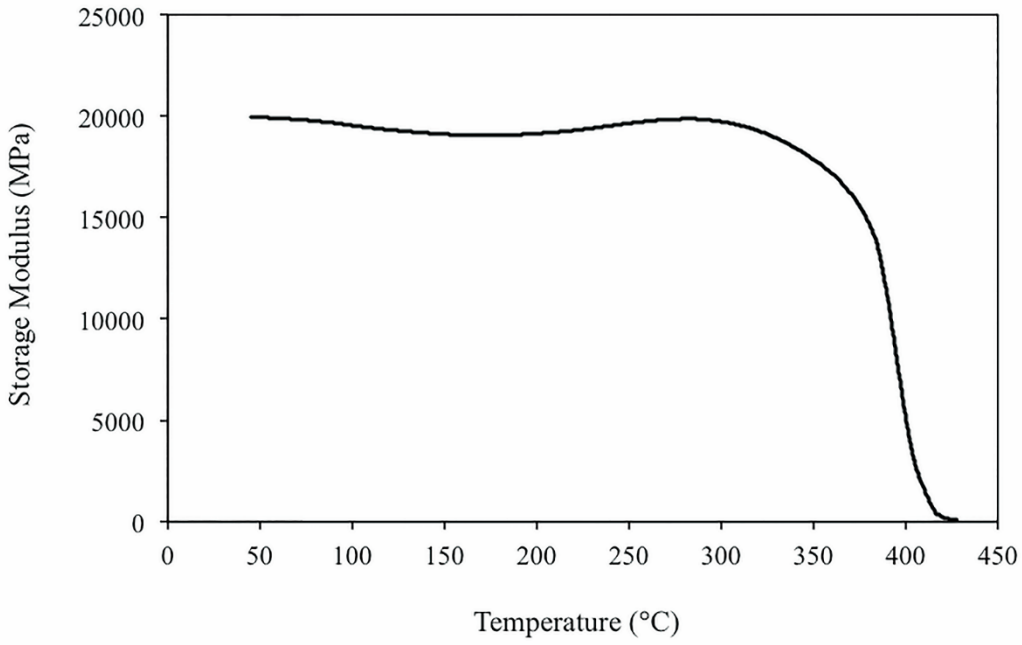

Figure 35. Storage modulus vs. temperature of dry BMI/quartz laminates [126]

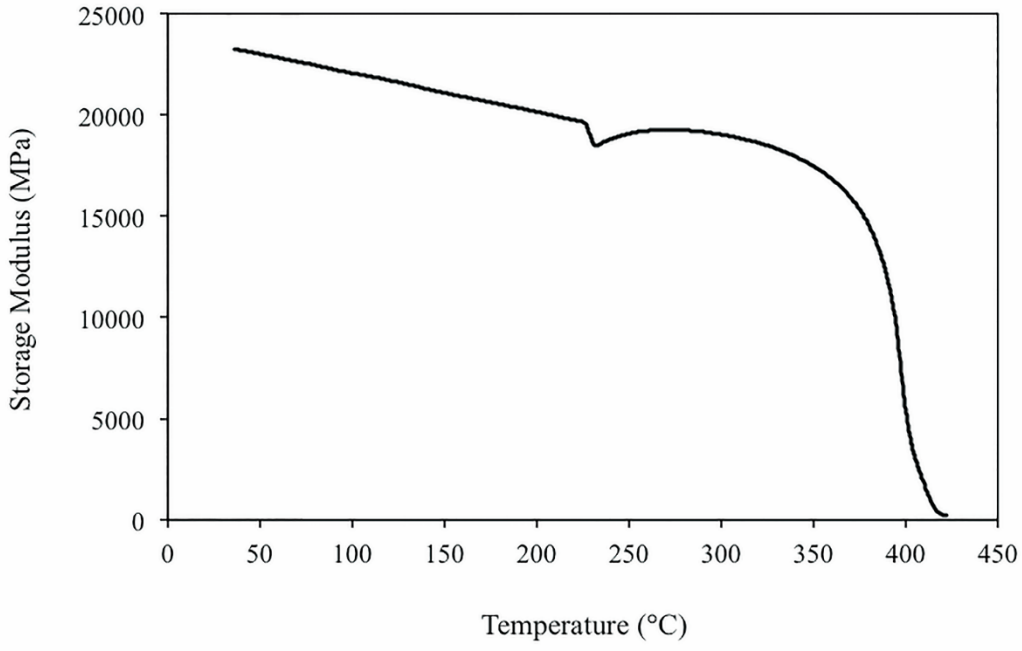

Figure 36. Storage modulus vs. temperature of over six month water contaminated BMI/quartz laminates [126]

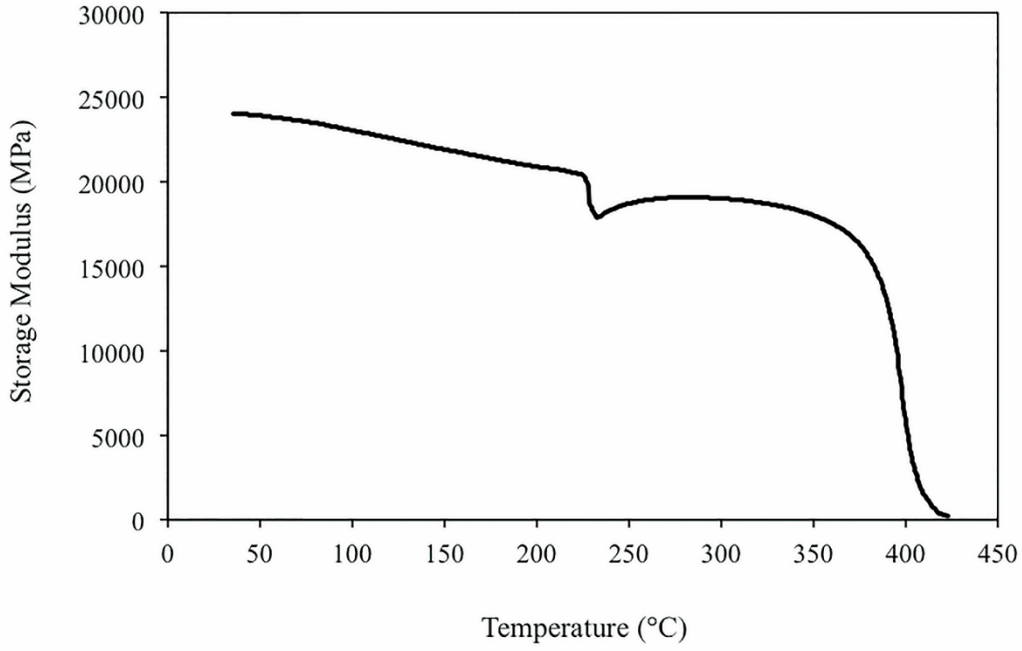

Figure 37. Storage modulus vs. temperature of over 4 year water contaminated BMI/quartz laminates [126]

The longevity of the quartz-reinforced BMI system is further supplemented by the non-varying T_g between the control and immersed laminates. Thermogravimetric analysis (TGA) was performed to quantify the amount of water that was removed before the onset of the glass transition point. Applying a ramp rate of 5°C/min on the TGA, a 1% loss of laminate weight was observed during the 55 minute ramp from 25 °C to 300 °C. During and after the T_g, moisture removal was noticed to be difficult to obtain and correlate as a result of the instantaneous composite mass and moisture content loss. Hence, it can be further stipulated that high-temperature desorption is not a catalyst of glass transition degradation, which additionally supports the remarkable durability of BMI/quartz composites.

Importantly, however, is an anomalous decrease and immediate recovery in storage modulus at 225 °C for specimens immersed over six months. This phenomenon was solely observed for long-term immersion specimens, which may be correlated to a moisture content/high temperature coupling. Equipment error was vigorously eliminated as a root cause and results were consistently repeated. It is assumed that fiber-matrix debonding is the result of this instantaneous decline, which will be discussed more thoroughly in Chapter 4.

3.2.4 Scanning Electron Microscopy

Micrographs of BMI/quartz specimens, for each aging period, were taken via scanning electron microscopy (SEM). Figure 38 shows the midsection (perpendicular to the edge) of dry, two-week, one-month, and four-year specimens. Only a portion of the observed fiber-matrix systems are shown due to sings of debonding (woven transvere fibers are not displayed). It should be noted that the six-month laminates were not shown as a

result of not demonstrating significant degradation under SEM analysis. Specimens in this figure were readied using a spinning platen, low to high grit sandpaper, and polishing solution. Relatively few manifestations of debonding were detected only in the laminates immersed for four years. The specific occurrence of these debonds is unclear, as the gravimetric data was recorded before micrographs were taken. Despite the ambiguity, the influence of these new pathways would presumably contribute to an apparent moisture increase. Although a sudden increase in moisture content was not observed, it is most likely that the moisture absorption and fiber-matrix separation develop gradually. This may explain the overall effects of non-Fickian behavior, non-varying flexure strength, and the few instances of debonds at 51 months of immersion.

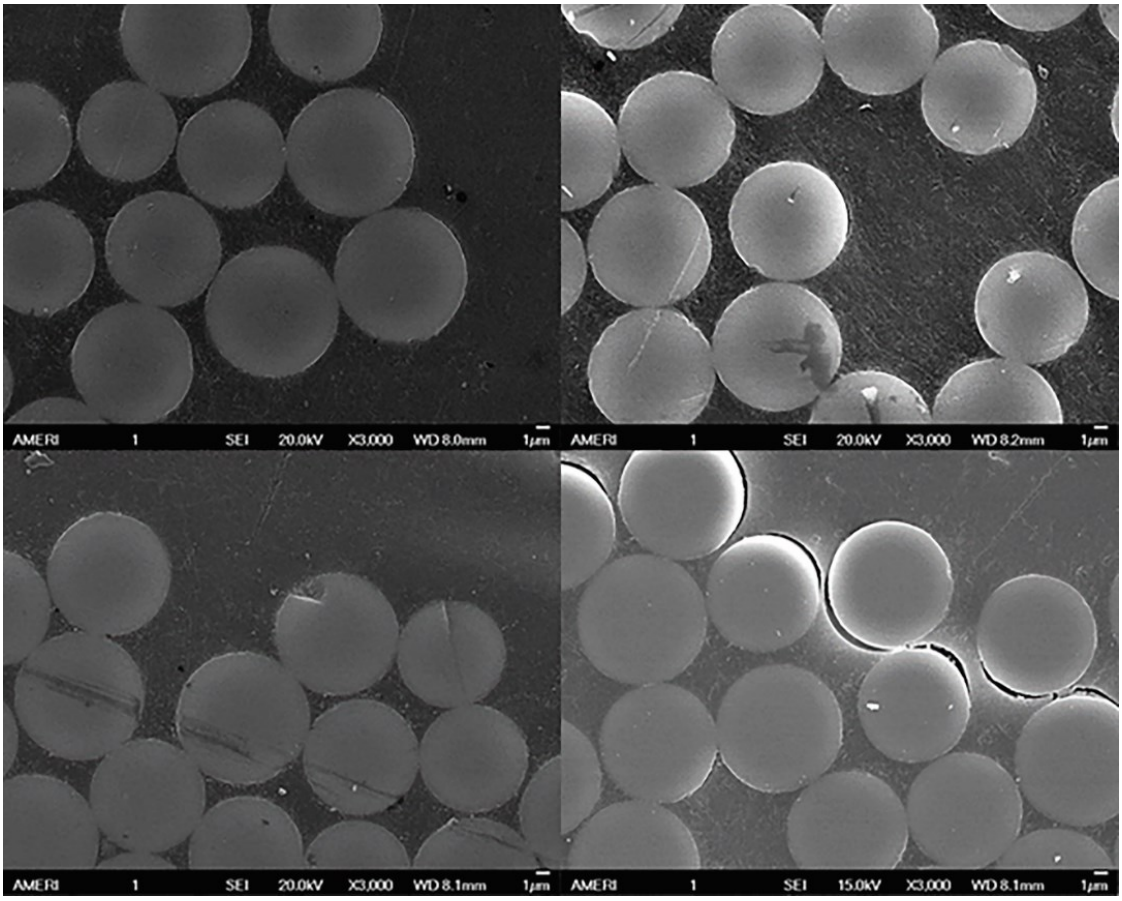

Figure 38. SEM micrographs of dry and moisture-contaminated BMI/quartz. Dry (top left), immersed two weeks (top right), one month (bottom left), and 51 months (bottom right) [126]

3.3 Conclusion

Six-ply BMI/quartz laminates were exposed to very-long-term water contamination procedure and were studied via flexural property assessment, dynamic mechanical analysis, and scanning electron microscopy. The four-year diffusion investigation was measured against the square root of time under full submersion. Moisture diffusion parameters were predicted by the 3D hindered diffusion model, which projected a moisture equilibrium of 1.723% for the four-year immersion time. The distinctly non-Fickian moisture absorption behavior resulted in water content of 1.529% by weight and was

consistent with the model projection. Despite the worst-case scenario of standing-water, such as precipitation pooling during ground storage, no significant decrease in flexural strength and no definitive change in glass transition temperature was detected for any specimen tested. Although SEM revealed the onset of debonding for specimens immersed for four years, areas of debond were relatively limited, and retention of flexural strength was preserved. Within the confines of the testing methods employed, the laminates exhibited excellent durability and resistance to water-induced degradation. As such, BMI/quartz composites are a viable option for load-bearing radome composite structures subject to long-term exposure in moisture-rich environments.

CHAPTER 4: Hygrothermally-Induced Fiber-Matrix Debond in BMI/quartz Laminates Measured by Dynamic Mechanical Analysis

4.1 Objective

This analysis is a continuation of Chapter 3 and its objective is twofold. Primarily it is to further investigate the anomalous decrease in storage modulus and its association to fiber-matrix debonds. Furthermore, this study will characterize the coactive effects of moisture contamination and elevated temperature on the mechanical and viscoelastic properties of quartz-reinforced BMI laminates.

4.2 Materials and Experimental Set Up

4.2.1 Material Machining

Again, the composite being investigated is a six-ply, eight-harness satin weave quartz fabric, style 581, embedded in a BMI resin, trade name HexPly® F650 [10]. The six ply laminates are composed of 60.3% fiber volume, 39.2% resin volume, and 0.4% void volume, as revealed by resin burn-off experiments. Laminates were cut from manufacturer's panel by the use of a wet diamond saw. DMA and flexure test laminate dimensions were 40 mm by 10 mm, with a thickness of 1.35 mm.

4.2.2 BMI/quartz Immersion

Composite laminates were dried at a constant temperature of 65 °C until an equilibrium weight was achieved. Laminates were immersed into containers filled with distilled water. Containers were placed into a 25 °C constant-temperature water bath. When removing composite specimens from immersion, they were fully dried with a lint-free cloth

to remove any residual water and weighed using a high-precision analytical balance. Gravimetric analysis was performed according to ASTM D5229 [73].

4.2.3 Dynamic Mechanical Analysis and Flexural Evaluation

For DMA and flexure test analysis, 1.21% and 1.52% moisture content by weight, were the immersion conditions in this investigation. Fully dry samples served as the control set. Moreover, two additional thermal conditions were analyzed for each moisture content: before anomalous transition (BT) and after anomalous transition (AT). BT describes the DMA situation wherein the laminate is taken to 220°C, right before the drop in storage modulus at 225°C. AT describes the situation immediately after the recovery from that drop, at a temperature of 260°C. Three composite laminates were used for DMA testing for each immersion condition and their respective BT and AT environments. Flexure test utilized four laminates in the same manner as DMA testing resulting in a total of 63 samples.

Samples were tested in a DMA (*TA Instruments* Q800), using a three-point bending clamp. During flexure tests, the Instron 5960 dual-column table frame was used with a three-point bending 5 kN flexure fixture. DMA tests were performed at a constant heating rate of 5°C/min, a frequency of 1 Hz and amplitude of 15 μm. T_g was found by the slope change of the storage modulus (E′) as a function of temperature, in accordance with ASTM D7028 [74]. Flexure testing was achieved with a thickness to span ratio of 20:1 at a constant crosshead rate of 0.9 mm/min. All flexure properties were calculated according to ASTM D790 [72]. Flexure and DMA data represents the average of each sample set. A 95% confidence interval was calculated on flexure data and analysis of variance with the same

interval was performed to analyze the interactions between immersion time and temperature.

4.3 Hygrothermal Contamination Results and Discussion

4.3.1 Dynamic Mechanical Analysis on BMI/quartz Laminates

Laminates of 0%, 1.21%, and 1.52% moisture content were analyzed via DMA and the storage modulus was plotted as a function of temperature, as shown in Figure 39. The rapid slope change in each curve occurs in a relatively short temperature range for the three curves shown. This sudden change occurs where the glass transition temperature of about 380°C is reached. The reported T_g of BMI/quartz is 316°C, which represents the onset of the glass transition. The dissimilarity between the measured and reported T_g may arise from lack of a standardized determination method and due to the thermocouple measuring in an oven environment instead of within the specimen, as suggested by Sims and Gnaniah [128]. An abrupt drop in storage modulus appears at an approximate temperature of about 225°C for the 1.21% and 1.52% moisture content laminates, which is followed by a modest recovery for all samples tested. This drop may be associated to the heat resistant constraints of the quartz fabric [50]. Drakonakis et al. [129] had similar findings for a set based carbon-carbon reinforced composite, where a decrease in storage modulus was observed at 220°C, followed by an increase at 320°C and fall once more over 350°C, which was said to be the result of thermal degradation and high temperature crosslink reactions. It should be noted that in the aforementioned study, there is no mention of moisture absorption or drying of laminates until moisture free weight is achieved. According to results in Figure 39, the significant difference in moisture uptake leads to the conclusion that the drop in storage modulus is dependent on water contamination and thermal degradation. It is worth noting

that a static force experiment with load of 0.001N and a temperature ramp rate of 5°C/min was performed on laminates via DMA in order to verify the occurrence of the premature drop in E′ with such a miniscule load. DMA results revealed the occurrence of a decrease in storage modulus, hence indicating that force is not an instrumental factor.

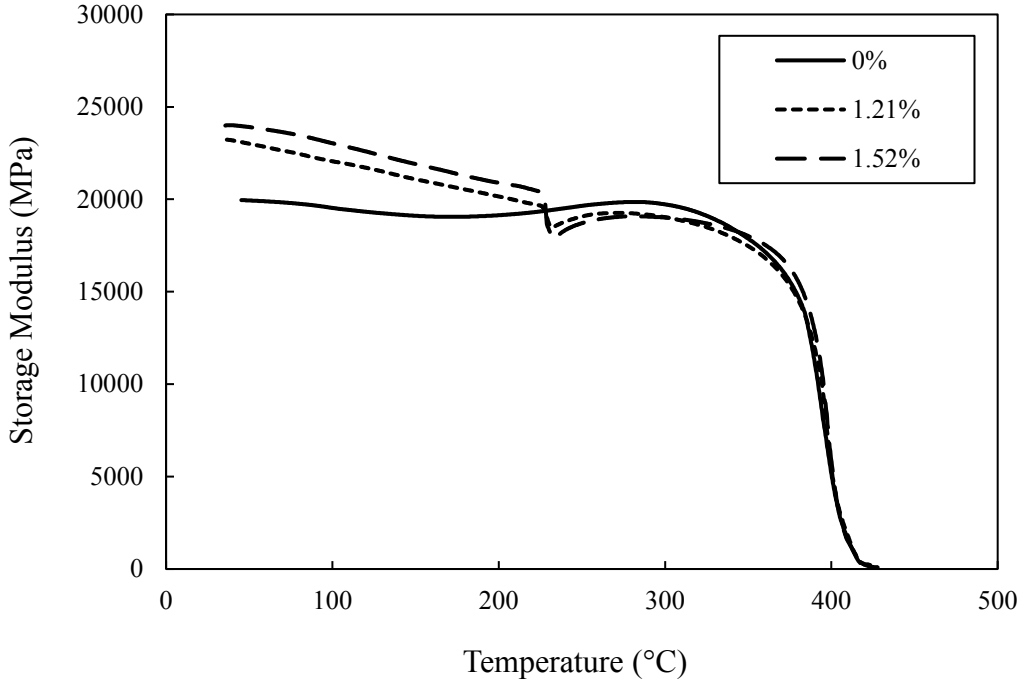

Figure 39. Storage modulus vs. temperature of dry and moisture-contaminated laminates

To further understand the anomalous drop, DMA testing was performed at various heating rates and moisture contents. Figure 40 shows the result of the experiments and indicates where no drop occurred (blue) and the occurrence of one (red). Table 9 was created by process of elimination as to save time and material. For example, if there is no indication of a sudden drop for 20°C/min at 0 and 0.2 wt%, it is safe to assume that there will not be a drop at lower temperature rates. Rates of 15°C/min and 5°C/min ramp rates

at each 0 and 0.2 wt% were tested for verification. The same process of elimination was performed for the red area. Figure 41 characterizes coupled temperature rates and moisture contents where no anomalous decrease in storage modulus is noticed. Conversely, Figure 42 and Figure 43 demonstrate the anomaly in storage modulus before glass transition temperature is reached. The white area in Figure 40 describes the unknown effects of the couplings and is in need of further study. Eventually, the limiting values of Figure 40 will be the moisture equilibrium (1.726 %) and the in-service temperature rate of the aircraft radome composite. Storage modulus curves in Figure 41 (blue), Figure 42 (blue), and Figure 43 (blue) coincide with Table 9 and Figure 40. Furthermore, as moisture content increases, the anomalous drop moves to the left (red curves) for the constant heat rates of 5°C/min and 10°C/min. Therefore, this demonstrates that this anomalous descent in storage modulus increases significantly with an increase in moisture. Additionally, with an increase in heating rate from 5°C/min to 10°C/min at a constant moisture content of 1.2 wt% the so called anomalous drop occurs at the same temperature of 225°C.

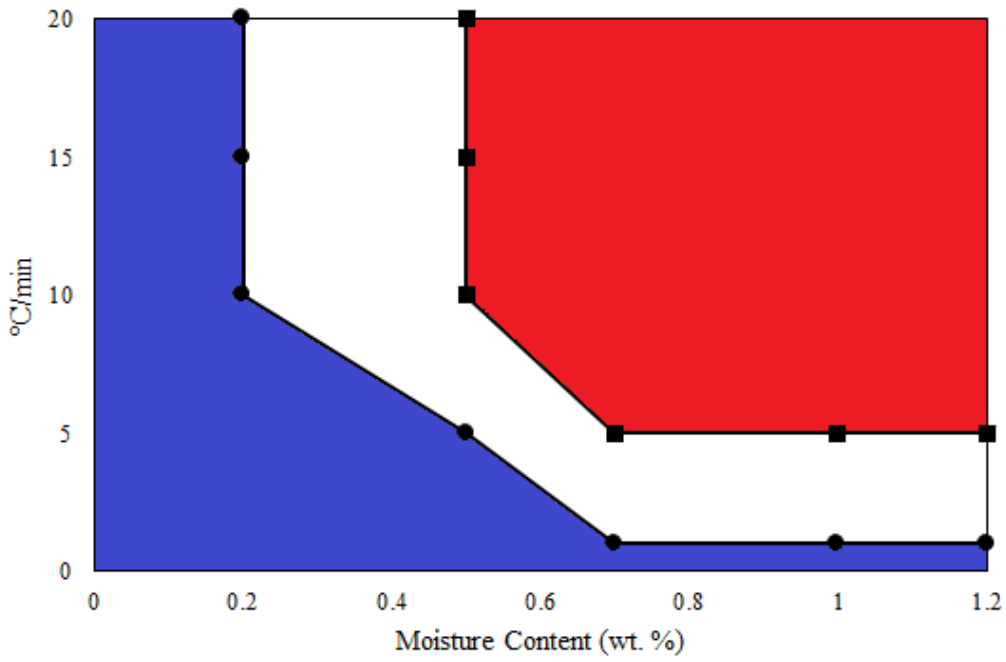

Figure 40. Ramp-rate and moisture content; critical (red), non-critical (blue), and unknown (white) debond areas in BMI/quartz

Table 9. Coupled ramp-rate and moisture content

Source of Variation	0wt%	0.2wt%	0.5wt%	0.7wt%	1wt%	1.2wt%
1°C/min						
5°C/min						
10°C/min						
15°C/min						
20°C/min						

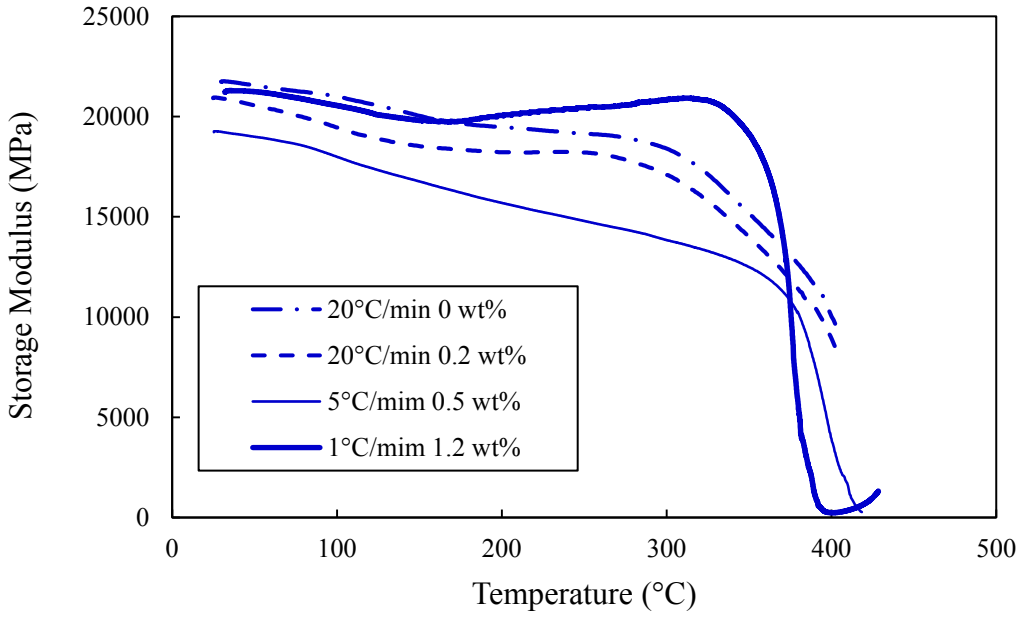

Figure 41. No anomalous descent in storage modulus vs. temperature for coupled ramp-rates and moisture contents

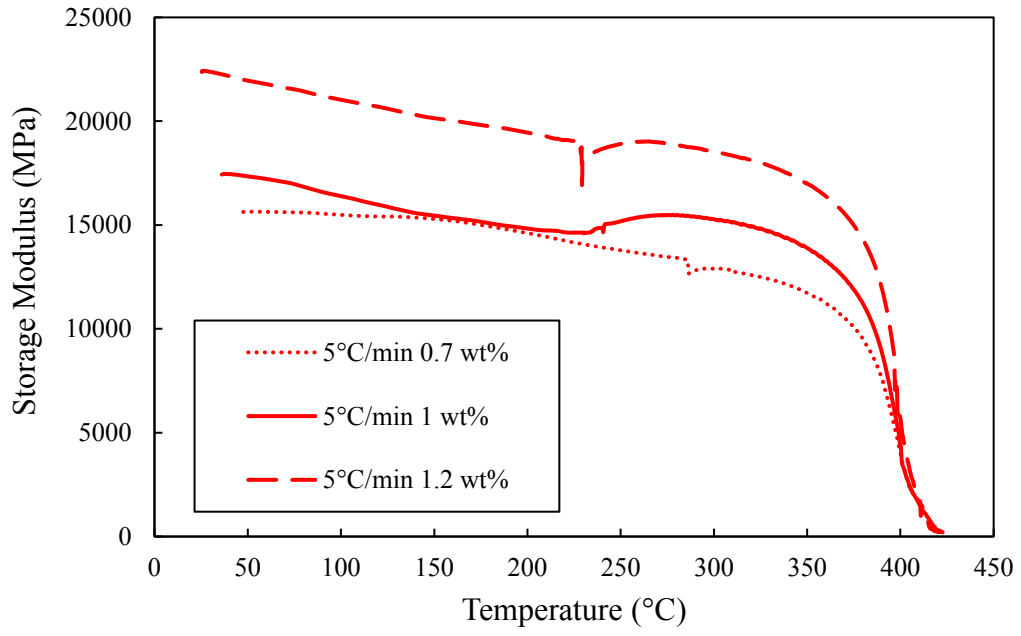

Figure 42. Anomalous descent in storage modulus vs. temperature at a constant 5°C/min and increasing moisture content

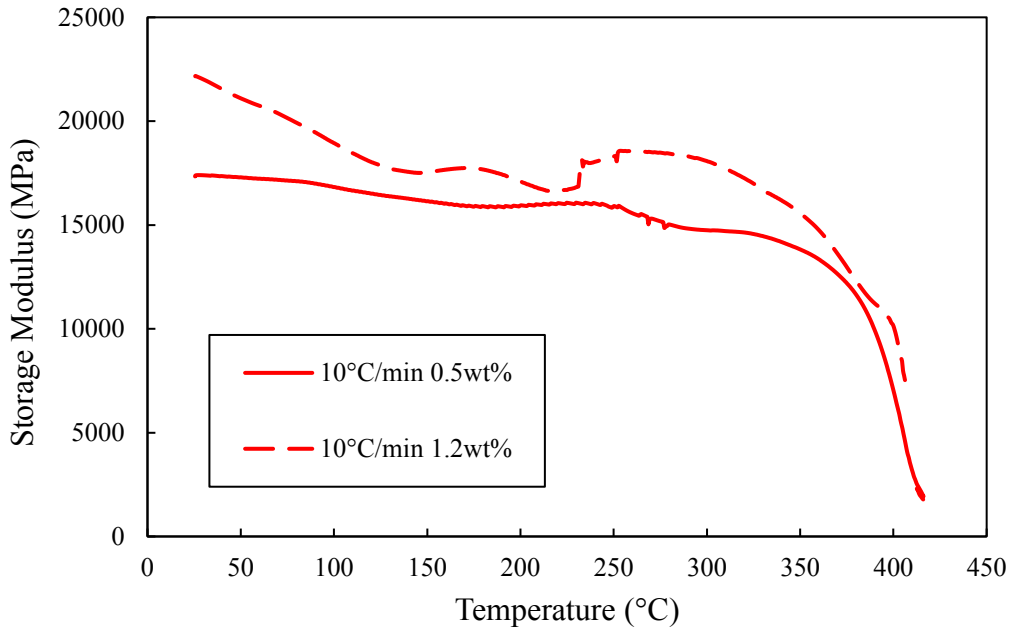

Figure 43. Anomalous descent in storage modulus vs. temperature at a constant 10°C/min and increasing moisture content

4.3.2 Flexural Test of BMI/quartz Laminates

Figure 44, Figure 45, and Figure 46 depict the flexural stress curves of 0%, 1.21% and 1.52% moisture content laminates, respectively, at BT and AT temperatures. In the dry case, after going through the designated temperatures, AT flexural strength is approximately 4.71% greater than BT. This is not the case in both the 1.21% and 1.52% laminates, where AT flexural strength is significantly lower. Strength between BT and AT in 1.21% and 1.52% laminates decreased by 10.05% and 7.97%, respectively. A comparison between flexure strengths and their respective BTs and ATs at each moisture content is shown in Figure 47. The 0% moisture content laminates showed no significant difference in strength with their respective BT, but as previously mentioned, AT is greater. On the contrary, flexure strength decreased for the water-contaminated laminates and the

loss in strength was at most 26%. Flexure failure of coupons at 1.52% moisture content are shown in both Figure 48 and Figure 49, which are representative of physical failure of tested samples.

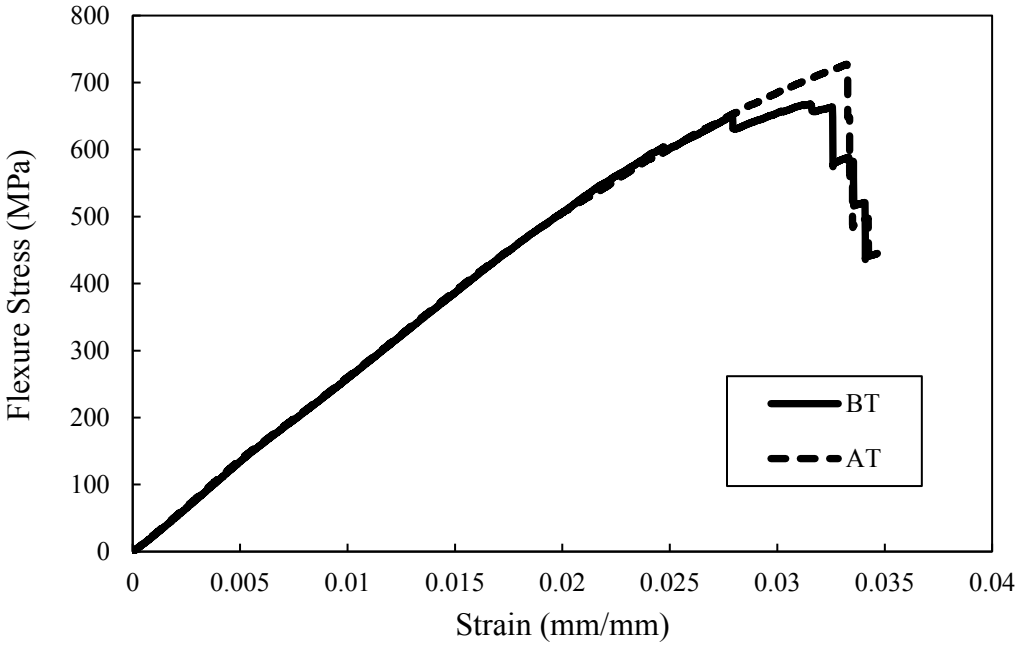

Figure 44. BT and AT experimental flexure stress vs. strain for dry laminates

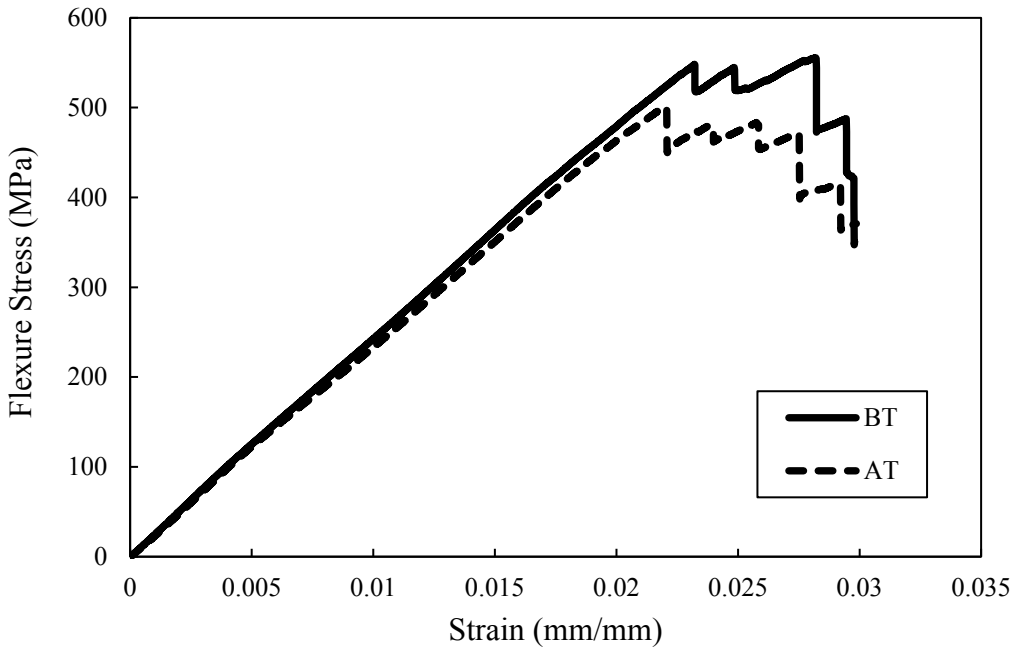

Figure 45. BT and AT experimental flexure stress vs. strain for 1.21% moisture content laminates

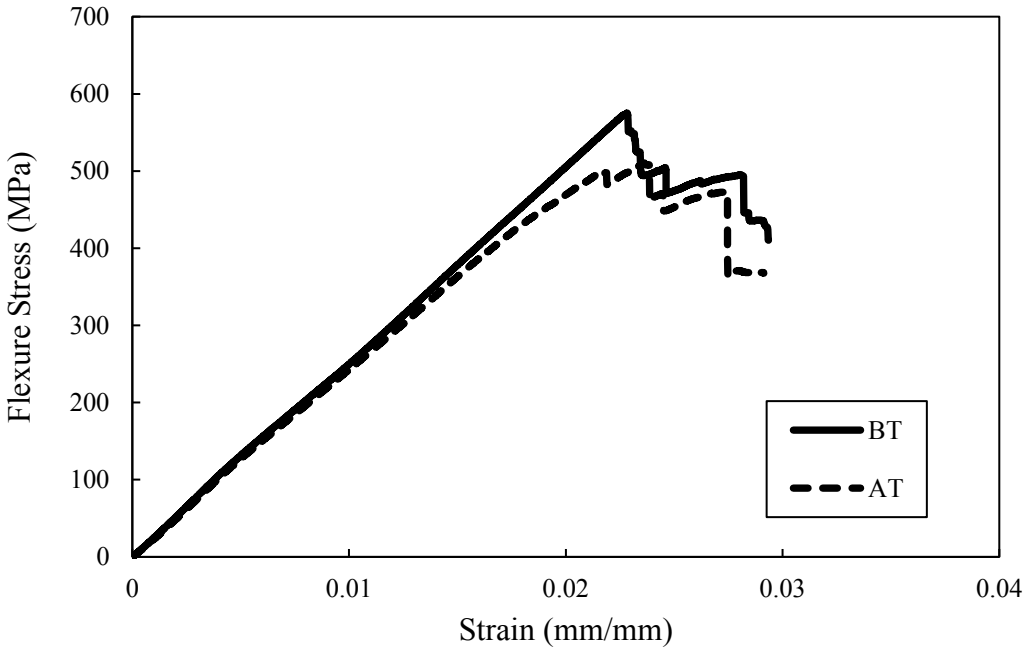

Figure 46. BT and AT experimental flexure stress vs. strain for 1.52% moisture content laminates

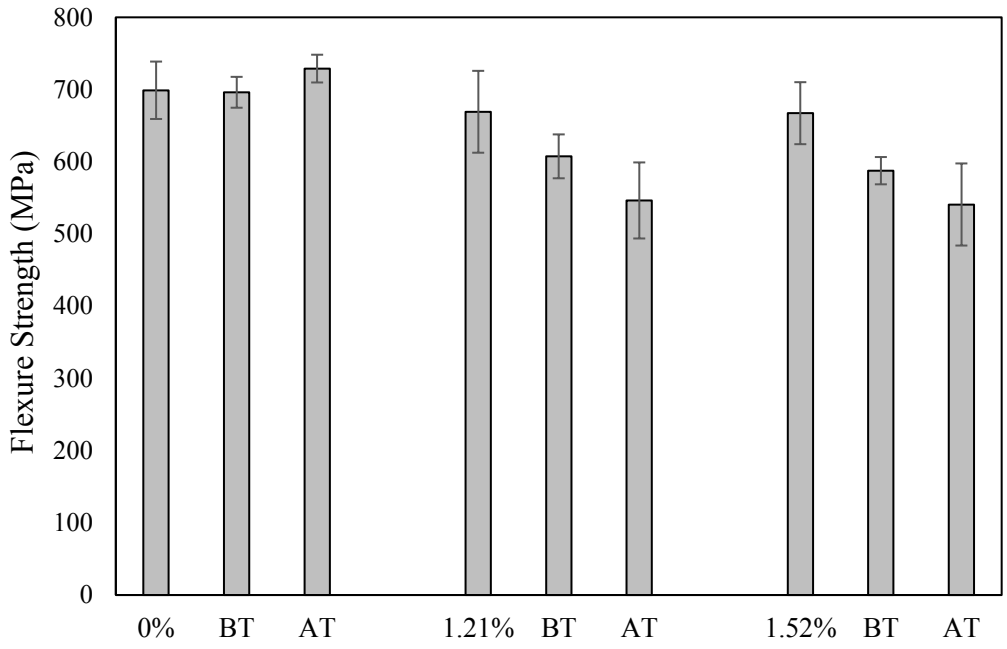

Figure 47. Flexure strength of 0%, 1.21 %, and 1.52 % laminates compared with strengths before (BT) and after (AT) anomalous drop in storage modulus

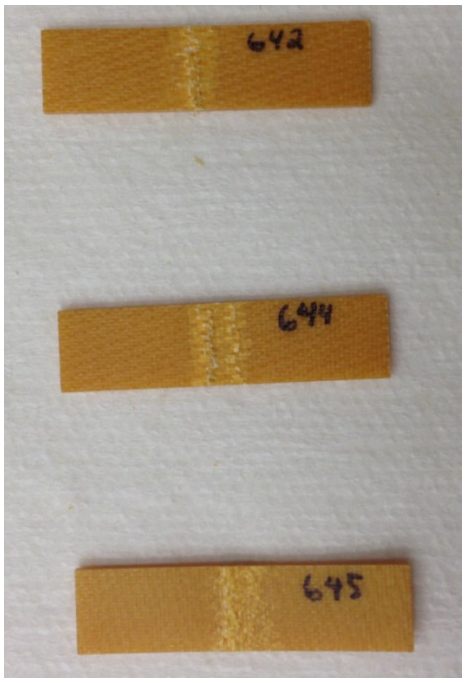

Figure 48. Compression area of BMI/quartz samples after flexural failure

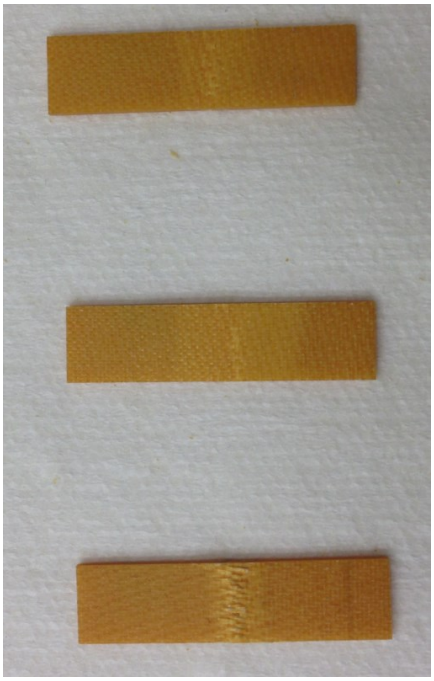

Figure 49. Tension area of BMI/quartz samples after flexural failure

A two-way analysis of variance with replication was performed to verify if there was a significant difference between all flexure strengths as a result of increasing temperature and water content. According to the statistical analysis and data gathered in Table 10, there is a significant interaction on flexure strength due to the increase of both moisture content and temperature. The confidence interval used is 95%, therefore the significance level or the probability of rejecting the null hypothesis is 5%. If the p-value (the probability of acquiring the same results from the experiment if the null hypothesis is true) is lower or equal to the significance level, the null hypothesis is rejected. P-values in Table 10 are lower than the significance level, thus the null hypothesis is rejected, resulting in averages of flexure stress not being relatively similar and the interaction being significant. This further is clarified by the F-statistic, where F critical (F crit) is the limiting value of the F probability distribution of flexure stress in this analysis. Since F values are

all higher than F crit, the sample means are significantly different. Interaction plots of moisture/temperature and their effect on flexure strength are presented in Figure 50 and Figure 51. The 0% moisture curve in Figure 50 has the highest flexure strength. In the latter figure, the 1.21% and 1.52% constant moisture contents have analogous reductions in strength. Figure 51 shows the effect of constant temperature with increasing moisture content. The greatest flexural strength occurs at 0% moisture content and a temperature of 260 °C. When moisture content is increased at 260 °C, strength is the poorest when compared with 25 °C and 220 °C. Interaction plots denote that an increase in temperature at a constant moisture content had a similar degrading effect on both of the moisture-contaminated laminates. In addition, for increasing moisture content at constant temperature, degradation increased relatively but with a worse-case scenario at 1.52% moisture content and temperature of 260°C.

Table 10. Analysis of variance statistics

Source of Variation	F	P-value	F crit
Temperature	10.094	0.001	3.354
Moisture Content	27.015	0.000	3.354
Interaction	4.943	0.004	2.728

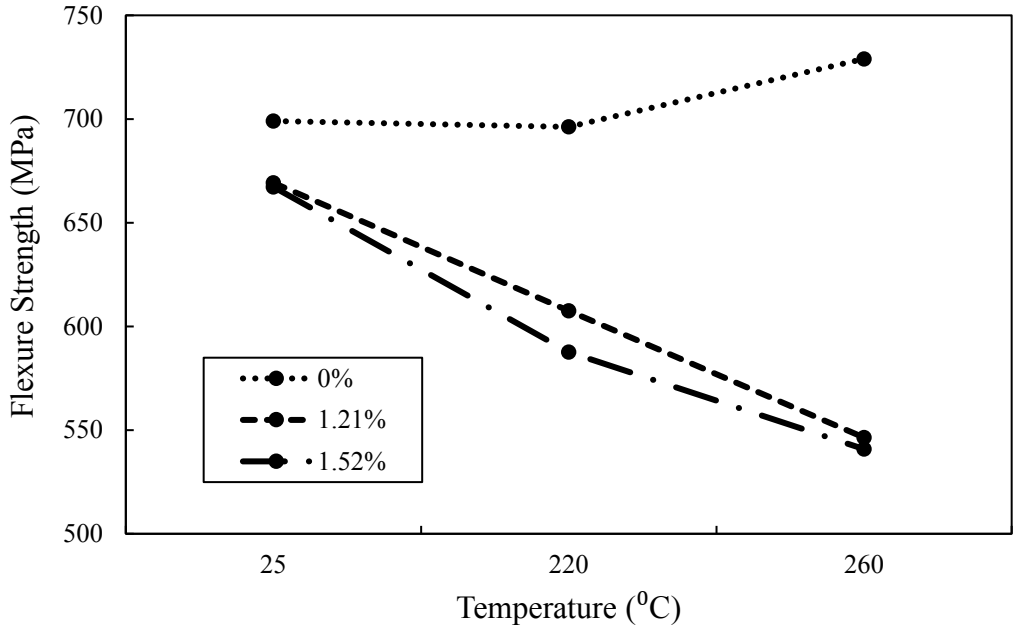

Figure 50. Effect of temperature increase on flexure strength at constant moisture content

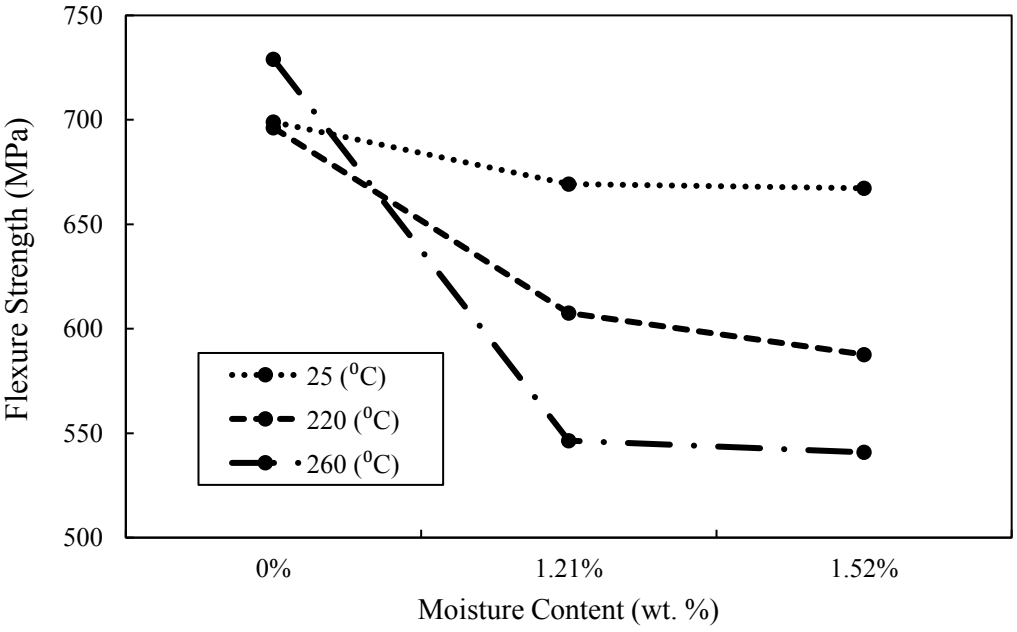

Figure 51. Effect of increasing moisture content on flexure strength at constant temperature.

4.3.3 Scanning Electron Microscopy

Scanning electron microscopy was performed on 1.21% and 1.52% BMI/quartz laminates with their respective BT and AT. Contaminated laminates were compared with an SEM image of a dry sample and are shown in Figure 52 and Figure 53. It is important to note that relatively few incidences of interphase debonding were found for each SEM image taken; the most significant are shown. AT laminates of 1.21% moisture content indicate signs of debonding at 260°C, but BT and no DMA laminates seem comparable to the dry. On the contrary, 1.52% laminates in all cases of contamination illustrate signs of debonding. Grace noticed that the contribution of debonds on the 1.52% case with no thermal analysis indicates slow non-Fickian behavior [52]. In the same study, flexure tests were performed where flexure strength decreased by 5% from dry to 1.52% moisture contaminated specimens. The addition of thermal energy at 220 °C causes wider debonding. At 260 °C, debonds become wider and multidirectional. Taken together, these results indicate that wider/multidirectional interphase separation and decrease in flexural strength play a significant role in the anomalous decrease in storage modulus.

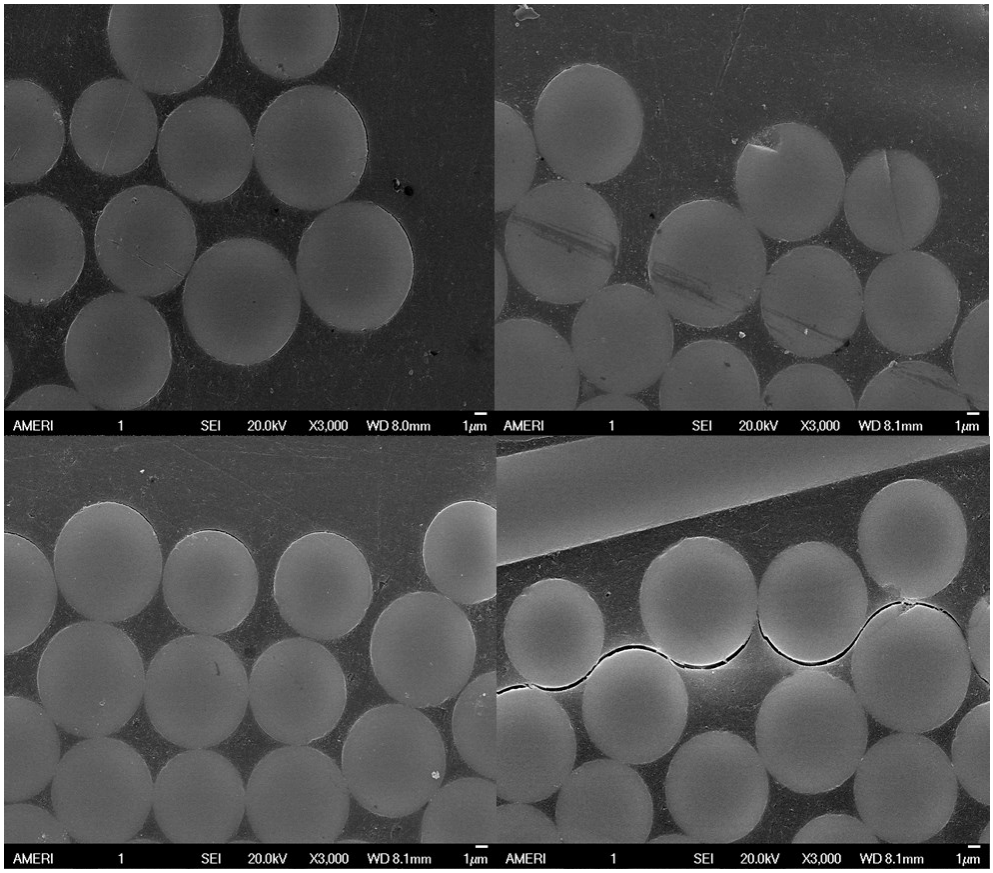

Figure 52. SEM images of BMI/quartz at 1.21% moisture content. Dry (top left), no DMA (top right), DMA 220 °C (bottom left), DMA 260 °C (bottom right)

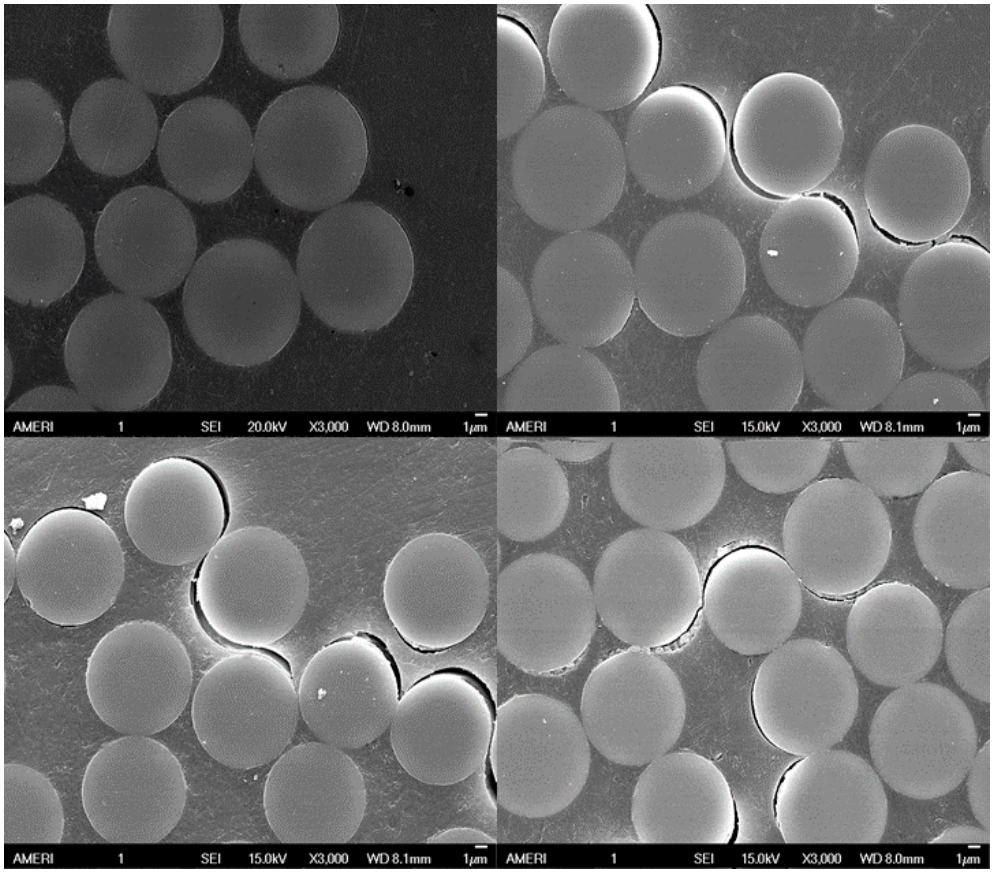

Figure 53. SEM images of BMI/quartz at 1.52% moisture content. Dry (top left), no DMA (top right), DMA 220 °C (bottom left), DMA 260 °C (bottom right)

Moreover, further analysis of the polymeric quartz composite was performed to verify the significance of the coupled moisture-temperature degradation. SEM micrographs of BMI/quartz specimens at approximately 1.20% moisture content that were taken to 220°C and 250°C in DMA are shown in Figure 54 and Figure 55, respectively. Micrographs taken represent a lengthwise cut at the mid-section of each specimen, that is, their length dimension points into the page. For a better perspective, specimens in both figures are displayed within white lines and are numbered. At 220°C, in Figure 54, three samples are shown and are numbered 1-3. The latter demonstrates no signs of debonding or delamination within each sample. The gap in temperature was narrowed down to get a

more accurate origin of debonding with respect to temperature. Contrarily to Figure 54 and in support of the anomalous descent in storage modulus, samples at 250°C in Figure 55 notably exhibit debonding and delamination in their mid-section. Degradation of the BMI composite is shown between the red lines of both samples in the latter figure. Of critical importance is the location of the delamination, which can be seen in Figure 56. Although SEM images were taken at the mid-section of the specimens as shown in the figure, it is believed that this type of degradation occurs along the length direction of the composite specimen.

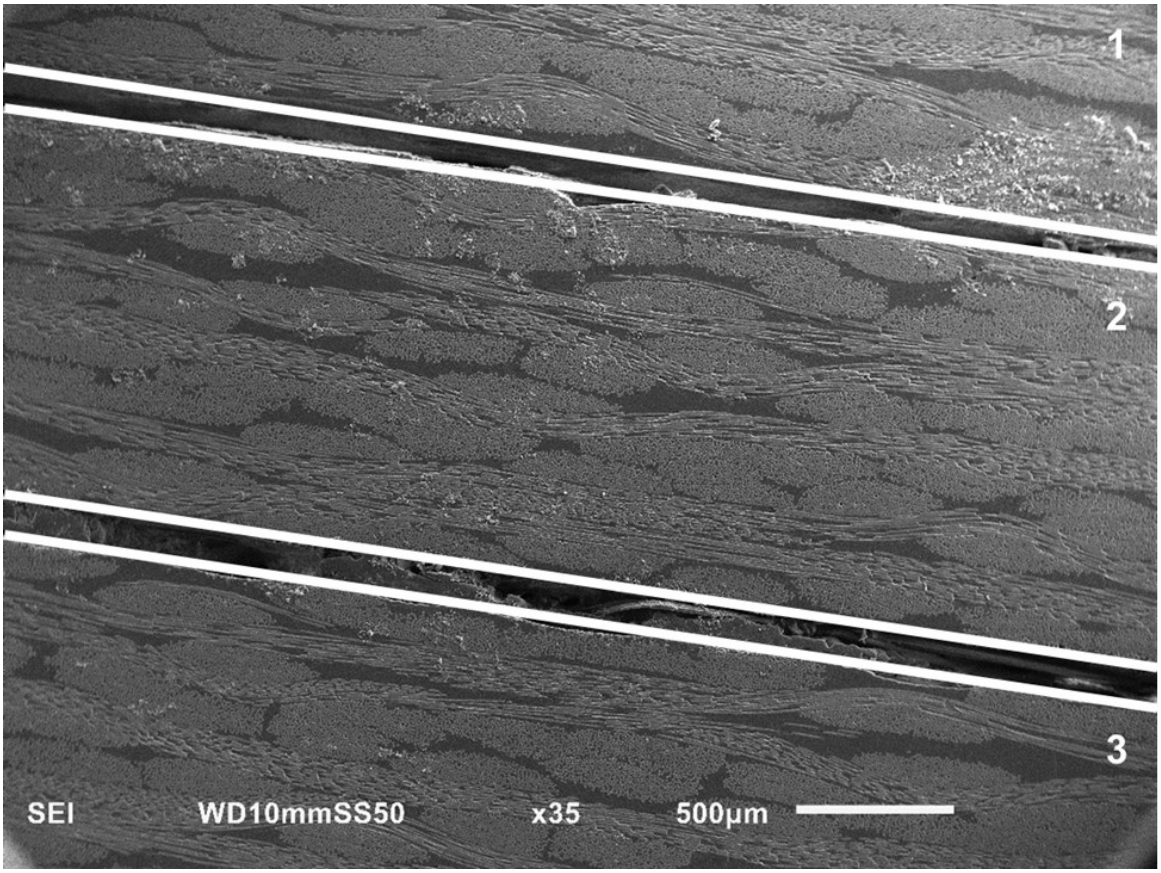

Figure 54. SEM images of BMI/quartz at 1.20% moisture content after DMA at 220°C

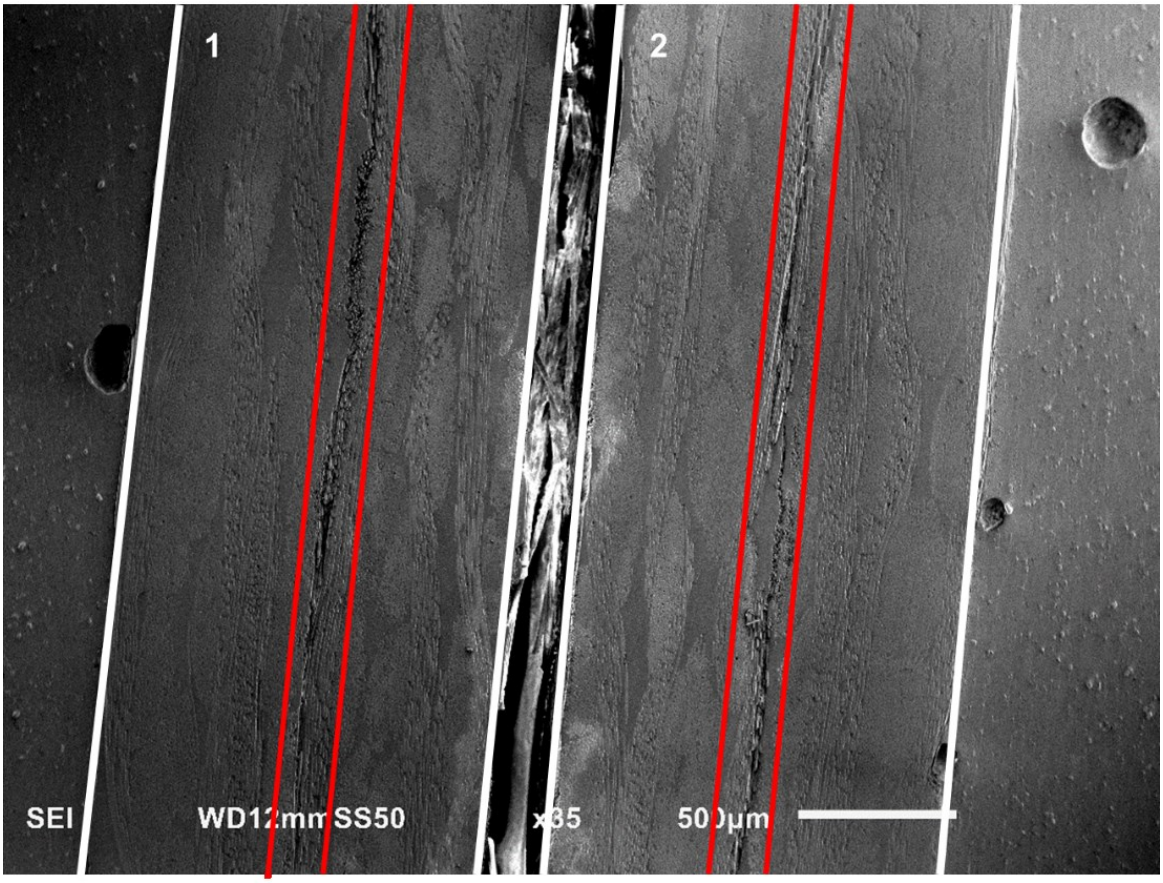

Figure 55. SEM images of BMI/quartz at 1.20% moisture content after DMA at 250°C

This result is justified by a measure of total thickness directly upon removal from the DMA. Thickness of a total of eight specimens, four at 220°C and four at 250°C were measured. Samples removed after 220°C showed no variation in thickness. Conversely, all samples extracted at 250°C exhibited an increase in thickness of about 1.67%. The increase in thickness is detrimental to radome performance, and compromises both dielectric thickness and structure integrity. The overall dilatational expansion may be indicative of steam pressure delamination [61].

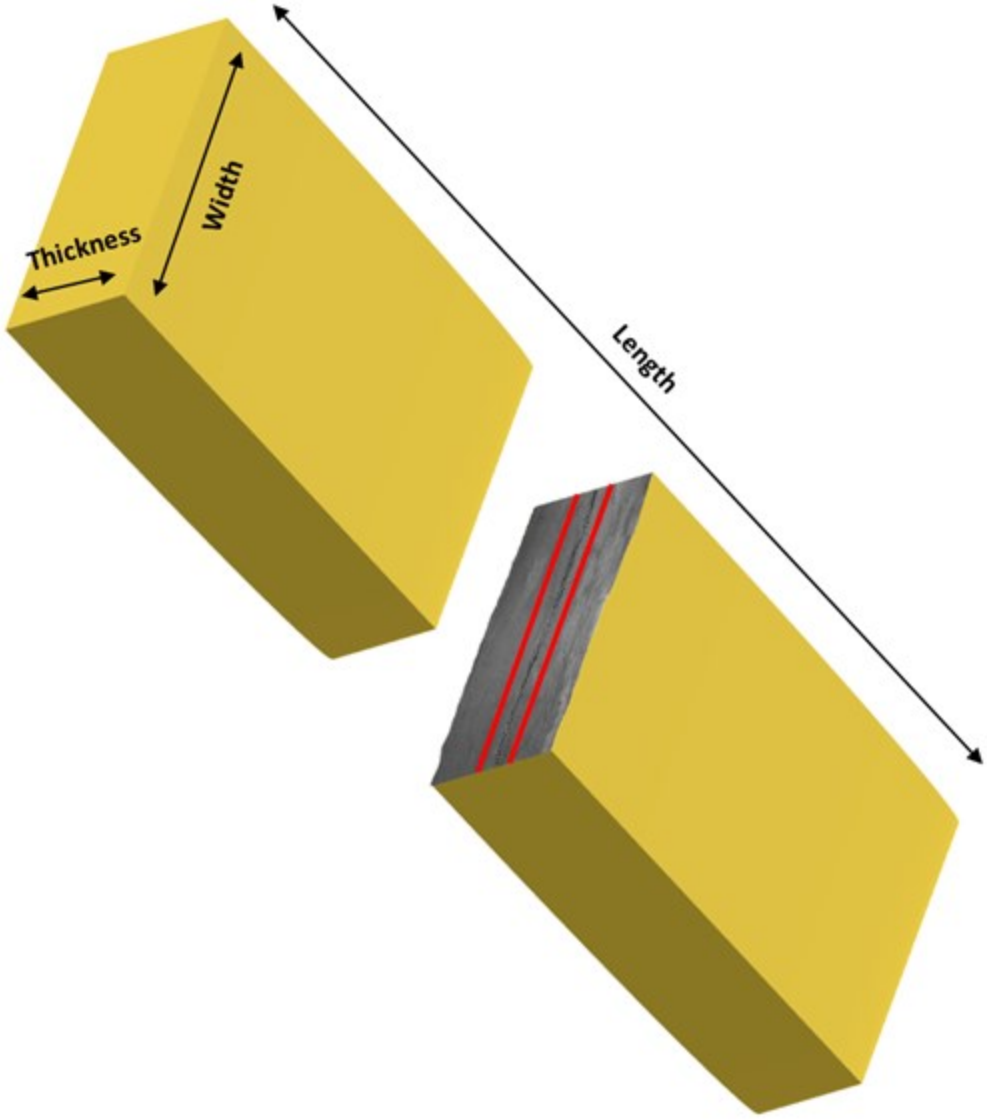

Figure 56. Representation of delamination in a BMI/quartz specimen

The synergistic effects of moisture and temperature have demonstrated their deleterious consequences on BMI/quartz radome material. Although the findings in this chapter are of paramount significance, the method of finding and determining debonding sites necessitates imperative acknowledgement. DMA, particularly its heating rate mechanism, was an instrumental tool in the discovery of the decrease in storage modulus before T_g is reached. Despite the use of the recommended ramp rate of 1°C/min for better accuracy of T_g and storage modulus curve, a rate of 5°C/min was applied. The adapted rate

instigated the necessary thermal shock that lead to the anomalous drop and debonds in the bismaleimide composite. Had a 1°C/min been exercised, as shown in Figure 40 and Table 9, no decreased in storage modulus would have been noticed.

4.4 Conclusion

Laminates under immersion were assessed via dynamic mechanical analysis, flexure examination, and microscopy tests to provide additional data of the deleterious impact on flexure properties before and after an anomalous decrease in storage modulus. This pre-glass-transition event is of invaluable importance for the sake of preventing catastrophic failure of aircraft radome structures. In addition to providing a further insight on the performance and service life of BMI/quartz as a radome composite, this study identified DMA as an invaluable tool for evaluating debonds in the composite material. To the best of our knowledge, the abnormal decrease in storage modulus on a BMI composite (before reaching T_g) has not been published.

CHAPTER 5: Langmuir Diffusion Model Evaluation of BMI/quartz at Different Immersion Temperatures

5.1 Langmuir Model and Arrhenius Correlation

During service conditions, aircraft composites may be exposed to a wide range of temperatures and various sources of moisture contamination. As a result, the temperature effects on moisture diffusion are of major concern to radome performance. Moisture ingress is known to be a thermally stimulated event and its dependence on diffusion coefficient can be articulated via the Arrhenius equation,

$$D_z = D_{zo} e^{-E_a/RT} \tag{33}$$

where D_z is the through thickness edge diffusivity in the z spatial direction, D_{zo} is the pre-exponential factor (diffusivity in the z spatial direction when temperature approaches infinity), E_a is the activation energy, R is the gas constant (8.314 J / mol·K), and T is temperature in Kelvin. The exponential in this equation denotes the strong correlation between diffusivity and T^{-1}. Therefore, adherence to the Arrhenius relationship is of particular significance in regards to predicting moisture content during the service life of a fiber-reinforced composite.

In this chapter, the one-dimensional hindered model (Langmuir-type model) from Equation (15) will be used to predict moisture content at any given point in time. Samples of different planar areas (55 x 55, 34 x 34, and 14 x 14 mm) were immersed in temperatures of 25°C, 37°C, and 50°C are examined in order to characterize the diffusion temperature dependent behavior of the bismaleimide composite. Furthermore, the Arrhenius equation

is applied to the diffusivities recovered, in order to verify the accuracy of the Langmuir model predictions.

5.2 Experimental Set Up of BMI/quartz

5.2.1 Material Machining

The material used was the same as for the previous chapter: A six-ply BMI matrix embedded with an eight-harness satin weave quartz fabric, style 581, trade name HexPly® F650 [10]. The balanced, quartz reinforce fabric laminates were machined into three different aspect ratios from the manufacturer's panel by the use of a wet diamond saw as shown in Figure 57. The dimensions of the machined samples were chosen to provide three significantly different ratios between planar surface and edge surface area. A total of 45 samples were cut to area aspect ratios of 20, 12.5, and 5 with planar dimensions of 55 x 55, 34 x 34, and 14 x 14 mm respectively. Each individual set of ratios contained 15 test samples with a thickness of 1.35 mm.

5.2.2 Environmental Conditioning

Following sample machining, samples were dried at 80°C by vacuum oven and stored in a desiccator in order to remove all residual moisture. After removal from oven and desiccator, dry samples were weighed and measurements were recorded. Five samples of each aspect ratio were subsequently fully immersed in distilled water and placed in constant temperature water baths of 25°C, 37°C, and 50°C.

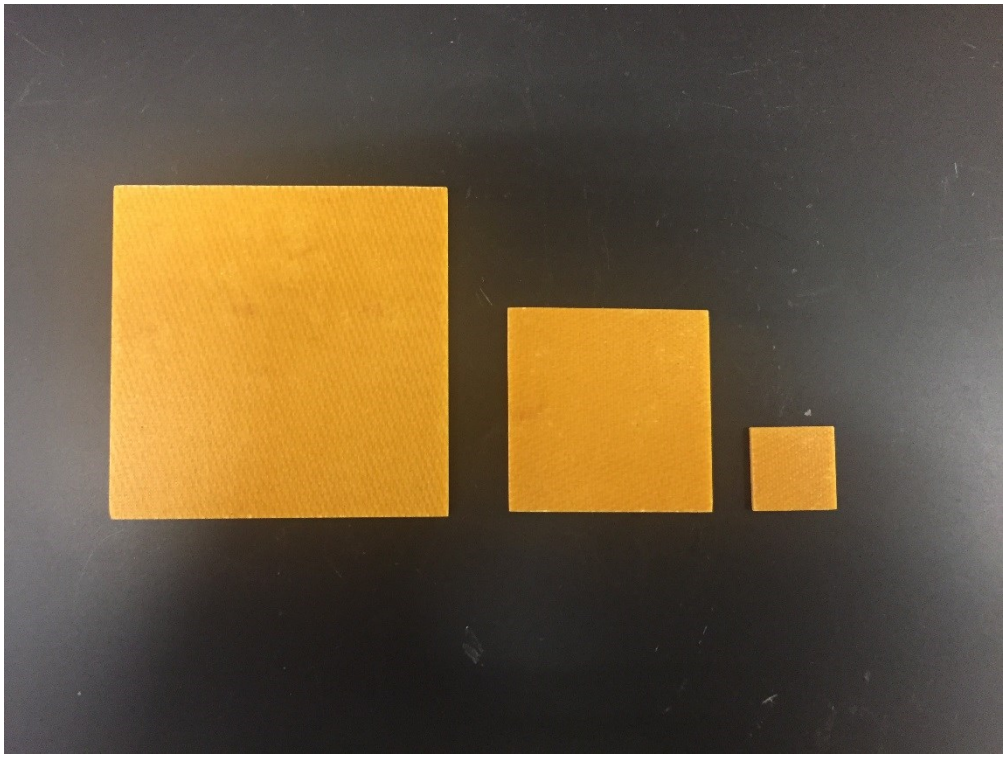

Figure 57. Machined BMI/quartz samples (55x55, 34x34, and 14x14 mm)

5.3 Modeling BMI/quartz Absorption Behavior

5.3.1 Langmuir Model

Non-conformity to the typical Fickian absorption behavior was expected for the BMI-quartz composite [19, 51, 52]. The concentration profiles and the absorption dynamics ($D_z, M_\infty, \beta, \gamma$) of BMI/quartz laminates in this chapter are predicted by the one-dimensional hindered model, repeated here from Equation (15), given by

$$M(t)_L = \frac{\beta}{\gamma+\beta} M_\infty \left(1 - \frac{8}{\pi^2}\sum_{p=0}^{\infty} \frac{1}{(2p+1)^2} e^{-\pi^2 t\left(D_z \frac{(2p+1)^2}{h^2}\right)}\right) + M_\infty \left(1 - \frac{\gamma}{\gamma+\beta} e^{-\beta t} - \frac{\beta}{\gamma+\beta}\right) \quad (34)$$

This approach was used instead of the three–dimensional hindered diffusion model due to the error between the experimental data and the model prediction. The failure of the 3D-HDM to recover model parameters is a consequence of temperature and the area aspect ratio, which is defined by

$$Area\ Aspect\ Ratio = \frac{Planar\ Area}{Edge\ Area} \tag{35}$$

This erroneous prediction is somewhat shown by Grace [51], where it was demonstrated that a significant difference in edge area between samples can lead to high error when recovering diffusion parameters.

The hindrance model was applied to the experimental data using a least-squares regression scheme. This method involved the minimization of the following error function,

$$E(t) = \sum_{i}^{n} \left[M_i(t)_L - M_{iexp}(t)_L \right]^2 \tag{36}$$

where $M(t)_L$ is the theoretical moisture content predicted by the Langmuir model and $M_{iexp}(t)_L$ is the experimentally obtained moisture content. The model variables that contribute to the minimization of the error function are the through thickness diffusion coefficient D_z, moisture equilibrium content M_∞, the probability per unit time that a bound molecule will become mobile β, and the probability per unit time that a mobile molecule will become bound γ.

5.3.2 One-Dimensional Hindered Diffusion Model Predictions

The hindered diffusion scheme was implemented in MathWorks' Matlab® alongside the gravimetric data in order to recover the necessary parameters for the Langmuir fits. Parameters from 15 months of immersion and their hindrance coefficient are provided in Table 11. The proposed model demonstrated an excellent correlation with experimental moisture uptake data for all water immersed sample sets. All experimental data and their respective fits establish a linear uptake with a deviation from the Fickian equilibrium plateau. A 95% confidence interval was calculated and illustrated for all gravimetric data. In addition, the magnitudes of the induced moisture content measurement error, at any given time, are expressed via root-mean-square error (RMSE). Values of the RSME are provided in Table 12.

The six-ply data sets and their respective Langmuir fits at 25°C, 37°C, and 50°C are shown in Figure 58 - Figure 69. Similarly, individual error bars are also plotted with their corresponding planar dimensions. Figure 61, Figure 65 and Figure 69 depict plots of 25°C, 37°C, and 50°C, correspondingly. Each of the latter three figures contains a combination of 55 x 55, 34 x 34, and 14 x 14 mm sample sets, with error bars not shown for ease of visibility. The 14 x 14 mm experimental data exhibits a significant decline of pseudo-equilibrium and moisture equilibrium when compared to the associated higher dimensioned specimens. It can be observed that samples of 34 x 34 and 55 x 55 mm, have closely related moisture uptake trajectories at each corresponding temperature. Therefore, the lower pseudo-equilibrium for the 14 x 14 mm samples is indicative of the role that temperature and aspect ratio play with respect to diffusion with in the material. Similarly,

samples of 14 x 14 mm immersed at 50°C have an analogous moisture profile to that of the 34 x 34, and 55 x 55 mm samples immersed in the same temperature shown in Figure 69.

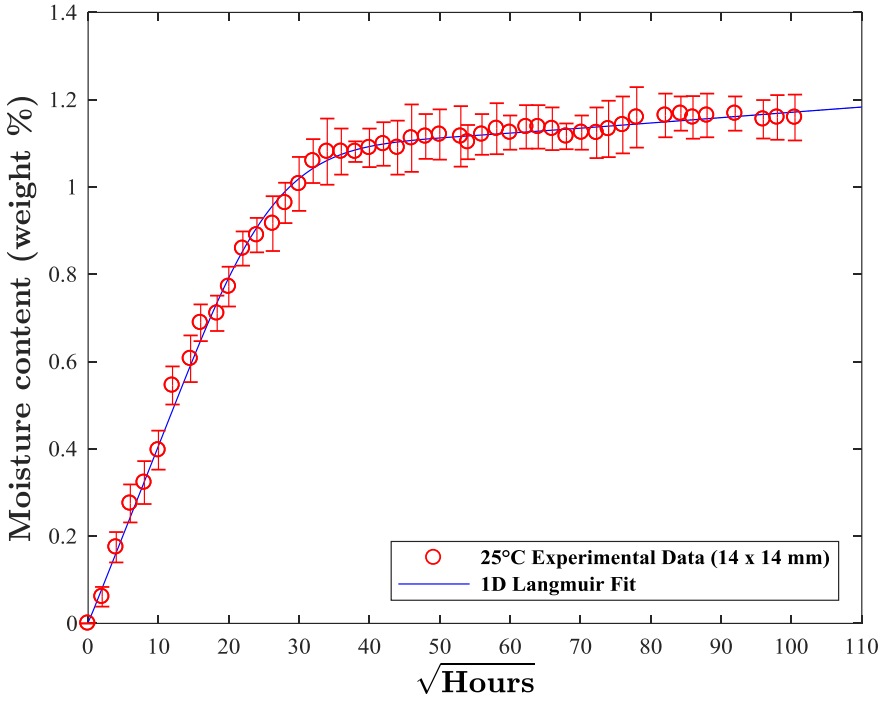

Figure 58. 1D Langmuir diffusion model prediction and corresponding gravimetric data for six-ply laminate samples of 14 x 14 mm planar dimensions immersed in 25°C distilled water

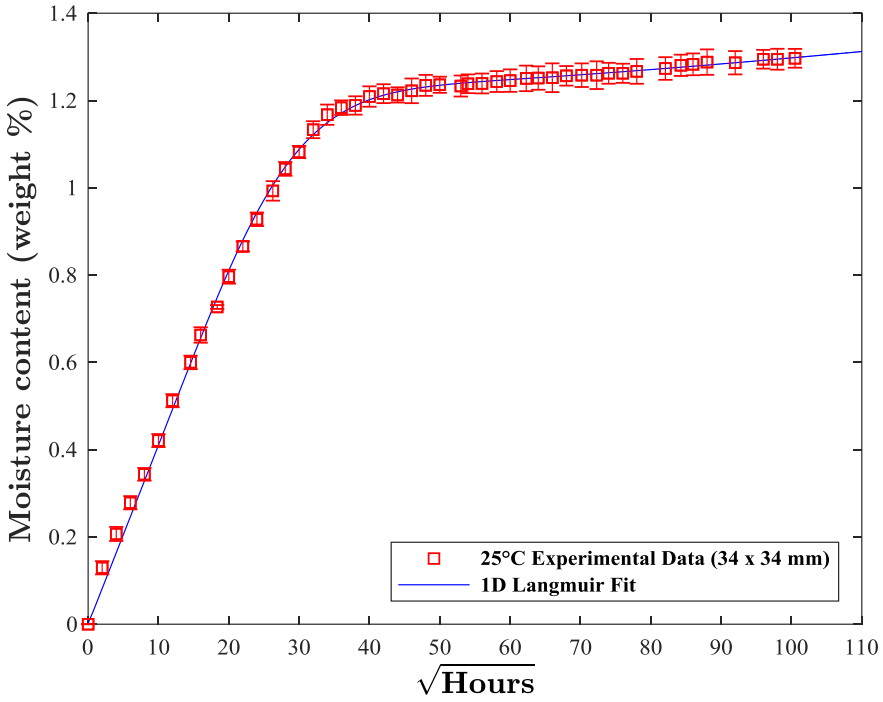

Figure 59. 1D Langmuir diffusion model prediction and corresponding gravimetric data for six-ply laminate samples of 34 x 34 mm planar dimensions immersed in 25°C distilled water

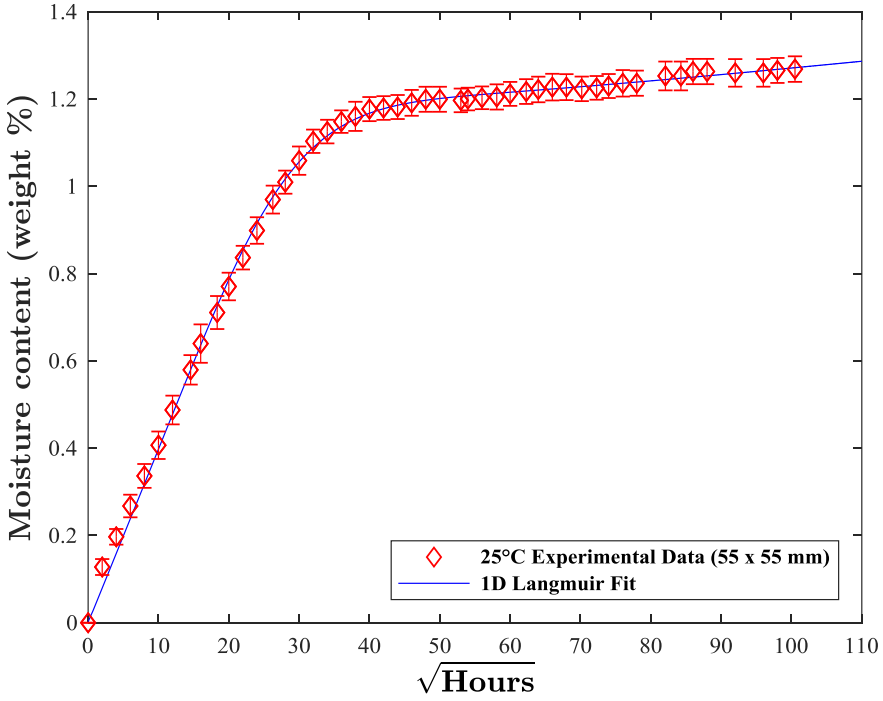

Figure 60. 1D Langmuir diffusion model prediction and corresponding gravimetric data for six-ply laminate samples of 55 x 55 mm planar dimensions immersed in 25°C distilled water

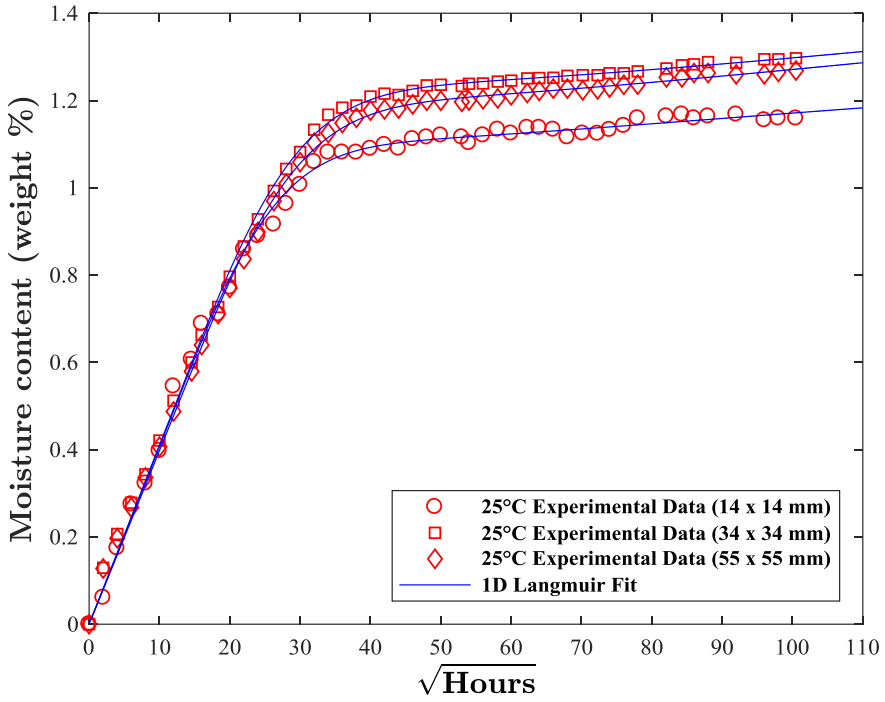

Figure 61. All immersed 25°C six-ply laminate samples 1D Langmuir diffusion model predictions and corresponding gravimetric data (without error bars)

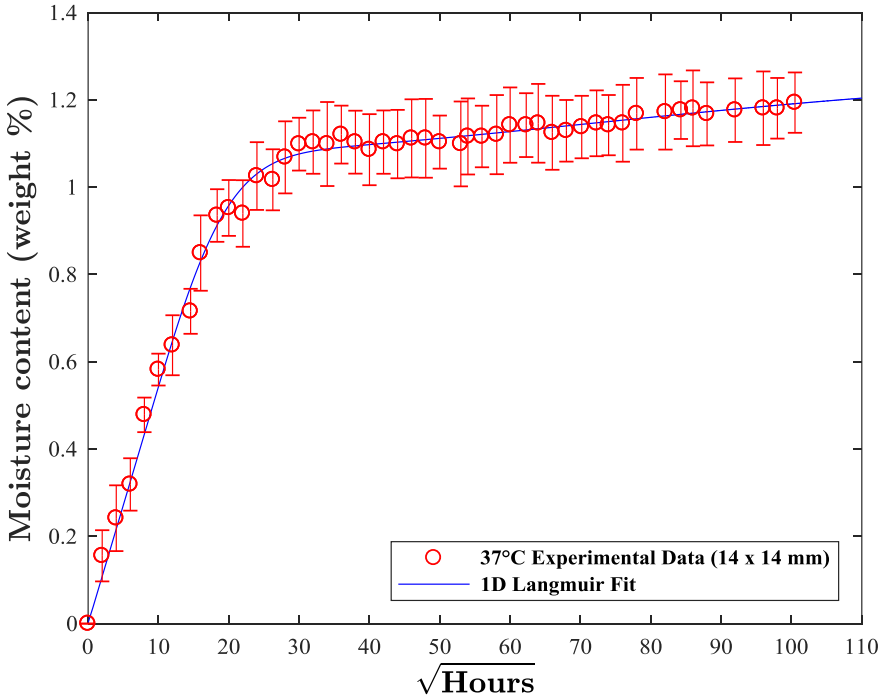

Figure 62. 1D Langmuir diffusion model prediction and corresponding gravimetric data for six-ply laminate samples of 14 x 14 mm planar dimensions immersed in 37°C distilled water

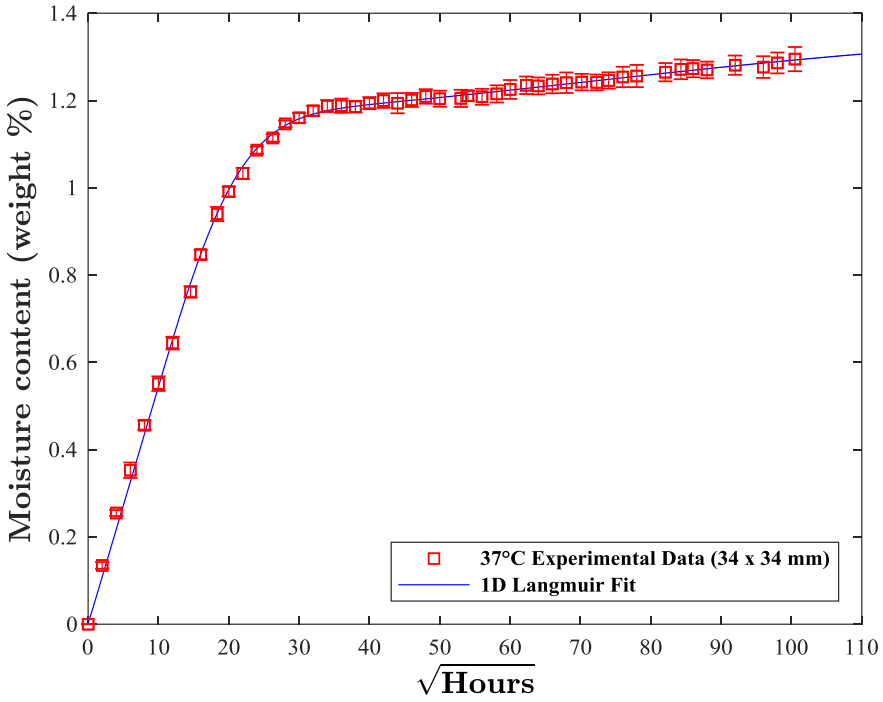

Figure 63. 1D Langmuir diffusion model prediction and corresponding gravimetric data for six-ply laminate samples of 34 x 34 mm planar dimensions immersed in 37°C distilled water

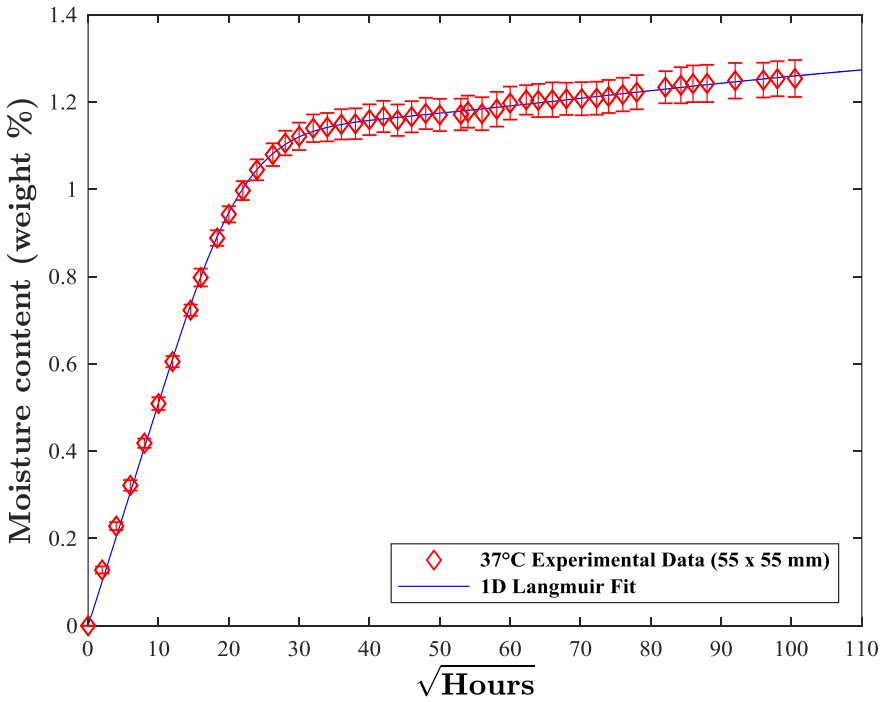

Figure 64. 1D Langmuir diffusion model prediction and corresponding gravimetric data for six-ply laminate samples of 55 x 55 mm planar dimensions immersed in 37°C distilled water

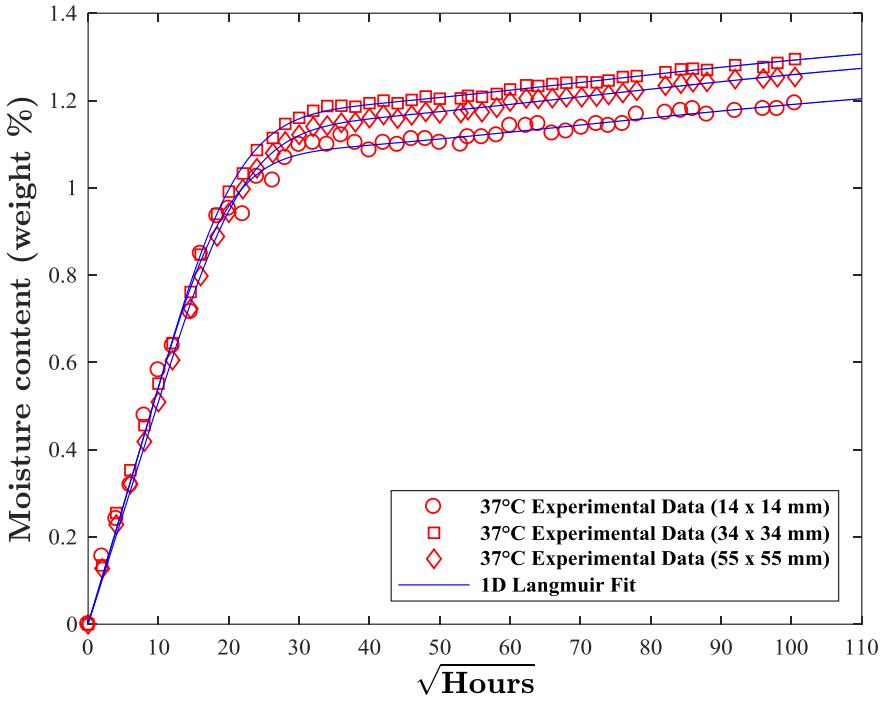

Figure 65. All immersed 37°C six-ply laminate samples, 1D Langmuir diffusion model predictions and corresponding gravimetric data (without error bars)

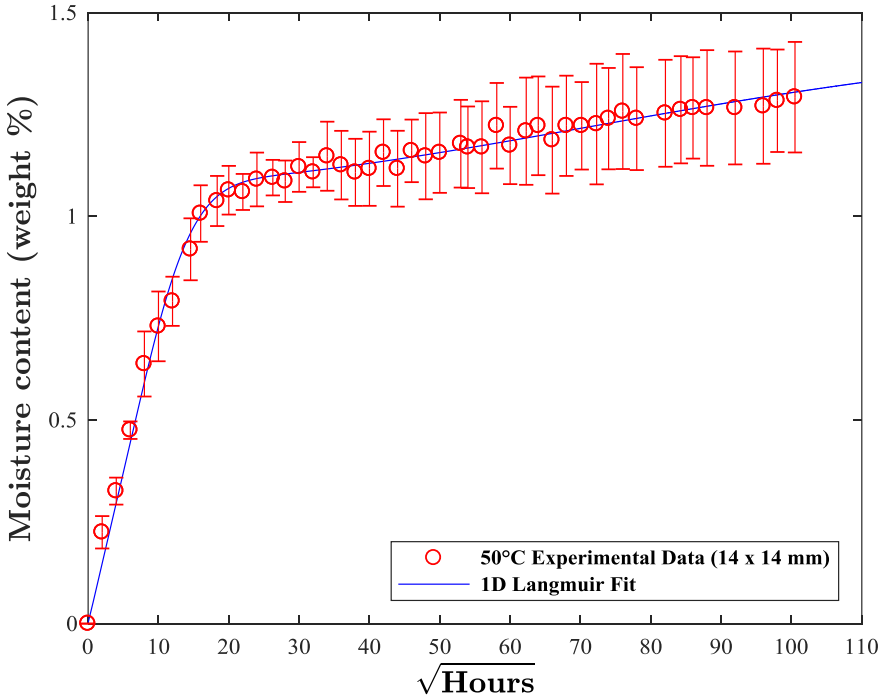

Figure 66. 1D Langmuir diffusion model prediction and corresponding gravimetric data for six-ply laminate samples of 14 x 14 mm planar dimensions immersed in 50°C distilled water

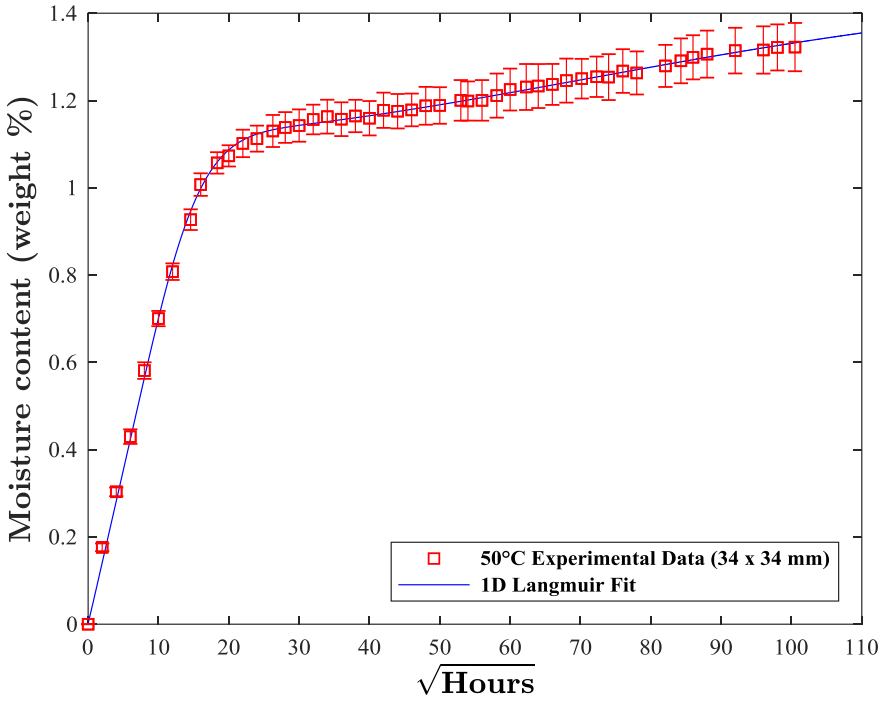

Figure 67. 1D Langmuir diffusion model prediction and corresponding gravimetric data for six-ply laminate samples of 34 x 34 mm planar dimensions immersed in 50°C distilled water

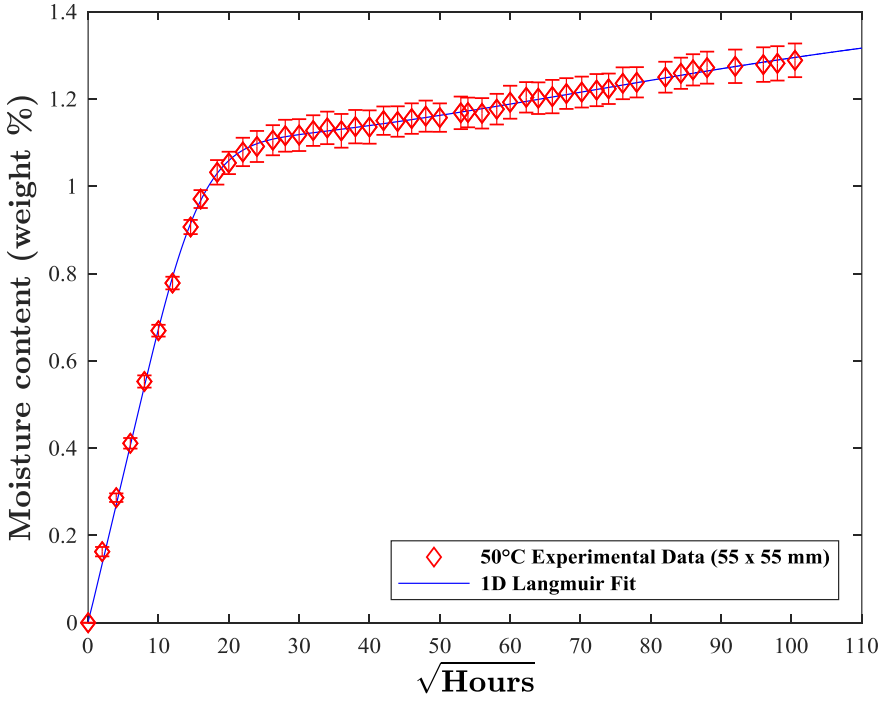

Figure 68. 1D Langmuir diffusion model prediction and corresponding gravimetric data for six-ply laminate samples of 55 x 55 mm planar dimensions immersed in 50°C distilled water

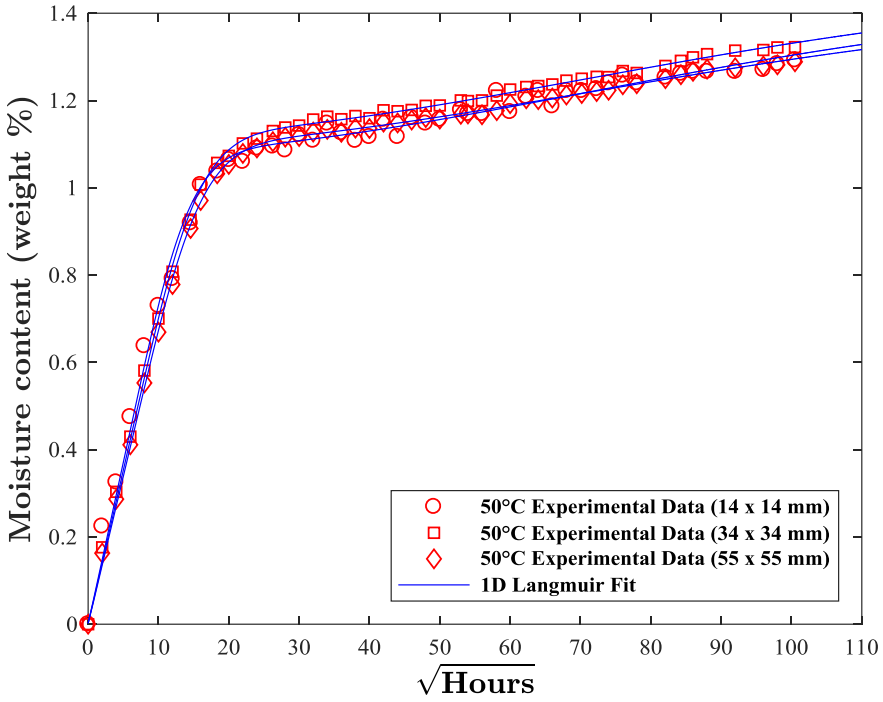

Figure 69. All immersed 50°C six-ply laminate samples 1D Langmuir diffusion model predictions and corresponding gravimetric data (without error bars)

The similar diffusion data for the bismaleimide composites is displayed distinctively in Figure 70, Figure 71, and Figure 72. In each plot, one planar dimension is shown at 25°C, 37°C, and 50°C. As expected, the thermally activated process demonstrates an acceleration in moisture ingress as a consequence of temperature increase. The thermal influence of the moisture behavior at each temperature allows for the application of the Arrhenius equation. Taking the natural logarithms of Equation (33) yields a linear relationship as shown by

$$ln(D_z) = ln(D_{zo}) - {}^{E_a}/_{RT} \tag{37}$$

As a consequence of linearizing Equation (33), the activation energy and pre-exponential can be determined by generating a plot of the natural logarithm of the through thickness diffusivity vs. the inverse of temperature. Acquiring the slope and the ordinate intercept of the Arrhenius fits in Figure 73 results in the activation energies and pre-exponentials for all three planar dimensions, which can be observed in Table 13. The range of activation energies gathered fall within the typical values of moisture diffusion in thermosets (35 to 50 kJ/mol) as demonstrated by Bao and Yee [84]. Their findings in BMI/carbon composites were comparable to E_a and D_{zo} parameters. Hence, the 1D Langmuir model demonstrates accurate predictions in regards to the temperature dependent diffusivities of the polymeric thermoset composite.

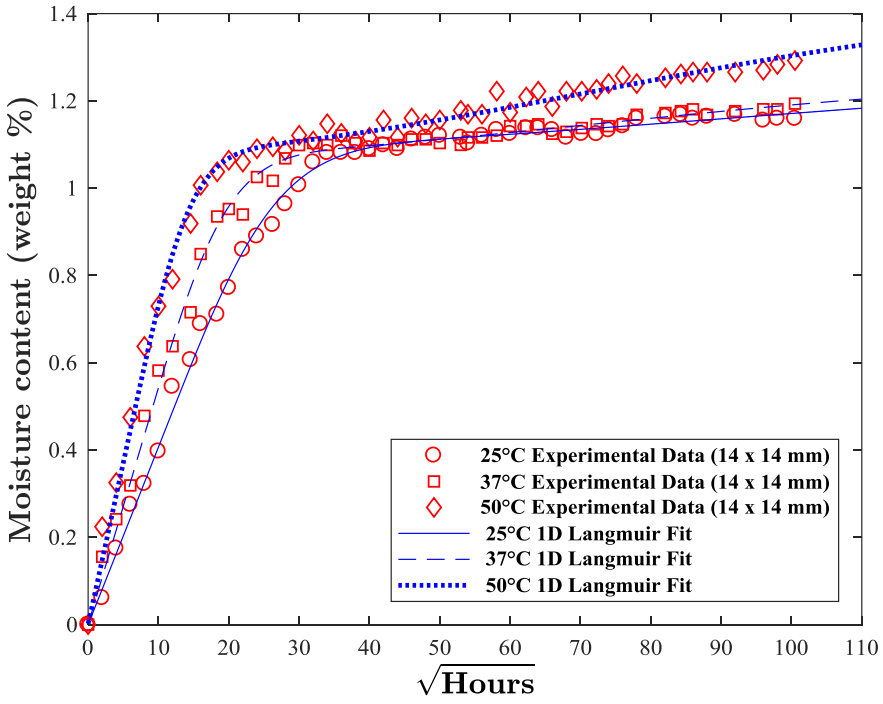

Figure 70. 1D Langmuir diffusion model predictions and corresponding gravimetric data for all six-ply laminate samples of 14 x 14 mm planar dimensions immersed at analogous temperatures

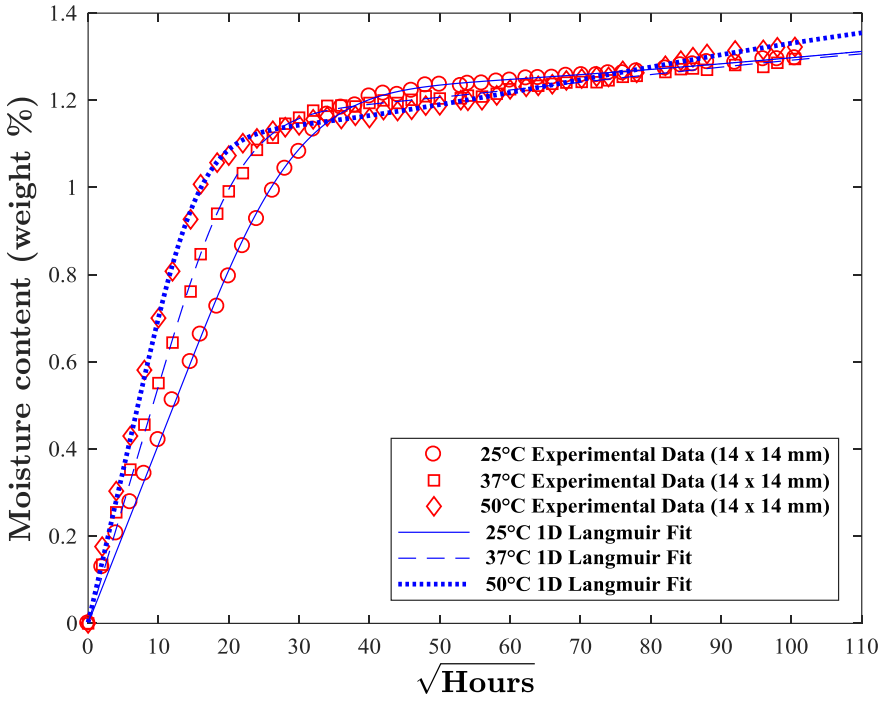

Figure 71. 1D Langmuir diffusion model predictions and corresponding gravimetric data for all six-ply laminate samples of 34 x 34 mm planar dimensions immersed at analogous temperatures

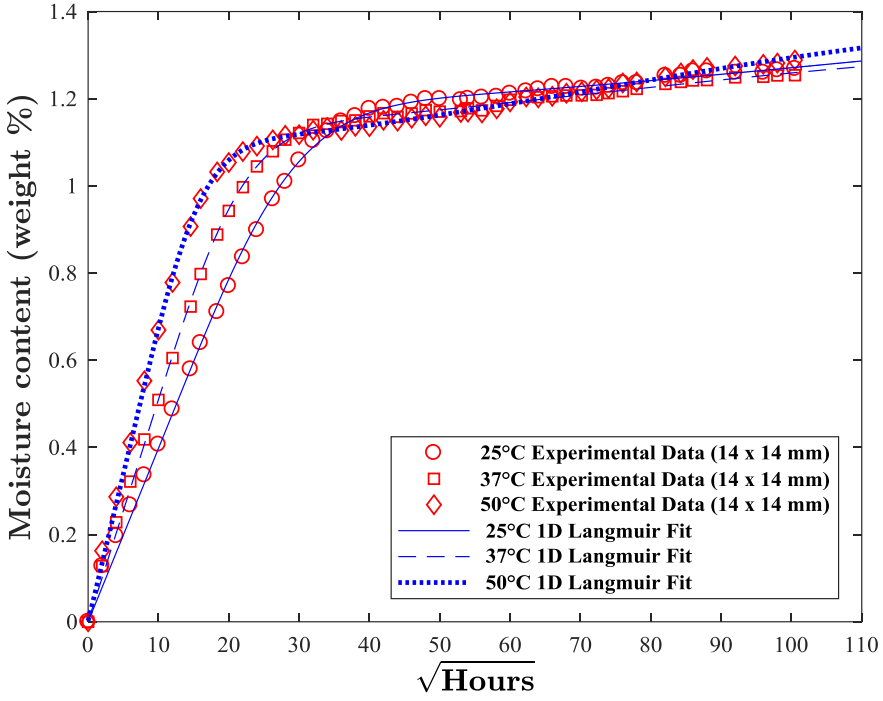

Figure 72. 1D Langmuir diffusion model predictions and corresponding gravimetric data for all six-ply laminate samples of 55 x 55 mm planar dimensions immersed at analogous temperatures

Table 11. BMI/quartz hygrothermal Langmuir parameters

Sample Sets	D_z *(mm^2/hr)*	β *(hr^{-1})*	γ *(hr^{-1})*	M_∞ *(wt. %)*	μ
25°C (14x14 mm)	4.98×10^{-4}	6.04×10^{-5}	1.03×10^{-5}	1.272	0.855
25°C (34x34 mm)	4.05×10^{-4}	2.47×10^{-5}	7.49×10^{-6}	1.586	0.767
25°C (55x55 mm)	4.05×10^{-4}	3.59×10^{-5}	9.30×10^{-6}	1.485	0.794
37°C (14x14 mm)	9.17×10^{-4}	9.94×10^{-5}	1.79×10^{-5}	1.262	0.848
37°C (34x34 mm)	7.81×10^{-4}	1.00×10^{-4}	1.78×10^{-5}	1.368	0.849
37°C (55x55 mm)	7.23×10^{-4}	9.71×10^{-5}	1.79×10^{-5}	1.338	0.844
50°C (14x14 mm)	1.69×10^{-3}	1.00×10^{-4}	3.32×10^{-5}	1.435	0.751
50°C (34x34 mm)	1.43×10^{-3}	1.00×10^{-4}	3.07×10^{-5}	1.457	0.765
50°C (55x55 mm)	1.37×10^{-3}	9.83×10^{-5}	2.90×10^{-5}	1.415	0.772

Table 12. Moisture equilibrium and RSME

Sample Sets	M_∞ *(wt. %)*	$RSME$
25°C (14x14 mm)	1.272	1.75×10^{-2}
25°C (34x34 mm)	1.586	1.33×10^{-2}
25°C (55x55 mm)	1.485	1.29×10^{-2}
37°C (14x14 mm)	1.262	2.06×10^{-2}
37°C (34x34 mm)	1.368	1.03×10^{-2}
37°C (55x55 mm)	1.338	7.60×10^{-3}
50°C (14x14 mm)	1.435	2.27×10^{-2}
50°C (34x34 mm)	1.457	9.20×10^{-3}
50°C (55x55 mm)	1.415	7.10×10^{-3}

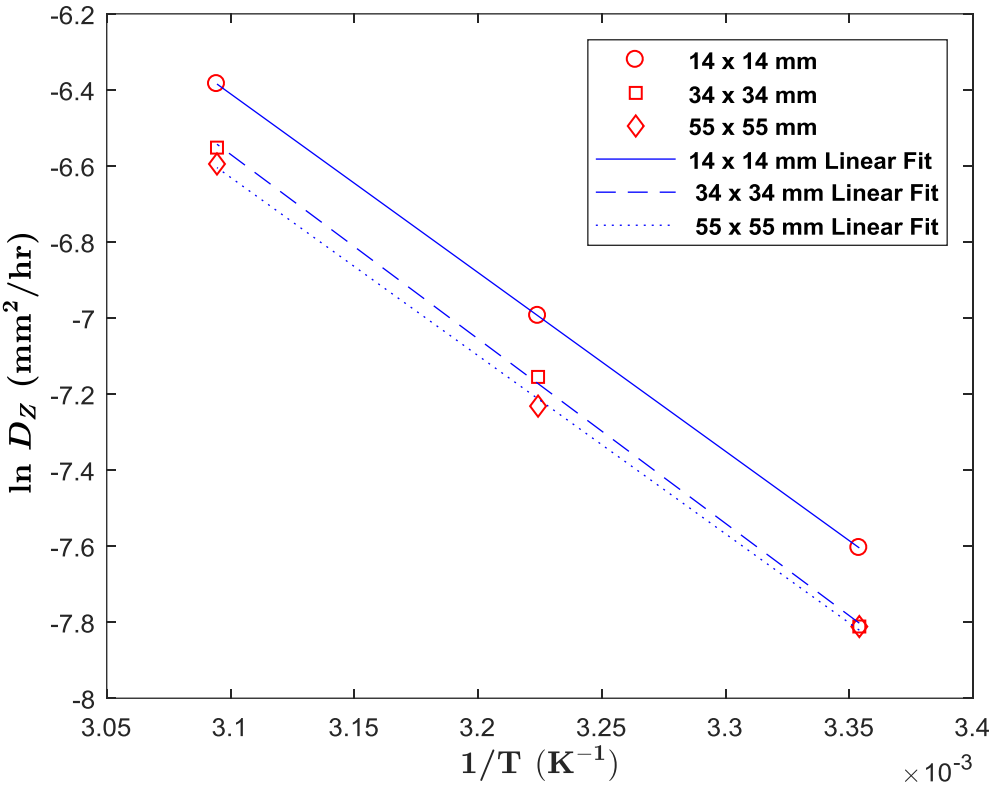

Figure 73. Arrhenius plot of each sample size at 25°C, 37°C, and 50°C with corresponding linear fits

Table 13. Activation energies and pre-exponentials with respective dimensions

Planar Dimension *(mm)*	E_a *(kJ/mol)*	D_{zo} *(mm^2/hr)*
14 x 14	39	3521
34 x 34	40	4811
55 x 55	38	2711

Final moisture uptake parameters are illustrated against temperature and planar dimensions in Figure 74-Figure 78. These plots demonstrate the dependence of moisture

absorption dynamics in regards to thermal variation and specimen sizing. The through thickness diffusivity, shown in Figure 74, is absolutely temperature dependent. Although the diffusion coefficient does not fluctuate significantly with planar dimensions, a slight increase in diffusivity for the 14 x 14 mm composites was observed at each temperature. This finding interestingly denotes the importance of the area aspect ratio during moisture absorption. The ratio of planar to edge area of 5 for the 14 x14 mm BMI/quartz material is significantly lower than 12.5 and 20 for that of the 34 x 34 and 55 x 55 mm samples, respectively. Grace [40] noticed a similar effect where diffusion through the edges (a long the fiber direction) in a 6-ply quartz-reinforced BMI composite is 11 times greater than through its thickness. For this reason, when planar area is reduced, additional moisture tends to enter the material through the edges than through the thickness direction.

Probabilities of molecular binding and unbinding are shown in Figure 75 and Figure 76, accordingly. Both β and γ have analogous behavior with increasing aspect ratio but vary with respect to temperature. The probability per hour that a bound molecule will become mobile, β, is noticed to be lower at 25°C with noticeably higher and slightly equivalent values at 37°C and 50°C. At the similar temperature of 25°C, the 14 x 14 mm composites have a greater β than their larger dimensioned specimen. The probability per hour that a mobile molecule will become bound, γ, is lowest at 25°C, with the greatest contribution to fluid flow dynamics at 50°C. Based on the β and γ plots of the 14 x 14 mm samples immersed at 25°C, water molecules are more likely to detach and not bind to polar sites in the bismaleimide matrix. This decrease in water-polymer chain attachment greatly clarifies the importance between temperature and area aspect ratio.

Long-term moisture content for the 6-ply BMI/quartz composite has been reported as 1.726 wt.% [52]. Moisture equilibrium values predicted by the 1D hindrance model are between 1.262 and 1.586 wt.%. The overall decrease in projected M_∞ and pseudo-equilibrium is attributed to the long-time (5 years) accumulation of moisture (in the form of humidity) of stored manufactured panels. These laminates, even if stored in hot and dry environments [122], have the propensity to absorb fluids. Although samples were dried according to ASTM D5229 [73] standards (until a moisture equilibrium dry weight was reached), the remains of strongly interconnected bound water may exist and higher activation of desorption is needed to remove excess moisture. Removal of excess water with higher temperatures may induce thermal cracking, oxidation, mass loss, or a combination of all three events [123]. In regards to the strongly interconnected bound water, hydrogen bonding can still occur with mobile water molecules. Nevertheless, laminates were all subjected to equivalent environmental conditions. Despite there being no consistent behavior in M_∞ prediction, a trend in increasing temperature was detected for the various dimensioned specimens. The 34 x 34 mm samples were noticed to have slightly higher M_∞ in all immersed temperatures. While a relatively greater equilibrium was noticed, it is difficult to conclusively correlate this result to temperature or area aspect ratio as more data may be needed to make a stronger verdict. In the case of all three different ratios under immersion at 50°C, similar moisture equilibrium contents were recovered. The equality in the results at 50°C are not surprising, as it is known that an increase in temperature causes an acceleration in the moisture absorption process, thus reaching equilibrium at a faster rate.

Hindrance values recovered in this study lie between 0.751 and 0.855. The projected 5-year value of μ, from Table 7, is 0.805, which is in close proximity to the predicted values for all temperatures and dimensions. The proximity of the predicted value strengthens the validity of 1D Langmuir model predictions. There is no significant variation or tendency identified in μ as shown in Figure 78. As in M_∞, more data is needed to determine the total effect of water as a result of temperature and area aspect ratio variations for the BMI/quartz composite.

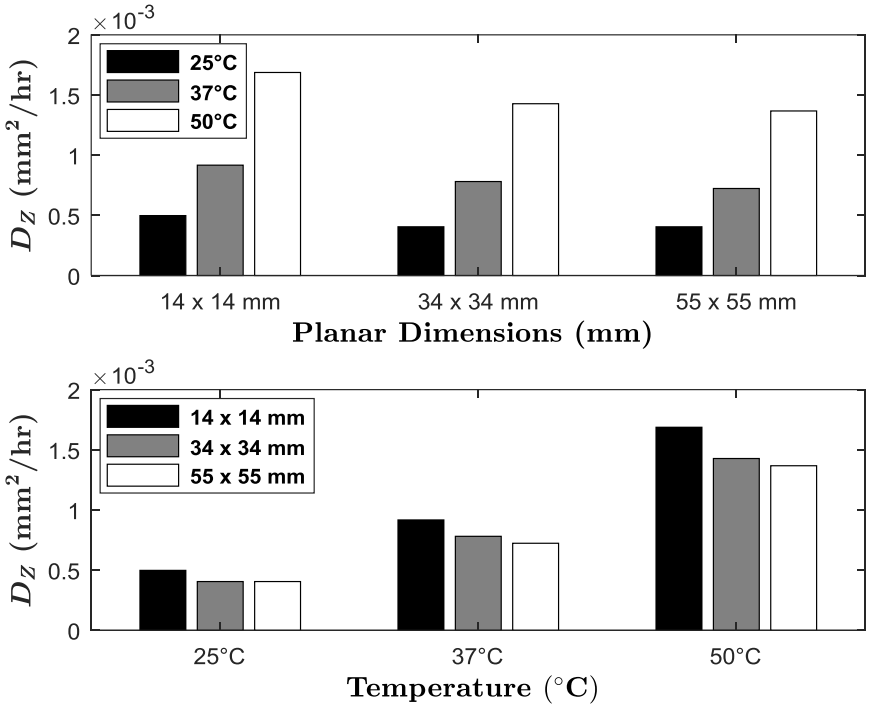

Figure 74. A comparison of all D_Z, planar dimensions, and submersion temperatures

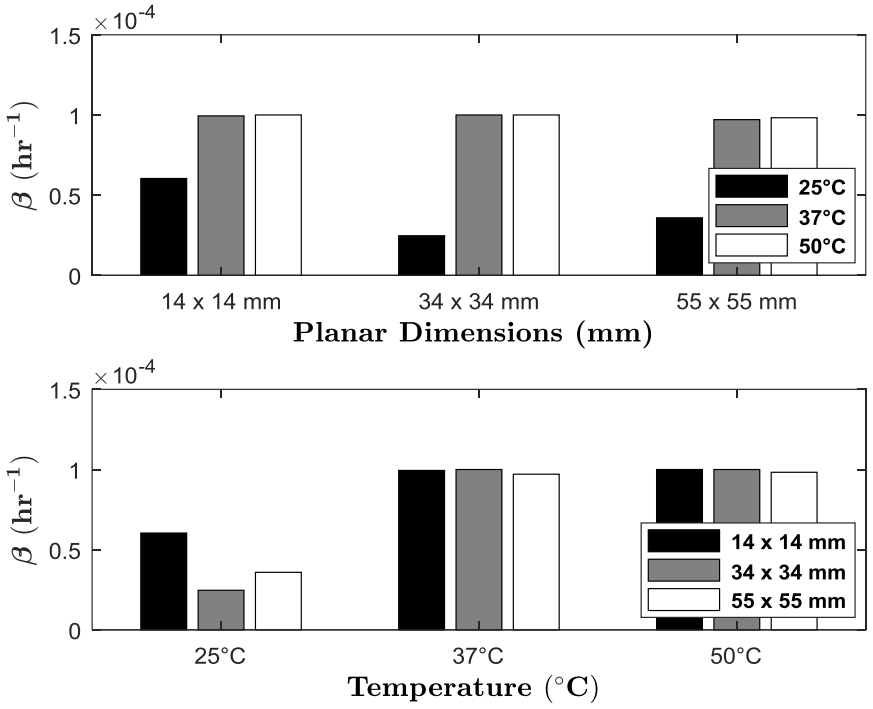

Figure 75. A comparison of all β, planar dimensions, and submersion temperatures

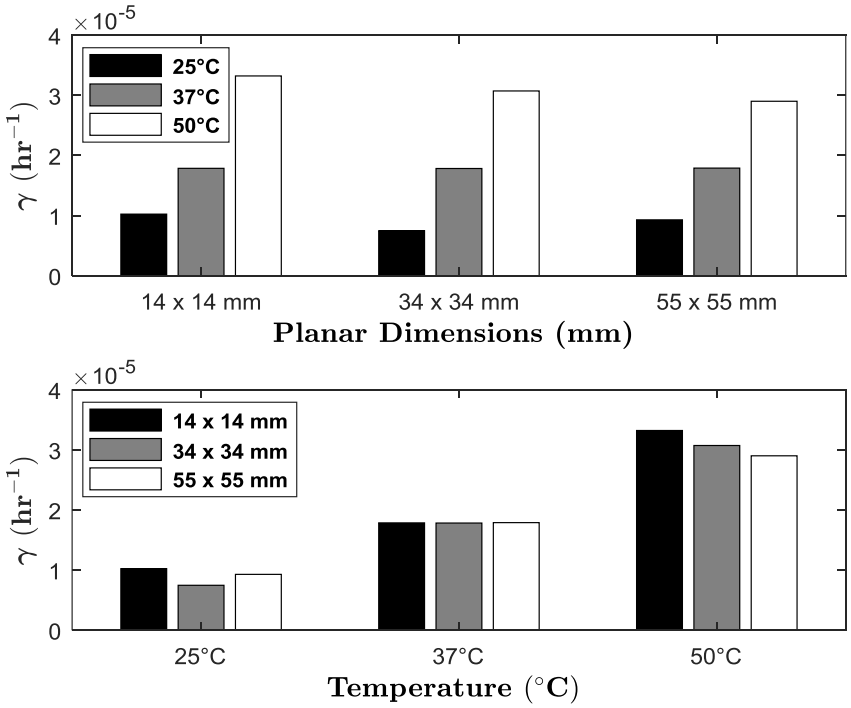

Figure 76. A comparison of all γ, planar dimensions, and submersion temperatures

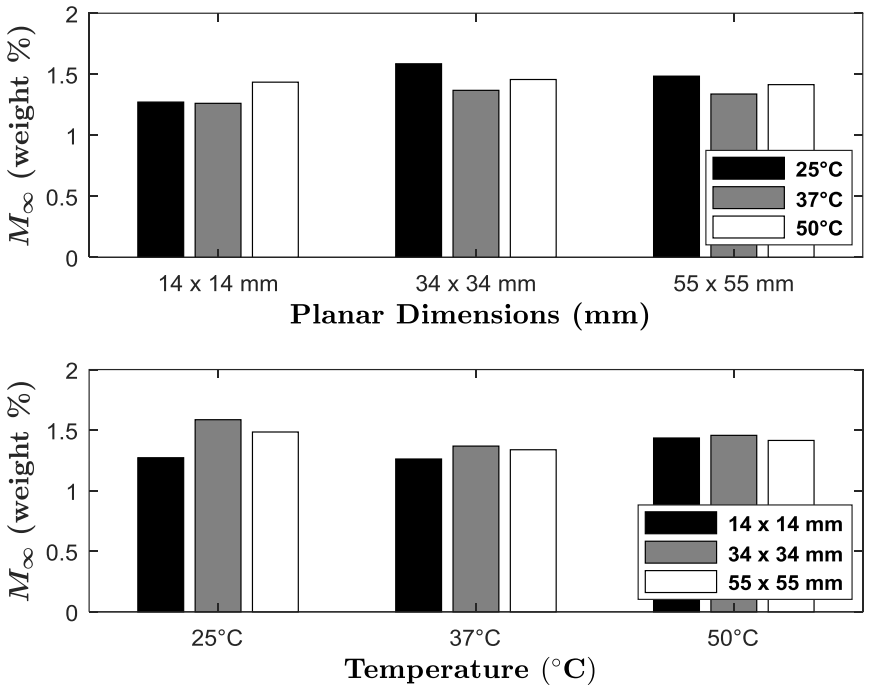

Figure 77. A comparison of all M_∞, planar dimensions, and submersion temperatures

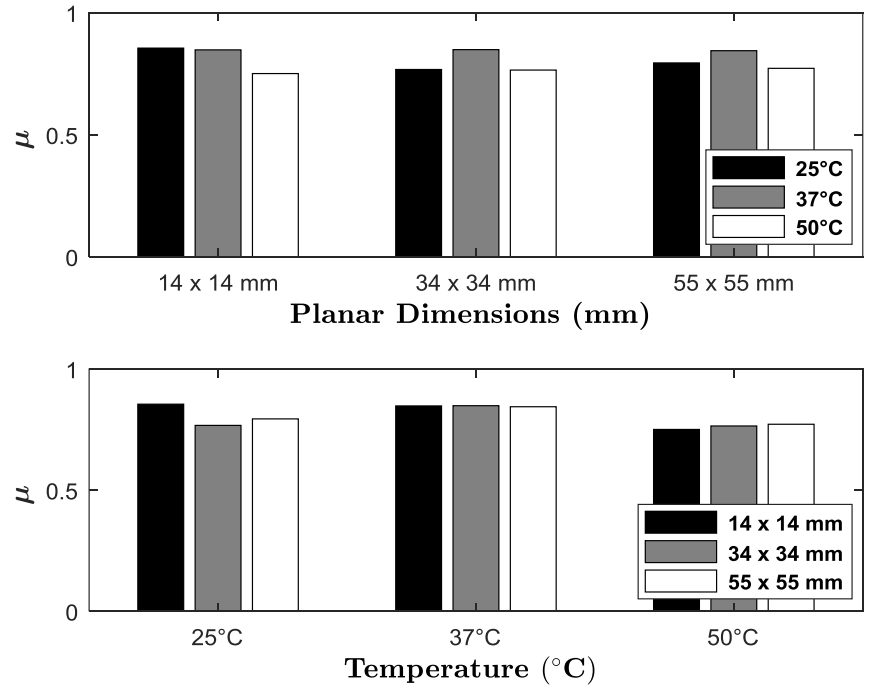

Figure 78. A comparison of all μ, planar dimensions, and submersion temperatures

5.4 Conclusion

The hygrothermal moisture absorption behavior of 6-ply quartz-reinforced bismaleimide laminates was monitored gravimetrically during a 15-month time frame at immersion temperatures of 25°C, 37°C, and 50°C. Samples undergoing moisture uptake were machined into dimensions of 55 x 55, 34 x 34, and 14 x 14 mm with corresponding ratios of 20, 12.5, and 5. The predictive one-dimensional hindrance diffusion model was implemented to reveal the nature of the moisture diffusion dynamics as a consequence of immersion temperature and specimen dimensioning. In combination with the hindrance model, a parameter recovery method employing least-squares regression was presented. The recovery method and the predictive model were both applied successfully to the water ingress data showing less than 1% error for the recovery of the non-Fickian parameters D_z, M_∞, β, and γ. In addition, RMSE values demonstrated excellent accuracy between the one-dimensional hindrance model and the experimental data.

Moisture absorption parameters exhibited a dependence on both area aspect ratio and temperature. A decrease in temperature from 50°C to 25°C was noticed to cause a reduction in the moisture uptake profile after pseudo-equilibrium for the 14 x 14 mm laminates, with area aspect ratio of 5. Samples with an area aspect ratio of 12.5 and 20 had no significant change in uptake profiles. For each area ratio, the diffusion process was accelerated due to an increase in thermal energy. Since the increase in temperature increased the rate of moisture ingress, the Arrhenius equation was utilized. It was concluded from both the diffusivities recovered and from the Arrhenius plot that the activation energies and pre-exponentials calculated were similar to those of BMI/carbon composites found in the existing literature.

Moisture equilibrium and diffusivity values predicted were between 1.262 and 1.586 wt.% and 4.05 x 10^{-4} and 1.69 x 10^{-3} mm^2/hr, respectively. Although M_∞ values were lower than previously reported research, the hindrance coefficient of 0.805, from the same study, was in the neighborhood of the values recovered. β and γ exhibited significant correlations to thermal activity and laminate dimensioning. Despite the noticeable trends in the binding and unbinding parameters, their relation to the hindrance coefficient further confirms the accuracy of the hindrance model predictions. Collectively, the results presented in this chapter strengthen the validity of the Langmuir model to accurately predict moisture content in BMI/quartz specimens used in aircraft radome structures.

CHAPTER 6: Concluding Remarks and Recommendations for Future Work

6.1 Concluding Remarks

Quartz-fiber-reinforced bismaleimide is commonly utilized in radomes due to the material's resultant low dielectric properties, corrosion resistance, heat retardant characteristics, and relative low vulnerability to moisture ingress. BMI/quartz as a radar housing structure is crucial to the existence of the radar detection system by shielding its constituent antenna from hazardous conditions such as lightning, high temperature from engine exhaust, debris, moisture, hail or bird strike, and aircraft-related fluids such as fuels, lubricants, and solvents. Furthermore, the material's ability to provide long term structural integrity and impact protection while maintaining transparency to electromagnetic waves has led to its wide spread use in the aerospace industry. However, one of the pivotal drawbacks of the polymeric composite structure is its sensitivity to moisture absorption in nearly all operational environments.

Accurate prediction of composite degradation in mechanical, viscoelastic, and electrical properties due to moisture diffusion is important to aircraft radome design and performance. In addition, knowing the effects of moisture within an aircraft environment leads to the damage prevention of the polymeric composite. Water alone has a high dielectric constant that can degrade radar performance by casting shadows on radar image. Additional water ingress into a BMI/quartz structure can further diminish composite properties via thickness swelling, high temperature thermal spiking, and freeze/thaw cycles. These type of events can produce cracks, delamination, and fiber-matrix debonds.

Regulations set by the FAA and military give basic requirements about examining degradation of polymeric composites used for radome structures that can be found to be short and non-specific. NATO's AGARD advisory report regarding suitable radome material for avionic systems provides guidance to better asses environmental degradation on aircraft composites. In this report, test methods to evaluate dielectric, moisture absorption, and flexural properties include a resonant cavity method, ASTM D570, and ASTM D790. Utilizing AGARDS advisory report as an aid to evaluate degradation, ASTMs D790, D5229, D7028, and a resonant cavity method were adopted in order to investigate the performance of BMI/quartz under hygrothermal immersion.

6.1.1 Dielectric Study of BMI/quartz

In the initial investigation, BMI/quartz specimen were fully submerged in distilled water, propylene glycol, and deicing fluid for up to 1300 hours at 25°C. Gravimetric measurements of fluid uptake were recorded and dielectric properties were measured as a function of fluid content using a split-post dielectric resonator operating at X-band (10 GHz). An approximate linear relationship between fluid content and dielectric properties was observed. Furthermore, each contaminant's physical and electrical properties were observed to have a proportional response to an electric field when inside the composite samples. A 1% increase in water, deicing fluid, and propylene glycol content resulted in a 7.8%, 4.5%, and 2.5% increase in relative permittivity, respectively. Likewise, these contaminants caused an increase in loss tangent of 378.5%, 593.0%, and 441.5% for a 1% increase by weight, respectively. Approximately 1300 hours of immersion at room temperature resulted in a fluid content by weight of 1.31%, 3.41%, and 4.28% for water, deicing fluid, and propylene glycol, respectively.

In the second part of this dielectric study, the BMI/quartz was compared to epoxy/glass radome composites during full immersion in distilled water at a temperature of 25°C and immersion time of 1300 hours under X-band frequency. Although the bismalimide composite had an outstanding increase of 1.31% moisture content compared to that of epoxy/7781 and epoxy/4180's increase of 0.52% and 0.95%, its relative permittivity and loss tangent were significantly lower or approximately equivalent for the immersion time. During full moisture desorption of both BMI/quartz and epoxy/glass specimens, dielectric values of all three materials systems returned to their initial state, which was that prior to moisture contamination. Hence, for short immersion periods, a simple desorption method can be implemented in order to reverse compromised dielectric properties.

6.1.2 Long-Term Durability of BMI/quartz

Six-ply quartz-fiber-reinforced bismaleimide laminates were exposed to a four-year water contamination investigation and were studied via flexural property assessment, dynamic mechanical analysis, and scanning electron microscopy. Moisture diffusion parameters were predicted by the 3D-HDM, these being edge diffusivity, through thickness diffusivity, and moisture equilibrium with values of 1.98×10^{-3}, 1.73×10^{-4}, and 1.723% respectively. Additional parameters predicted were the binding probabilities and hindrance coefficient (γ, β, and μ) with values of 2.98×10^{-6}, 12.5×10^{-6}, and 0.807, correspondingly. The non-Fickian behavior resulted in water content of 1.529% by weight and was consistent with the model projection. An anomalous decrease in storage modulus prior to glass transition temperature was noticed, but is discussed in further detail in a consecutive study. Despite the worst-case scenario of full immersion, no significant decrease in flexural

strength and change in glass transition temperature was detected in the laminates. Although SEM revealed areas of debonding for specimens immersed for four years, structural integrity was maintained.

6.1.3 Hygrothermal Induced Debonds

Prior to the glass transition temperature, an anomalous decrease in storage modulus was noticed in moisture-contaminated BMI/quartz specimens. In the absence of water contamination and elevated temperature, no such drop was observed. Conversely, in the absence of loading, a drop was observed. However, the concurrent application of the two contributing factors has a significant effect on the flexural strength of the specimen. SEM images are suggestive of fiber-matrix debonding as the cumulative result, which leads to this effect. In addition, DMA may prove to be instrumental as a debond detection tool for fiber-reinforced composites. In summary, the experimental results indicate the existence of a scenario in which no individual service limit has been reached, yet a significant loss in mechanical properties has occurred. Furthermore, the concurrent application of moisture and high temperatures is likely quite common for in-service radome structural composites, and therefore warrants additional and significant study.

6.1.4 Hygrothermal Langmuir Diffusion Model Evaluation

The ability to use experimental data prior to reaching moisture equilibrium was investigated by means of a 1D-HDM ("Langmuir-type") diffusion model. Projections in moisture content were accurately made for samples with dimensions of 55x55, 34x34, and 14x14 mm and thickness of 1.35 mm. Laminates immersed in water baths of 25°C, 37°C, and 50°C were analyzed gravimetrically along with one-dimensional predictive model in

order to characterize the diffusion temperature/area-aspect-ratio dependent behavior of the bismaleimide composite. Application of both least-squares regression method and the predictive model showed less than 1% error for the recovery of the non-Fickian parameters D_z, M_∞, β, and γ. Furthermore, the Arrhenius equation was applied to diffusivities recovered to verify the accuracy of the model predictions. M_∞ and D_z were projected between 1.262 and 1.586 wt.% and 4.05 x 10^{-4} and 1.69 x 10^{-3} mm^2/hr, respectively. β and γ exhibited a strong correlation to immersion temperature and aspect ratio. The hindrance coefficient, which is dependent on the binding probabilities, was accurately recovered between 0.751 and 0.855. Similar prediction of five year immersed BMI/quartz laminates were projected with an analogous hindrance coefficient of 0.805, hence strongly supporting the accuracy of the hindrance model predictions.

6.2 Recommendations and Future Work for BMI/quartz Radome

6.2.1 Suggestions for Preventing Degradation of a Contaminated BMI/quartz Radome

It was observed, in Chapter 2 that with low levels of moisture the dielectrics of the BMI/quartz composite began to deteriorate. However, with a simple desorption process, the dielectrics of the composite reversed to their initial state. The fluid contents achieved in the dielectric degradation investigation are likely representative of a worst-case scenario for in-service composites, which are only occasionally exposed to these fluids rather than continually immersed. Therefore, in aircraft radome structures, a simple desorption method, can be an effective periodic practice for decelerating the dielectric degradation process. Also, this method can possibly prevent mechanical and viscoelastic property impairment. Moisture removal of a radome structure can be performed periodically via an autoclave.

6.2.2 Suggestions for Preventing Moisture/Heat-Rate Debonding

The synergistic ramifications between moisture content and temperature ramp rate are known to lead to delamination and fiber-matrix debonds in the bismaleimide composite. Removal of the deleterious combination between these coupled factors is important to the durability and performance of the BMI radome. Effortless removal of moisture can be achieved by modifying void content in such a way that it would accelerate desorption but not degrade its mechanical integrity. Moreover, keeping radome structures distant form high rate thermal energy sources, such as high-temperature engine exhaust gases, would prevent structure damage.

6.2.3 Finalizing Plot of Hygrothermally Induced Debonds in BMI/quartz and Utilization in Polymer Composites

The overlaying objectives of the heat rate vs. moisture content plot in Figure 40 are unfinished. The main purpose of this plot is to quantify the overall coupling of heat rate and moisture effects on BMI/quartz. This means that more data is needed in Figure 40 in order to construct an accurate model of the operating service limits of the radome composite. For example, the moisture limit for this plot would be located at the moisture equilibrium of BMI/quartz, which is 1.726 wt.%. The rate of heating limit is dependent on the environment and usage of the polymeric material. Furthermore, the correlation between moisture, heat rate, and debonds has established DMA as a potential method for uncovering possible fiber matrix debonds and delamination in BMI/quartz. Although the findings shown in Chapter 4 are for the BMI/quartz radome composite, they can also have a profound impact in similar polymeric composites. The type of environment where these

plot-types would be most significant are those that are exposed to significant variation in thermal energy and moisture absorption.

6.2.4 Effect of Fluid Molecule Interaction Inside Radome Composite

In a radome environment, various aerospace fluid types may be exposed to the composite structure. Depending on the type of fluid and environment, radome properties can be deleteriously altered. The most probable culprit in polymeric composite property degradation can be attributed to the molecular binding between the polymer chain and fluid molecules. The nature of how molecules bind will determine radome performance, which can be characterized by the chemical structure of both fluid and composite material. Chemical properties such as electronegativity, dipole moment, vapor pressure, heat capacity, viscosity, number of molecules, etc. are detrimental to the accurate prediction of both dielectric and moisture absorption behaviors. In addition, the outside environment of an aircraft has an important role in detailing the rate of binding and unbinding. Effectively knowing or understanding how radome materials and fluid molecules interact in specific environments may reduce the rate of dielectric, viscoelastic, and mechanical property failure.

6.2.5 Recommendation for the Three-Dimensional Hindered Diffusion Model

The use of thin composite samples to determine moisture absorption effects on dielectric, viscoelastic, and mechanical properties is efficient in both cost and time. However, variation in parameter recovery in this research, which was found to be dependent in area aspect ratio and immersion temperature, determine the use of thin laminates to be ineffective. The laminate physical properties, which include void content,

resin content, fiber content, ply thickness, and ply count of the BMI composite are critical to variations in parameter recovery as a result of dissimilarities in area aspect ratio and immersion temperature. Accommodations of the physical laminate characteristics and immersion environment into the 3D-HDM would greatly expand the effectiveness of the method.

References

[1] Niu MCY. Organic Matrices. Composite Airframe Structures - Practical Design Information and Data (3rd Edition): AD Adaso/Adastra Engineering LLC; 1992. p. 51.

[2] Ratna D. Bismaleimide Resins. Handbook of Thermoset Resins: Smithers Rapra Technology; 2009. p. 127-32.

[3] Fink JK. Bismaleimide Resins. Reactive Polymers Fundamentals and Applications - A Concise Guide to Industrial Polymers (2nd Edition): Elsevier; 2013. p. 291.

[4] Costa ML, De Almeida SFM, Rezende MC. The Influence of Porosity on the Interlaminar Shear Strength of Carbon/Epoxy and Carbon/Bismaleimide Fabric Laminates. Composites Science and Technology. 2001;61(14):2101-8.

[5] Stone DEW, Clarke B. Ultrasonic Attenuation as a Measure of Void Content in Carbon-Fibre Reinforced Plastics. Non-Destructive Testing. 1975;8(3):137-45.

[6] Zhu H, Wu B, Li D, Zhang D, Chen Y. Influence of Voids on the Tensile Performance of Carbon/Epoxy Fabric Laminates. Journal of Materials Science & Technology. 2011;27(1):69-73.

[7] Hurdelbrink II KR, Siddique Z, Altan MC. The Coupled Effect of Microvoids and Hydraulic Fluid Absorption on Mechanical Properties of Quartz/BMI Laminates. In: Proceedings of 29th Asc Technical Conference. UC San Diego, La Jolla, CA, 2014. p. 15.

[8] Hurdelbrink II KR, Guloglu GE, Anderson JP, Grace LR, Siddique Z, Altan MC. Effect of Microvoids on Anomalous Moisture Absorption of Quartz/BMI Composite Laminates. In: Proceedings of ASME 2014 International Mechanical Engineering Congress and Exposition. Montreal, Quebec, Canada, 2014. p. 8.

[9] Bao L-R. Moisture Absorption and Hygrothermal Aging in a Bismaleimide Resin and its Carbon Fiber Composites. Ann Arbor: University of Michigan; 2001.

[10] Hexply F650 Product Data Sheet. Connecticut: Hexcel Corporation; 2005.

[11] Ju J, Morgan RJ. Characterization of Microcrack Development in BMI-Carbon Fiber Composite Under Stress and Thermal Cycling. Journal of Composite Materials. 2004;38(22):2007-24.

[12] Cox SB, Tate LC, Caraccio AJ, Wright MC, Sampson JW, Taylor BJ, et al. Process Optimization of Bismaleimide (BMI) Resin Infused Carbon Fiber Composite. Florida: NASA; 2013.

[13] Chen X, Yuan L, Zhang Z, Wang H, Liang G, Gu A. New Glass Giber/Bismaleimide Composites with Significantly Improved Flame Retardancy, Higher Mechanical Strength and Lower Dielectric Loss. Composites Part B: Engineering. 2015;71(0):96-102.

[14] Zhuo D, Gu A, Liang G, Hu J-t, Yuan L, Chen X. Flame Retardancy Materials Based on a Novel Fully End-Capped Hyperbranched Polysiloxane and Bismaleimide/Diallylbisphenol a Resin with Simultaneously Improved Integrated Performance. Journal of Materials Chemistry. 2011;21(18):6584-94.

[15] Landman D. Advances in the Chemistry and Applications of Bismaleimides. In: Pritchard G, editor. Developments in Reinforced Plastics—5: Processing and Fabrication. Dordrecht: Springer Netherlands; 1986. p. 39-81.

[16] Strong AB. Fundamentals of Composites Manufacturing: Materials, Methods and Applications. United States: Society of Manufacturing Engineers; 2008. p. 140.

[17] Peros V, Trawinski D, Ruth J. Application of Fiber-Reinforced Bismaleimide Materials to Aircraft Nacelle Structures. Maryland: Martin Marietta Aero & Naval Systems; 1992. p. 1333-47.

[18] Guozheng L, Zengping Z, Jieying Y, Xiaolei W. BMI Based Composites with Low Dielectric Loss. Polymer Bulletin. 2007;59(2):269-78.

[19] Grace LR. The Effect of Moisture Contamination on the Relative Permittivity of Polymeric Composite Radar-Protecting Structures at X-Band. Composite Structures. 2015;128(0):305-12.

[20] Kumar BG, Singh RP, Nakamura T. Degradation of Carbon Fiber-Reinforced Epoxy Composites by Ultraviolet Radiation and Condensation. Journal of Composite Materials. 2002;36(24):2713-33.

[21] Kutz M. Effects on Epoxy Composites and Adhesives. Handbook of Environmental Degradation of Materials: Second Edition. Burlington, US: William Andrew; 2012. p. 743.

[22] De Vivo B, Lamberti P, Spinelli G, Tucci V. Evaluation of the Lightning strikes on Carbon Fibers Panels for Aircraft Structural Parts. COMSOL conference 2015 Grenoble. Grenoble: COMSOL; 2015. p. 5.

[23] Feraboli P, Kawakami H. Damage of Carbon/Epoxy Composite Plates Subjected to Mechanical Impact and Simulated Lightning. Journal of Aircraft. 2010;47(3):999-1012.

[24] Ozcelik O, Aktas L, Altan MC. Thermo-Oxidative Degradation of Graphite/Epoxy Composite Laminates: Modeling and Long-Term Predictions. eXPRESS Polymer Letters. 2009;3(12):797-803.

[25] Roy S, Singh S, Schoeppner G. Modeling of Evolving Damage in High Temperature Polymer Matrix Composites Subjected to Thermal Oxidation. J Mater Sci. 2008;43(20):6651-60.

[26] Aylor DM, Murray JN. The Effect of a Seawater Environment on the Galvanic Corrosion Behavior of Graphite/ Epoxy Composites Coupled to Metals. Maryland: Naval Surface Warfare Center; 1992.

[27] Cochran RC, Donnellan TM, Trabocco RE. Environmental Degradation of High Temperature Composites. Pennsylvania: Naval Air Development Center; 1992.

[28] Rao RMVGK, Chanda M, Balasubramanian N. A Fickian Diffusion Model for Permeable Fibre Polymer Composites. Journal of Reinforced Plastics and Composites. 1983;2(4):289-99.

[29] Blikstad M. Three-Dimensional Moisture Diffusion in Graphite/Epoxy Laminates. Journal of Reinforced Plastics and Composites. 1986;5(1):9-18.

[30] Rao RMVGK, Kumari HVS, Raju KS. Moisture Diffusion Behaviour of T300-914c Laminates. Journal of Reinforced Plastics and Composites. 1995;14(5):513-22.

[31] Liu W, Hoa SV, Pugh M. Water Uptake of Epoxy–Clay Nanocomposites: Experiments and Model Validation. Composites Science and Technology. 2008;68(9):2066-72.

[32] Glaskova T, Aniskevich A. Moisture Absorption by Epoxy/Montmorillonite Nanocomposite. Composites Science and Technology. 2009;69(15–16):2711-5.

[33] Burcham LJ, Eduljee RF, Gillespie JW. Investigation of the Microcracking Behavior of Bismaleimide Composites During Thermal Aging. Polymer Composites. 1995;16(6):507-17.

[34] Haque MH, Upadhyaya P, Roy S, Ware T, Voit W, Lu H. The Changes in Flexural Properties and Microstructures of Carbon Fiber Bismaleimide Composite after Exposure to a High Temperature. Composite Structures. 2014;108:57-64.

[35] Luo H, Lu G, Roy S, Lu H. Characterization of the Viscoelastic Behavior of Bismaleimide Resin before and after Exposure to High Temperatures. Mech Time-Depend Mater. 2013;17(3):369-99.

[36] Ray BC, Mula S, Bera T, Ray PK. Prior Thermal Spikes and Thermal Shocks on Mechanical Behavior of Glass Fiber- Epoxy Composites. Journal of Reinforced Plastics and Composites. 2006;25(2):197-213.

[37] Bera T, Mula S, Ray PK, Ray BC. Effects of Thermal Shocks and Thermal Spikes on Hygrothermal Behavior of Glass-- Polyester Composites. Journal of Reinforced Plastics and Composites. 2007;26(7):725-38.

[38] Shin EE, Morgan RJ, Zhou J, Lincoln J, Jurek R, Curliss DB. Hygrothermal Durability and Thermal Aging Behavior Prediction of High- Temperature Polymer- Matrix Composites and Their Resins. Journal of Thermoplastic Composite Materials. 2000;13(1):40-57.

[39] Zheng Q, Morgan RJ. Synergistic Thermal- Moisture Damage Mechanisms of Epoxies and Their Carbon Fiber Composites. Journal of Composite Materials. 1993;27(15):1465-78.

[40] Grace LR, Altan MC. Three-Dimensional Anisotropic Moisture Absorption in Quartz-Reinforced Bismaleimide Laminates. Polymer Engineering & Science. 2014;54(1):137-46.

[41] Tsenoglou CJ, Pavlidou S, Papaspyrides CD. Evaluation of Interfacial Relaxation Due to Water Absorption in Fiber–Polymer Composites. Composites Science and Technology. 2006;66(15):2855-64.

[42] Weitsman YJ, Weitsman Y. Fluid Effects in Polymers and Polymeric Composites. Boston, MA, UNITED STATES: Springer US; 2011. p. 13-4.

[43] Zhou J, Lucas JP. Hygrothermal Effects of Epoxy Resin. Part II: Variations of Glass Transition Temperature. Polymer. 1999;40(20):5513-22.

[44] Wang Y, Hahn TH. Afm Characterization of the Interfacial Properties of Carbon Fiber Reinforced Polymer Composites Subjected to Hygrothermal Treatments. Composites Science and Technology. 2007;67(1):92-101.

[45] Abdel-Magid B, Ziaee S, Gass K, Schneider M. The Combined Effects of Load, Moisture and Temperature on the Properties of E-Glass/Epoxy Composites. Composite Structures. 2005;71(3–4):320-6.

[46] Sun P, Zhao Y, Luo YF, Sun LL. Effect of Temperature and Cyclic Hygrothermal Aging on the Interlaminar Shear Strength of Carbon Fiber/Bismaleimide (BMI) Composite. Materials & Design. 2011;32(8-9):4341-7.

[47] Bao L-R, Yee AF. Moisture Diffusion and Hygrothermal Aging in Bismaleimide Matrix Carbon Fiber Composites—Part I: Uni-Weave Composites. Composites Science and Technology. 2002;62(16):2099-110.

[48] Bao L-R, Yee AF. Moisture Diffusion and Hygrothermal Aging in Bismaleimide Matrix Carbon Fiber Composites: Part II—Woven and Hybrid Composites. Composites Science and Technology. 2002;62(16):2111-9.

[49] Costa ML, De Almeida SFM, Rezende MC. Hygrothermal Effects on Dynamic Mechanical Analysis and Fracture Behavior of Polymeric Composites. Materials Research. 2005;8(3):335-40.

[50] Cloth, Quartz, Style 581 Fabric. AMS 3849B ed. Warrendale, PA: SAE International; 1994.

[51] Grace LR. Non-Fickian Three-Dimensional Moisture Absorption in Polymeric Composites: Development and Validation of Hindered Diffusion Model. Ann Arbor, MI: University of Oklahoma; 2012.

[52] Grace LR. Projecting Long-Term Non-Fickian Diffusion Behavior in Polymeric Composites Based on Short-Term Data: A 5-Year Validation Study. Journal of Materials Science. 2016;51(2):845-53.

[53] Cary RH. Avionic Radome Materials. Paris, France: Advisory Group for Aerospace Research and Development; 1974.

[54] Loos AC, Springer GS. Moisture Absorption of Graphite-Epoxy Composites Immersed in Liquids and in Humid Air. Journal of Composite Materials. 1979;13(2):131-47.

[55] Gibbins MN, Hoffman DJ. Environmental Exposure Effects on Composite Materials for Commercial Aircraft. Springfield, VA1982.

[56] Sugita Y, Winkelmann C, La Saponara V, Cheng L. Effect of a Deicing Fluid on the Durability of Carbon/Epoxy Composites. Mechanics of Composite Materials. 2011;47(3):313-22.

[57] Sugita Y, Winkelmann C, La Saponara V. Environmental and Chemical Degradation of Carbon/Epoxy Lap Joints for Aerospace Applications, and Effects on Their Mechanical Performance. Composites Science and Technology. 2010;70(5):829-39.

[58] Moffet ML, La Saponara V. Rheological Properties of Neat Epoxy Exposed to in-Service Aerospace Contaminants. Journal of Applied Polymer Science. 2013;130(6):3961-71.

[59] Popineau S, Rondeau-Mouro C, Sulpice-Gaillet C, Shanahan MER. Free/Bound Water Absorption in an Epoxy Adhesive. Polymer. 2005;46(24):10733-40.

[60] Hurdelbrink KI. The Synergistic Effects of Prepreg Humidity Exposure, Fabrication Pressure, and Hydraulic Fluid Absorption on Microstructure and Mechanical Properties of High-Performance Composite Laminates. Norman, Oklahoma: University of Oklahoma; 2017.

[61] Campbell FC. Structural Composite Materials. ASM International; 2010. p. 401-20.

[62] FAA. Advanced Composite Material. AMT Airframe Handbook (FAA-H-8083-31). Oklahoma City, Oklahoma: U.S. Department of Transportation; 2012. p. 41.

[63] FAA. Maintenance of Weather Radar Radomes. Washington, DC: U.S. Department of Transportation; 1977.

[64] Palocz-Andresen M. Decreasing Fuel Consumption and Exhaust Gas Emissions in Transportation Sensing, Control and Reduction of Emissions. In: ProQuest, editor. Heidelberg ; New York: Heidelberg ; New York : Springer; 2013.

[65] Mattingly JD. Elements of Propulsion : Gas Turbines and Rockets. Reston: Reston, VA, USA: American Institute of Aeronautics and Astronautics; 2006.

[66] Frasier SJ, Kabeche F, Figueras i Ventura J, Al-Sakka H, Tabary P, Beck J, et al. In-Place Estimation of Wet Radome Attenuation at X Band. Journal of Atmospheric & Oceanic Technology. 2013;30(5):917-28.

[67] Morgan D, Hardwick CJ, Haigh SJ, Meakins AJ. The Interaction of Lightning with Aircraft and the Challenges of Lightning Testing. 2012.

[68] Wang Y. Modeling of Lightning-Induced Thermal Ablation Damage in Anisotropic Composite Materials and Its Application to Wind Turbine Blades. Iowa: The University of Iowa; 2016.

[69] Boeing. Lightning Strikes: Protection, Inspection,and Repair. Aeromagazine. Seattle, WA: The Boeing Company; 2012. p. 18-28.

[70] 173 SC. Minimum Operational Performance Standards for Nose-Mounted Radomes. Washington, D.C.: RTCA, Incorporated; 1993.

[71] Radomes, General Specification. Department of Defense; 1975.

[72] Standard Test Methods for Flexural Properties of Unreinforced and Reinforced Plasticsand Electrical Insulating Materials. Pennsylvania: ASTM International; 2010.

[73] Standard Test Method for Moisture Absorption Properties and Equilibrium Conditioning of Polymer Matrix Composite Materials. Pennsylvania: ASTM International; 2012.

[74] Standard Test Method for Glass Transition Temperature (DMA Tg) of Polymer Matrix Composites by Dynamic Mechanical Analysis (DMA).

[75] Agilent Split Post Dielectric Resonators for Dielectric Measurements of Substrates: Agilent Technologies; 2006.

[76] Fick A. Ueber Diffusion. Annalen Der Physik. 1855;170(1):59-86.

[77] Aktas L, Hamidi YK, Altan MC. Combined Edge and Anisotropy Effects on Fickian Mass Diffusion in Polymer Composites. Journal of Engineering Materials and Technology. 2004;126(4):427.

[78] Garcia C, Fittipaldi M, Grace LR. Epoxy/Montmorillonite Nanocomposites for Improving Aircraft Radome Longevity. Journal of Applied Polymer Science. 2015;132(43):9.

[79] Shen C-H, Springer GS. Moisture Absorption and Desorption of Composite Materials. Journal of Composite Materials. 1976;10(1):2-20.

[80] Musto P, Ragosta G, Scarinzi G, Mascia L. Probing the Molecular Interactions in the Diffusion of Water Through Epoxy and Epoxy–Bismaleimide Networks. Journal of Polymer Science Part B: Polymer Physics. 2002;40(10):922-38.

[81] Cotugno S, Mensitieri G, Sanguigno L, Musto P. Molecular Interactions in and Transport Properties of Densely Cross-Linked Networks: A Time-Resolved FT-IR Spectroscopy Investigation of the Epoxy/H2O System. Macromolecules. 2005;38(3):801-11.

[82] Kotsikos G, Gibson AG, Mawella J. Assessment of Moisture Absorption in Marine Grp Laminates with Aid of Nuclear Magnetic Resonance Imaging. Plastics, Rubber & Composites. 2007;36(9):413-8.

[83] Liu W, Hoa SV, Pugh M. Water Uptake of Epoxy–Clay Nanocomposites: Model Development. Composites Science and Technology. 2007;67(15):3308-15.

[84] Bao L-R, Yee AF. Effect of Temperature on Moisture Absorption in a Bismaleimide Resin and Its Carbon Fiber Composites. Polymer. 2002;43(14):3987-97.

[85] Roy S, Xu WX, Park SJ, Liechti KM. Anomalous Moisture Diffusion in Viscoelastic Polymers: Modeling and Testing. Journal of Applied Mechanics. 1999;67(2):391-6.

[86] Jacobs PM, Jones FR. Diffusion of Moisture into Two-Phase Polymers. Journal of Materials Science. 1990;25(5):2471-5.

[87] Berens AR, Hopfenberg HB. Diffusion and Relaxation in Glassy Polymer Powders: 2. Separation of Diffusion and Relaxation Parameters. Polymer. 1978;19(5):489-96.

[88] Berens AR, Hopfenberg HB. Induction and Measurement of Glassy-State Relaxations by Vapor Sorption Techniques. Journal of Polymer Science: Polymer Physics Edition. 1979;17(10):1757-70.

[89] Carter HG, Kibler KG. Langmuir-Type Model for Anomalous Moisture Diffusion in Composite Resins. Journal of Composite Materials. 1978;12(2):118-31.

[90] Li J, Cantwell FF. Intra-Particle Sorption Rate and Liquid Chromatographic Bandbroadening in Porous Polymer Packings III. Diffusion in the Polymer Matrix as the Cause of Slow Sorption. Journal of Chromatography A. 1996;726(1):37-44.

[91] Masoud H, Alexeev A. Permeability and Diffusion through Mechanically Deformed Random Polymer Networks. Macromolecules. 2010;43(23):10117-22.

[92] Shao J, Baltus RE. Hindered Diffusion of Dextran and Polyethylene Glycol in Porous Membranes. AIChE Journal. 2000;46(6):1149-56.

[93] Grace LR, Altan MC. Non-Fickian Three-Dimensional Hindered Moisture Absorption in Polymeric Composites: Model Development and Validation. Polymer Composites. 2013;34(7):1144-57.

[94] Grace LR, Altan MC. Characterization of Anisotropic Moisture Absorption in Polymeric Composites Using Hindered Diffusion Model. Composites Part A: Applied Science and Manufacturing. 2012;43(8):1187-96.

[95] Khatavkar N, Kandasubramanian B. Composite Materials for Supersonic Aircraft Radomes with Ameliorated Radio Frequency Transmission-a review. RSC Advances. 2016;6(8):6709-18.

[96] Meyer JG. Polyurethane Foam: Dielectric Materials for Use in Radomes and Other Applications. Tacoma, WA: General Plastics Manufacturing Company; 2015.

[97] Viña J, García EA, Argüelles A, Viña I. The Effect of Moisture on the Tensile and Interlaminar Shear Strengths of Glass or Carbon Fiber Reinforced PEI. Journal of Materials Science Letters. 2000;19(7):579-81.

[98] Akay M, Ah Mun SK, Stanley A. Influence of Moisture on the Thermal and Mechanical Properties of Autoclaved and Oven-Cured Kevlar-49/Epoxy Laminates. Composites Science and Technology. 1997;57(5):565-71.

[99] Reid JD, Lawrence WH, Buck RP. Dielectric Properties of an Epoxy Resin and Its Composite I. Moisture Effects on Dipole Relaxation. Journal of Applied Polymer Science. 1986;31(6):1771-84.

[100] Fink BK, McCullough RL, Gillespie JW. The Influence of Moisture on Dielectric Behavior of Poly-Etheretherketone/Carbon Fiber Composites. Journal of Thermoplastic Composite Materials. 1992;5(2):90-104.

[101] Choi I, Kim JG, Lee DG, Seo IS. Aramid/Epoxy Composites Sandwich Structures for Low-Observable Radomes. Composites Science and Technology. 2011;71(14):1632-8.

[102] Blevis B. Losses Due to Rain on Radomes and Antenna Reflecting Surfaces. IEEE Transactions on Antennas and Propagation: IEEE; 1965. p. 175-6.

[103] Kurri M, Huuskonen A. Measurements of the Transmission Loss of a Radome at Different Rain Intensities. Journal of Atmospheric and Oceanic Technology. 2008;25(9):1590-9.

[104] Loss KR. Damage Tolerant Sandwich Panel Core with Low Moisture Affinity. In: Proceedings of American Society for Composites 29th Technical Conference on Composite Materials. San Diego, California, September 2014, 2014.

[105] Chang K. System Performance in Rain in a Radome-Enclosed Environment. International Journal of Infrared and Millimeter Waves. 1986;7(2):267-89.

[106] MSDS-Tks Fluid: Packaging Service Co., Inc.; 2012.

[107] Sebastian MT. Measurement of Microwave Dielectric Properties and Factors Affecting Them. Dielectric Materials for Wireless Communication. Amsterdam: Elsevier; 2008. p. 11-47.

[108] Krupka J, Gregory AP, Rochard OC, Clarke RN, Riddle B, Baker-Jarvis J. Uncertainty of Complex Permittivity Measurements by Split-Post Dielectric Resonator Technique. Journal of the European Ceramic Society. 2001;21(15):2673-6.

[109] Janezic MD, Kuester EF, Jarvis JB. Broadband Complex Permittivity Measurements of Dielectric Substrates Using a Split-Cylinder Resonator. In: Proceedings of 2004 IEEE MTT-S International Microwave Symposium Digest (IEEE Cat No04CH37535). 6-11 June 2004, 2004. p. 1817-20.

[110] Krupka J, Stephen AG, Krzysztof D, Brian MP. Comparison of Split Post Dielectric Resonator and Ferrite Disc Resonator Techniques for Microwave Permittivity Measurements of Polycrystalline Yttrium Iron Garnet. Measurement Science and Technology. 1999;10(11):1004.

[111] Krupka J, Derzakowski K, Abramowicz A, Tobar M, Geyer RG. Complex Permittivity Measurements of Extremely Low Loss Dielectric Materials Using Whispering Gallery Modes. In: Proceedings of 1997 IEEE MTT-S International Microwave Symposium Digest. 8-13 June 1997, 1997. p. 1347-50.

[112] Mazierska J, Krupka J, Jacob MV, Ledenyov D. Complex Permittivity Measurements at Variable Temperatures of Low Loss Dielectric Substrates Employing Split Post and Single Post Dielectric Resonators. 2004. p. 1825-8.

[113] Krupka J. Precise Measurements of the Complex Permittivity of Dielectric Materials at Microwave Frequencies.79:195-8.

[114] Krupka J. Developments in Techniques to Measure Dielectric Properties of Low-Loss Materials at Frequencies of 1–50 Ghz. Journal of the European Ceramic Society. 2003;23(14):2607-10.

[115] Handbook of Chemistry and Physics. 96th ed: CRC Press; 2015.

[116] Zahn M, Ohki Y, Fenneman DB, Gripshover RJ, Gehman VH. Dielectric Properties of Water and Water/Ethylene Glycol Mixtures for Use in Pulsed Power System Design. Proceedings of the IEEE. 1986;74(9):1182-221.

[117] Vishwam T, Parvateesam KS, Murthy KRV. Dielectric Spectroscopic Studies of Propylene Glycol/Aniline Mixtures at Temperatures Between 303K to 323K. International Journal of Engineering Research & Technology (IJERT). 2015;4(11).

[118] Agilent Basics of Measuring the Dielectric Properties of Materials: Agilent Technologies; 2006.

[119] Digest of Literature on Dielectrics. Washington, D.C.: National Academy of Sciences; 1977.

[120] Silvestrelli PL, Parrinello M. Water Molecule Dipole in the Gas and in the Liquid Phase. Physical Review Letters. 1999;82(16):3308-11.

[121] Cotinaud M, Bonniau P, Bunsell AR. The Effect of Water Absorption on the Electrical Properties of Glass-Fibre Reinforced Epoxy Composites. Journal of Materials Science. 1982;17(3):867-77.

[122] Hammond CL, Carroll JR. Environmental Effects on Composites. In: Proceedings of 19th Structures, Structural Dynamics and Materials Conference. MD, USA, 1978.

[123] Zhou J, Lucas JP. Hygrothermal Effects of Epoxy Resin. Part I: The Nature of Water in Epoxy. Polymer. 1999;40(20):5505-12.

[124] Delasi R, Whiteside JB. Effect of Moisture on Epoxy Resins and Composites. Dayton, Ohio: American Society for Testing and Materials; 1978.

[125] Li Y, Miranda J, Sue H-J. Hygrothermal Diffusion Behavior in Bismaleimide Resin. Polymer. 2001;42(18):7791-9.

[126] Rodriguez LA, García C, Grace LR. Long-Term Durability of a Water-Contaminated Quartz-Reinforced Bismaleimide Laminate. Polymer Composites. 2016:7.

[127] Surathi P, Karbhari VM. Hygrothermal Effects on Durability and Moisture Kinetics of Fiber-Reinforced Polymer Composites. La Jolla, California: University of California; 2006.

[128] Sims GD, Gnaniah SJP. Improved Procedures for the Determination of Tg by Dynamic Mechanical Analysis. In: Proceedings of 17th International Conference on Composite Materials. Edinburgh, UK, 27-31 July, 2009.

[129] Drakonakis VM, Seferis JC, Wardle BL, Nam J-D, Papanicolaou GC, Doumanidis CC. Kinetic Viscoelasticity Modeling Applied to Degradation During Carbon–Carbon Composite Processing. Acta Astronautica. 2010;66(7):1189-200.